AMERICAN UNIVERSITY OF BEIRUT

# THE EFFECT OF SAND COLUMNS ON THE RESPONSE OF CLAY UNDER CYCLED LOADING CONDITIONS

by
## AHMAD MAHMOUD KAHIEL

A dissertation
submitted in partial fulfillment of the requirements
for the degree of Doctor of Philosophy in Engineering
to the Department of Civil and Environmental Engineering
of the Maroun Semaan Faculty of Engineering and Architecture
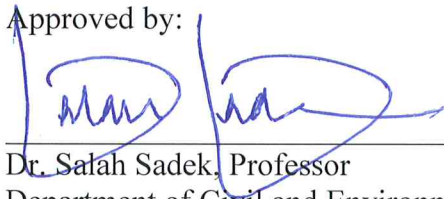at the American University of Beirut

Beirut, Lebanon
December 2019

AMERICAN UNIVERSITY OF BEIRUT


# THE EFFECT OF SAND COLUMNS ON THE RESPONSE OF

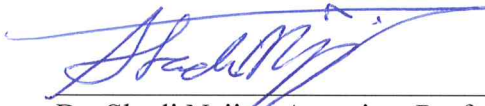# CLAY UNDER CYCLED LOADING CONDITIONS

by
## AHMAD MAHMOUD KAHIEL


Approved by:

_____

Dr. Salah Sadek, Professor                                           Advisor
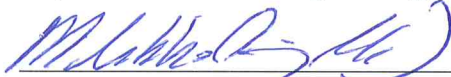Department of Civil and Environmental Engineering, AUB

_____

Dr. Shadi Najjar, Associate Professor                   Member of committee
Department of Civil and Environmental Engineering, AUB

_____
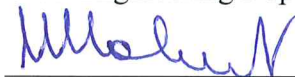
Dr. Grace Abou Jaoude, Associate Professor           Member of committee
Department of Civil Engineering, LAU

_____

Dr. Muhsin Rahhal, Professor                            Member of committee
Civil Engineering Department at the Faculty of Engineering, USJ

_____

Dr. Mounir Mabsout, Professor                              Chair of committee
Department of Civil and Environmental Engineering, AUB



December, 19, 2019

# AMERICAN UNIVERSITY OF BEIRUT

## THESIS, DISSERTATION, PROJECT RELEASE FORM

Student Name: __Kahiel__ __Ahmad__ __Mahmoud_____
                      Last            First         Middle

◯ Master's Thesis    ◯ Master's Project    ⊘ Doctoral Dissertation

[✓]     I authorize the American University of Beirut to: (a) reproduce hard or electronic copies of my thesis, dissertation, or project; (b) include such copies in the archives and digital repositories of the University; and (c) make freely available such copies to third parties for research or educational purposes.

[ ]     I authorize the American University of Beirut, to: (a) reproduce hard or electronic copies of it; (b) include such copies in the archives and digital repositories of the University; and (c) make freely available such copies to third parties for research or educational purposes after:

**One ---- year from the date of submission of my thesis, dissertation, or project.**
**Two ---- years from the date of submission of my thesis, dissertation, or project.**
**Three ---- years from the date of submission of my thesis, dissertation, or project.**

_____

Signature       Date    2020

*Ahmad Kahiel*    10/1/2020

# ACKNOWLEDGMENTS

# AN ABSTRACT OF THE DISSERTATION OF

Ahmad Mahmoud Kahiel    for    Doctor of Philosophy in Engineering
Major: Geotechnical Engineering

Title: The Effect of Sand Columns on the Response of Clay under Cycled Loading Conditions

The reliance on granular columnar inclusions for improving the bearing capacity of soft clays, reducing overall settlements, and accelerating consolidation due to applied static loads is an established ground modification solution. The improvement achieved by reinforcing soft clays with aggregate piers has been extensively studied and quantified both in experimental and real world application contexts. To date however, few attempts have addressed the resultant effect/improvement on the site response under dynamic loading conditions. This research effort investigates the effect of columnar granular inclusions on the cyclic resistance of isotropically and 1-dimensionally consolidated clay samples. A series of stress-controlled cyclic tests were conducted on both "control" and sand-column reinforced samples across a range of parameterized conditions. The effect of varying the cyclic stress amplitude and frequency as representatives of induced shear stresses and rate effects respectively was investigated under both drained and undrained conditions. Furthermore, the effects of a range of practical design values of area-replacement ratios and column densities were investigated. Image processing and tomographic techniques were utilized to assist in tracking sample deformation, particularly in the radial and axial directions. The pore water pressures generated during the various phases of loading were independently monitored for the clay matrix and at the granular column location. The effectiveness of granular columns under these parameters for design purposes were assessed and compared with current design practice.

Keywords: Stone column, aggregate piers, invasion, plugging, cyclic triaxial tests, image processing, reliability-based design.

# CONTENTS

Chapter

# ILLUSTRATIONS

# TABLES

# CHAPTER 1

# INTRODUCTION

Soil deposits constitute the upper most layer of the earth's crust upon which all manmade constructions are supported. Soils are a product of multifold-interrelated and complex processes of mechanical and chemical weathering and transportation. These processes result in spatially variable random fields of soil properties further confounded by placement conditions and environments: flat or sloping, wet or dry. Uncontrolled and somewhat random initial conditions of genesis, transportation and placement, coupled with at times modest and partial geotechnical data represent major challenges for engineers and researchers in their quest to predict performance, assess stability, and develop failure mitigation measures.

As urban centers and populations grow, demand on already limited/suitable sites for developments increases. As a result, less desirable/appropriate locations, typically those with problematic soil conditions, are left for engineers to devise safe and economic foundation solutions for. In their attempt to control soil and structure performance and to meet design requirements in such challenging sites, designers have adopted a variety of soil improvement techniques. The choice of a specific technique typically depends on prevailing soil type, site conditions, and sought degree and type of improvement, in addition to the availability of adequate equipment and local expertise. Granular columnar inclusions (otherwise referred to as "stone columns") in otherwise weak soils/matrices are amongst improvement techniques that are currently use on a wide and evolving scale. This is in part due to the relative simplicity of the technique and its applicability across a wide range/types of problematic soils spanning soft clays

1

to loose sands.

The installation of stone columns provides several advantages: (1) densifying native soil (in the case where loose sands are present), (2) providing shorter drainage paths to accelerate consolidate or mitigate against liquefaction, and (3) redistributing stresses across the site thus providing a more dependable and less variable foundation on which to build. This in turn will result in higher bearing capacities and cyclic resistances, reduced total and differential settlements, and faster dissipation of pore pressures (accelerated consolidation).
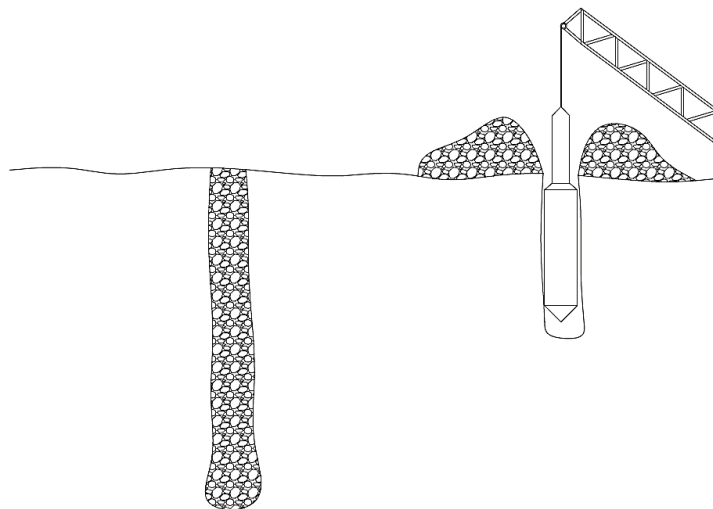


Figure 1. Vibro-floatation method for the intallation of stone columns

The installation of stone columns is achieved in one of two approaches and construction methods. The first method consists of using vibro-probes to install and densify granular columns in situ, using either a "dry placement approach" in which the aggregates are delivered at the base of the column once the matric is penetrated, or a "wet approach" where the aggregates are delivered from the ground surface through the annulus between the probe and the penetrated ground. (Figure 1). In this method a vibrating probe penetrates loose (or loosened) soil under its own weight. The probe is then used to compact the aggregates and form the stone column. The second method

2

involves ramming granular material inside a predrilled hole. This method evolved

significantly from its early applications (primarily in Japan) to forming a widely

recognized and in some instances "proprietary" family of techniques such as GeoPiers

among others. It was found that the installation method has no major effect on the

performance of the site and ultimate strength of the column.

Stone columns are typically installed either under large loaded areas

(embankments or rafts) or under single spread and combined footing. The behavior of

columns under large loaded area, excluding boundary columns, is studied by

considering a single column with tributary area that is a function of the spacing between

the columns (unit cell). This unit cell concept assumes that no lateral deformation can

take place at the boundaries of the cell. This assumption is considered reasonable given

the fact that any tendency to deform laterally will be counteracted by an equivalent

tendency from neighboring unit cells. However, , for individually loaded columns/small

group of columns, the surrounding soil will be unconstrained to deform laterally and

thus will have a different failure mechanisms that couldn't be modelled in the unit cell

concept.

The basis of the design and behavior of stone columns in single and group

configurations in sands and clays under static loading conditions has been extensively

researched (Najjar, 2013a). However, to date, only a very limited number of studies

have addressed the performance of stone columns subjected to repeated loading. The

importance of studying the behavior of soils under cycled loading emerges from the fact

that soils thus loaded, fail at applied stresses that are lower than their nominal static

strengths. The situation is more severe when the repeated loading exhibits a stress

reversal, which was found to have a detrimental effect on soil behavior. Figure 2 shows

the results of a cyclic triaxial test on a clay having a static strength of ~70kPa. As noted

from the figure, the soil was subjected to a sinusoidal loading with an amplitude of

~50kPa. Although the loading amplitude was lower than the static strength of the soil,

failure was reached after 22 cycles of loading.
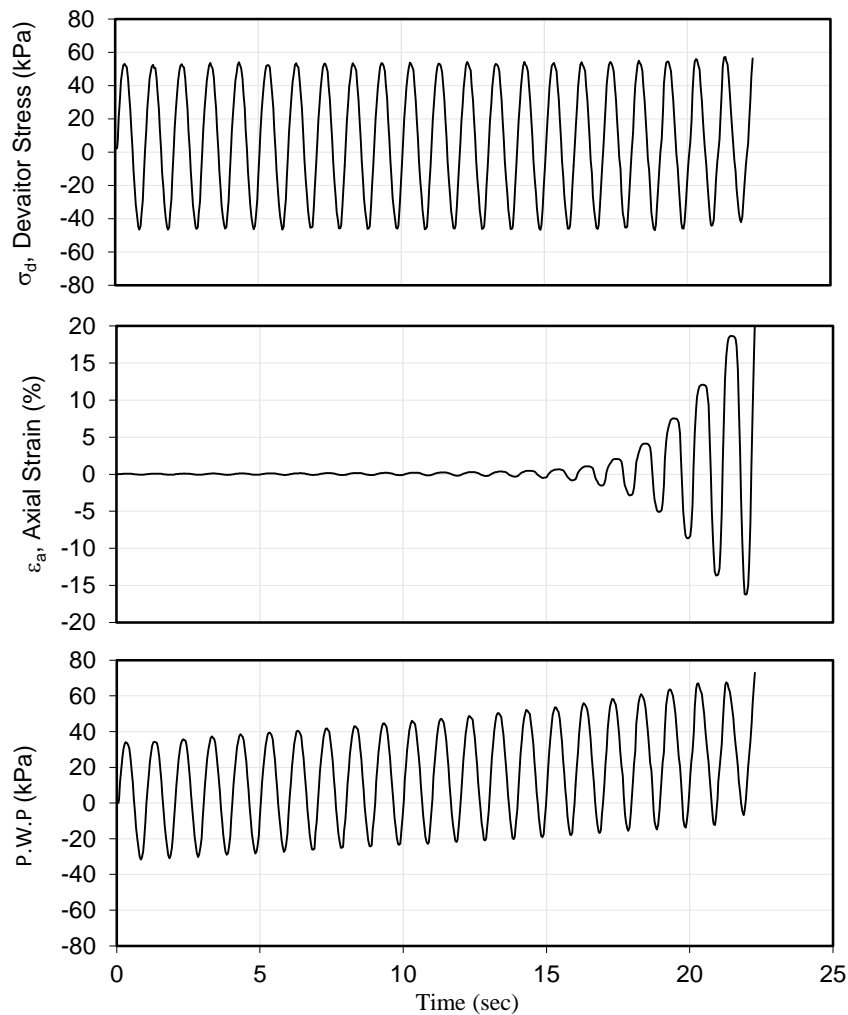


Figure 2. Cyclic triaxial test of Achrafieh clay sample

The scenarios/sources corresponding to repeated loads being applied on soil

deposits are numerous and significant. Earthquakes for instance represent a major

source of repeated loading that induces propagating shear stresses across the soil profile

(Figure 3a). Wind loads may cause structures to sway, which in turn is translated into

4

compressive and uplift forces exerted at the level of the footings on underlying soil (Figure 3c). Another source of repeated/periodic loading may be associated with the cycles of filling and discharging of large storage tanks for water or hydrocarbons etc. (Figure 3b). It should be noted that soil elements in these three loading patterns are subject to different stress paths and start from different initial states of stress. As a result, the earthquake loading could be best represented by simple shear loading, while wind and water tanks cause stress paths that are comparable to triaxial and 1-D loading mechanisms, respectively.
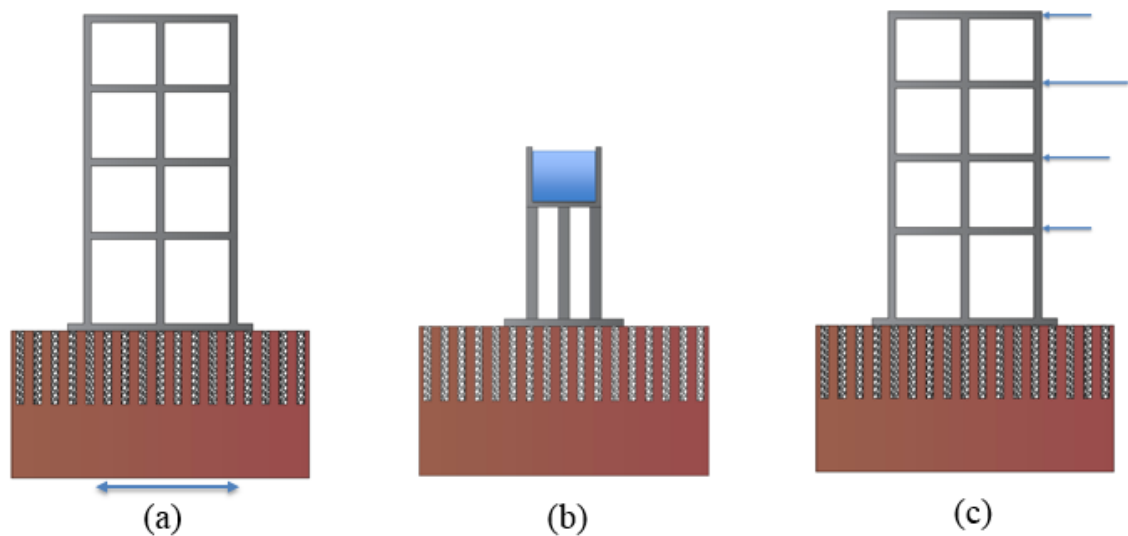


Figure 3. Applications involving repeated loading

Earthquakes occur in nature as a result of sudden fractures driven by the continuous motion and straining of earth tectonic plates. These fractures produce complex wave patterns that propagate through the earth crust reaching the surface. The intensity of the shaking can vary from mild (barely felt by humans) to strong ground motions that might lead to devastating damage scales. Measured ground accelerations reflect the complexity of the ground motion induced by earthquakes; this complexity renders its replication in a laboratory setup an arduous and intricate task. Thus,

significant simplifying assumptions are tolerated in attempts to establish a base-understanding of the response of soils during such events. Figure 4 shows a typical acceleration record along three orthogonal directions during an earthquake. The variability in the amplitude, frequency content and duration across the three directions is clearly demonstrated.
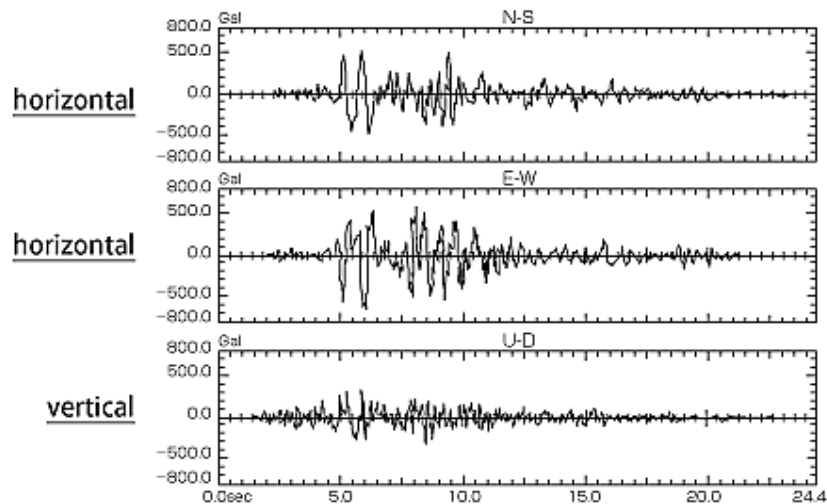


Figure 4. Acceleration time history of a typical earthaquake record along three orthogonal directions

This ground shaking may lead to liquefaction in sandy sites and cyclic mobility and/or loss of strength in clayey sites. These phenomena are manifested as excessive settlements in structures, lateral spreading for mildly sloping grounds, slope failures, damage to infrastructure and in some cases even loss of lives.

Available research on discrete columnar inclusions in soil under repeated loading includes analytical approaches, small scale testing, centrifuge testing, and finite element analyses. The results from these various sources/efforts show signification discrepancies and contradictions in reference to the expected system behavior.

One of the most compelling and daunting challenges in geotechnical engineering research is the ability and need to develop and adopt methods (experimental

6

and/or numerical) which are able to replicate/capture in-situ conditions. This is of critical importance given the stress-dependent nature of the material response. Most laboratory experimental procedures suffer from some limitations in that regard particularly in reference to the challenge of stress-level conditions and loading patterns and path replication. The basic simplification that is widely adopted in dealing with geo-materials in the realm of analytical and/or numerical simulations is to treat soils as a "continuum". However, in reality a soil "element"/block is generally constituted of independent and/or cemented individual particles holding each other through a complex web of contact forces and interactions. This assumption, though it may seem as unworkable, has the real advantage of simplifying the modelling of soil behavior and maintaining an acceptable level of compatibility with actual/observed behavior. The challenges raised by both experimental and analytical modeling of the behavior of stone columns are further compounded by the "distinct" nature of the composite matrix-granular column system.

The actual behavior/response of stone columns is in fact a function of the specific application they are used in/for. For instance, a stone column installed under an "isolated" footing will undoubtedly have different behavior than a similar column located at the center of a large array of columns under a wide foundation (Figure 5). The former type of columns will be unrestrained to deform with the surrounding soil in the lateral direction until reaching typical bearing capacity failure, whereas the latter is likely to exhibit uniaxial (~1-D) deformations/response.
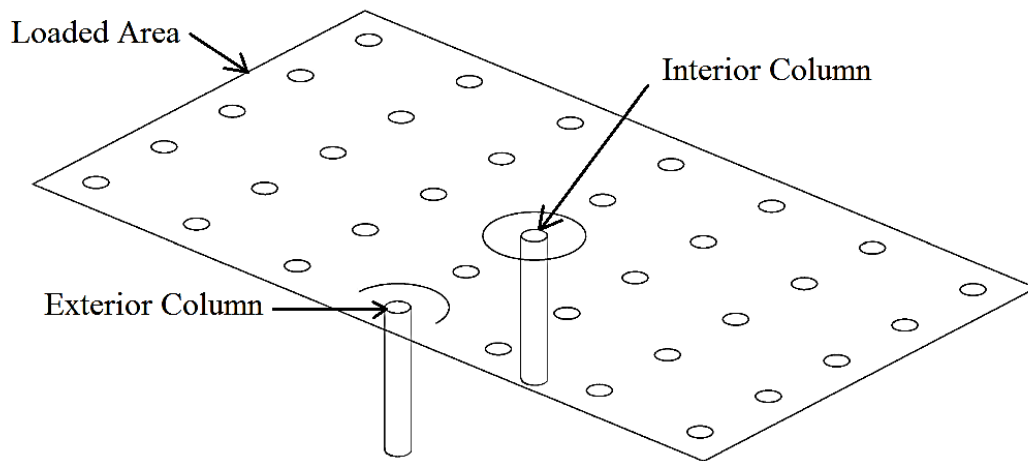
Figure 5. Site reinforced with stone columns showing interior and exterior columns

As such, columns in the central region of a grid will exhibit a different behavior as compared to peripheral columns. Since all the columns will be simultaneously loaded, lateral deformation at the periphery of the zone of influence of an interior column is assumed to be zero; thus each unit can be analyzed separately. Two field cases can be noted: equal strain and free strain: Equal strain conditions are encountered under rigid rafts where the column and the surrounding soil undergo equal settlements. In this case, the contribution of each (soil and column) will be based on their relative constrained moduli assuming no lateral deformation is taking place in the soil and the column. However in realty, the column will deform laterally and thus lower stress concentration factors will result (Castro & Sagaseta, 2009). Free strain conditions on the other hand, are expected to be applicable/present under large embankments. It is assumed that under these conditions stresses are uniformly distributed between the column and the soil (stress concentration factor equals unity). As a result it is expected that the soil will settle more than the columns and shear stresses will develop at the interface between the column and the soil. It is interesting that even in such cases, recent research showed that due to arching effects, stone columns will still bear higher

8

stresses than the surrounding soil even in free strain cases. (Basack, Indraratna, &
Rujikiatkamjorn, 2015).

In the balance of the work presented in this thesis, the effects of the presence of
columnar granular inclusions of different densities in a saturated clay soil, consolidated
under isotropic and 1-D initial conditions are explored. A series of cyclic tests were
conducted on saturated clay samples reinforced with sand columns for different design
parameters. These parameters included area replacement ratio, column density,
amplitude and frequency of loading, boundary conditions (drained/undrained, laterally
restrained/unrestrained). Image processing and tomographic techniques were utilized in
tracking sample and column deformation during loading. Results are analyzed and
conclusions/recommendations presented for design purposes.

It is important to note here that the structure of the thesis as presented is in fact
divided/written as separate "papers" that address the various aspects of interest
identified in the objectives of this work: Nature of the response, effect of variability of
material characteristics, conditions at the contact between matrix soil and granular
column (inter-penetration), laboratory setup and advanced techniques of image
processing and monitoring of load concentrations and pore pressures.  Specifically:
Chapter 2 presents the background and research works done to explore the nature of the
interaction/invasion of the clay matrix material into the granular inclusions under
different conditions; Chapter 3 includes a thorough presentation and discussion of the
Cyclic Triaxial setup used in the cycled loading tests including the many/major
modifications which were designed, built and incorporated specifically for the purpose
of the work; The results of the extensive testing program carried out as part of the study
of the response of granular inclusions/matrix clay systems to repeated loading under

varying conditions are presented and discussed in Chapter 4. In Chapter 5, the image capturing, analysis and interpretation technique and resulting enhancements in reference to establishing local deformations and associated stress concentrations at various levels within the sample are presented. The uncertainty in model parameters and its impact on the anticipated overall response in explored in Chapter 6. Finally conclusions from and overall contributions of the work are presented in Chapter 7.

# CHAPTER 2

# CLAY INVASION INTO SANDS AND GRAVELS

## 2.1 Abstract

The invasion of fine materials into a porous network is typically encountered in various engineering applications. Interactions between these two media at the interface level can govern the mechanical and hydraulic design procedure. This paper aims to quantify the invasion length of clays into porous coarse granular packing via experimental and theoretical approaches. We conduct an experimental program for different clay liquidity indices, granular-packing grain sizes and applied stress ranges. The experimental program along with the dimensional analysis guided the development of three upper bound prediction models for the invasion length. Hollow friction piles and ball penetrometers inspired the development of these models.

## 2.2 Introduction

Soils are multi-phased granular materials. This property renders soil pores vulnerable to invasion by finer geo-materials when subjected to applied pressures and hydraulic gradients at the interface. Previous research has examined this phenomenon within various engineering applications and include smear zone characterization around stone columns, filter design, mud-cake formation in oil boreholes, mud loss in rock fractures, grouting, and settlement of layered clay-gravel sites. These are all field applications in which the invasion of fines into the pores of coarser media could be a major concern in the design and construction.

Geotechnical engineers frequently use stone columns as a soil improvement technique. Stone columns can act as drainage paths that accelerate the dissipation of loading-induced pore water pressure. Additional benefits are an increase in load bearing capacity and a reduction of total and differential settlements (see (Mitchell, 1981), (Balaam & Booker, 1985), (Parsa Pajouh, Fatahi, & Khabbaz, 2010), and (Aboshi, Mizuno, & Kuwabara, 1991)). However, the installation process involves high compaction pressures and results in both mixing and disturbance of the in-situ soil. The smear zone refers to this disturbed area which could have a detrimental effect on the hydraulic conductivity of the stone column. Consequently there is a reduction in the efficiency when dissipating the generated pore water pressure through the stone column.

Extensive research has investigated the impact of the smear zone on the performance of stone columns. An early study presented analytical solutions for radial and vertical consolidation in sites with sand drains (Baron, 1948). This research included solutions for the degree of consolidation with time and considered the presence and absence of smear zones around the drain. Results showed that the presence of the smear zone significantly slows the consolidation process. The intensity of retardation

appears to be a function of the thickness and permeability of the smear zone. More recent studies investigated the free and equal strain conditions within a unit cell which contains a central column. These studies considered the effect of column spacing, moduli and Poisson's ratios, well resistance, the soil layer thickness, and radial deformation of the column (Alamgir, Miura, Poorooshasb, & Madhav, 1996), (Han & Ye, 2001; Han & Ye, 2002), and (Castro & Sagaseta, 2009).

The hydraulic conductivity and volume compressibility of the smear zone in these studies appeared to vary nonlinearly with radial distance from the center of the column (see (Rujikiatkamjorn & Indraratna, 2014)). Results suggested that the extent of this variation is a function of the installation technique, diameter of the mandrel/vibro-float, and energy exerted during compaction. Additionally, a smear zone radius of 1.6 times the well radius and a horizontal permeability of one third of that of the in-situ soil is satisfactory for vertical drain design purposes (Hird & Moseley, 2000). The variation of the horizontal permeability after the installation of vertical drains is 4 to 5 times the radius of the drain measured in laboratory tests (Indraratna & Redana, 1998). Results of large-scale laboratory experiments based on pore water pressure measurements at different distances from the drain showed that the radius of the smear zone is four times the mandrel radius (see (Sharma & Xiao, 2000)). Parabolic variations of soil permeability and compressibility with distance from the column result in the closest predictions to in-situ test measurements (Deb & Behera, 2016). As a result, larger drains with wider spacing are more efficient than smaller drains with closer spacing due to smear zone effects (see (M. R. Madhav, Park, & MIURA, 1993)).

All previous studies investigated the disturbance of in-situ soil outside the column. However, clogging and invasion of finer matter into the pores also effects the

13

internal structure of the column. The construction process results in three distinct zones around the stone column (Weber, Plötze, Laue, Peschke, & Springman, 2010)): the invasion, smear, and densification zones. The thickness of the invasion zone is one-third of the column radius and attributed to the material grain size, clay strength, and applied load. Furthermore, the clogging of stone columns is more severe when the area replacement ratio decreases and the stress concentration ratio increases (Deb & Shiyamalaa, 2015).

On the other hand, a variety of previous research has investigated the flow of viscous fluids in porous media. This work resulted in the continuum, capillary bundle, and numerical models which estimate the flow rate of fluids into porous media. (See (Sochi, 2010) for an extensive description).

Filter design studies have examined the percolation of fine grains into the pores of a coarser matrix in attempts to protect the base material in dams. Results suggest that the governing factor in the design is the minimum constriction diameter. Equation 1 presents a successful filter design relationship (Peck & Terzaghi, 1948):

$$D_{15}/d_{85} < 4 \tag{1}$$

where $D_{15}$ is the filter grain size with a 15% passing, and $d_{85}$ refers to the base material grain size with an 85% passing. Researchers also investigated the clogging and bridging phenomena of pores in a porous network (Valdes & Santamarina, 2008). The authors concluded that for orifice to particle diameter ratios < 3, stable bridges form, while for an orifice to particle diameter > 5, no bridging occurs. Earlier research found that reductions in permeability due to clogging occur more rapidly when the clay concentration in the suspension increases (Baghdikian, Sharma, & Handy, 1987).

Grouting is a soil improvement technique that improves the mechanical behavior

of soils and rocks. The technique consists of injections of cementing material into the voids/fractures of the soil/rock. Relative particle sizes of the grout and soil can provide reliable estimates of soil groutability (Mitchell, 1970). (Kim & Whittle, 2009) presented a particle network model to simulate filtration mechanism during cement injection. Predictions of pressures along the injected sand column where closer to experimental magnitudes in comparison to first-order absorption models that adopts a constant filtration rate. The water to cement ratio and degree of grout saturation have significant effects on the injected grout. When the grouting pressure, saturation, and water to cement ratio increase, the injected grout volume rises (Q. Wang, Wang, Sloan, Sheng, & Pakzad, 2016).

This study investigates the invasion of clay through an experimental program that includes different grain sizes. We develop models that predict the clay invasion length for a range of water contents, grain sizes for the granular packing, and applied stress. Three analytical models based on force equilibrium define upper bounds for the invasion length.

## 2.3   Experimental Study

The experimental program design aims to investigate the invasion of clay with water contents which range from one to half of the liquid limit into granular packings with different grain sizes. A syringe and an oedometer act as chambers for the test specimens. Figure 6 shows a schematic plot of the two test devices with the corresponding water content ranges.

15
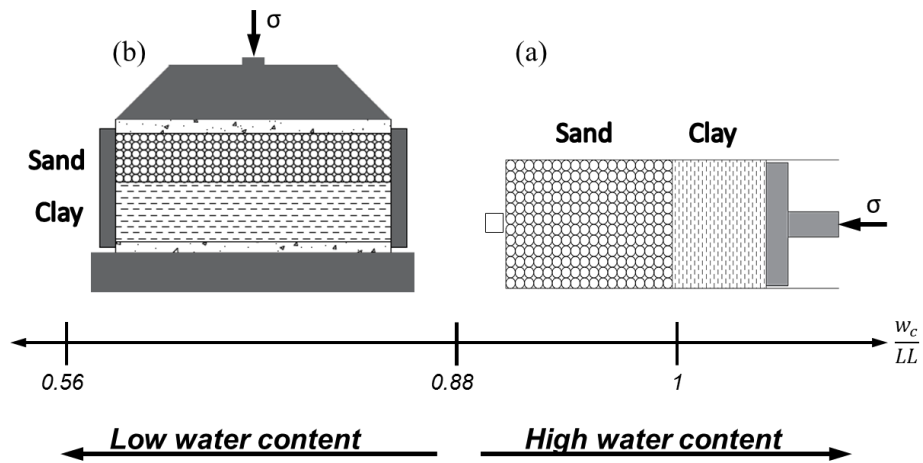
Figure 6. Devices utilized in the experimental program for different water contents: (a) Syringe, (b) Oedometer

### 2.3.1 Selected Soil

Kaolinite SA1 represented the fine invading slurry/clay. This clay has a liquid limit of 48% measured with fall cone tests. The consolidation test revealed a virgin compression index ($C_c$) of 0.22 and a recompression index ($C_r$) of 0.06 (ASTM Committee D-18 on Soil and Rock, 2004). The undrained shear strength to the initial effective confining pressure ratio $(s_u/\sigma'_{3,0})$ is approximately 0.3.

The selection of four uniformly graded granular materials considers a wide range of pore sizes (0.6mm to 6mm) to study the effects of size on the degree of clay invasion. The materials include: 3 and 6-mm glass beads, Ottawa 10/20 sand, and KAUST 20/30 sand. The selection of the ratio of clay particles size to the size of voids in the granular packing prevent clogging or bridging. Orifice diameter to particles diameter ratio are 100, 250, and 750 for the combination of Kaolinite SA1 with KAUST 20/30, Ottawa 10/20, and 3mm-glass beads. All ratios are far from the entrapment/bridging range (Valdes & Santamarina, 2008). This choice of materials

ensures that the clay invasion into the pores of the granular packing only stops due to the development of resisting shear planes which equalize the driving force.

### 2.3.2 Syringe Tests

The granular material fills half of the vertically positioned syringe and the slurry clay ($w_c = LL$) is added, leveled, and slowly pushed until it interfaces with the granular material (Figure 1a). The syringe pump pushes the clay into the granular packing contained within the specimen chamber (syringe) at a constant flow rate until it reaches the maximum torque capacity of the syringe pump motor. We measure the invasion length once the invasion stops. Two syringes with diameters of 25.7mm and 20.0mm result in maximum applied pressures of 100 and 156 kPa respectively. The high flow rate ensures that the invasion occurs under undrained conditions.

### 2.3.3 Oedometer Tests

This section of the experimental program uses a clay slurry with a starting water content which equals the liquid limit of the clay. Figure 7b presents the experimental set-up. The equipment is the typical oedometer ring with 50.5mm diameter (Figure 7b). We consolidate the clay specimens to defined pre-consolidation pressures (12, 30, and 100 kPa) which correspond to water contents of 0.88, 0.82, and 0.73 respectively. Following equilibrium, specimens are unloaded and a granular layer of measured weight and height is added and leveled. The applied load increments on the composite specimens range from 6kPa to 1MPa, with the displacement monitored over time until complete pore water pressure dissipation.

Table 1 summarizes a total of 16 tests in both parts of the experimental program and includes the corresponding boundary conditions.

Table 1. Experimental study: tests, materials and boundary conditions.

| Device | Test ID | Granular-Packing Material | Applied Pressure [kPa] | Clay $w_c$/LL | Clay Pre-consolidation Stress [kPa] |
|---|---|---|---|---|---|
| Syringe (Sy) | 1 | GB-6mm | 100 | 1 | N/A |
| | 2 | GB-3mm | 100 | 1 | N/A |
| | 3 | Ottawa 10/20 | 100 | 1 | N/A |
| | 4 | KAUST 20/30 | 100 | 1 | N/A |
| | 5 | GB-3mm | 150 | 1 | N/A |
| | 6 | Ottawa 10/20 | 150 | 1 | N/A |
| | 7 | KAUST 20/30 | 150 | 1 | N/A |
| Oedometer (Oed) | 8 | GB-3mm | 6→1000 | 0.88→0.56 | 12 |
| | 9 | Ottawa 10/20 | 6→1000 | 0.82→0.56 | 30 |
| | 10 | KAUST 20/30 | 6→1000 | 0.73→0.56 | 100 |
| | 11 | GB-3mm | 6→1000 | 0.88→0.56 | 12 |
| | 12 | Ottawa 10/20 | 6→1000 | 0.82→0.56 | 30 |
| | 13 | KAUST 20/30 | 6→1000 | 0.73→0.56 | 100 |
| | 14 | GB-3mm | 6→1000 | 0.88→0.56 | 12 |
| | 15 | Ottawa 10/20 | 6→1000 | 0.82→0.56 | 30 |
| | 16 | KAUST 20/30 | 6→1000 | 0.73→0.56 | 100 |

## 2.4    Experimental Results and Analysis

### 2.4.1    Syringe Tests

Figure 7a shows of the invasion of kaolinite at the initial, intermediate, and final time-steps. Observations note the uniform invasion of the slurry with a stable plane normal to the direction of flow. The invasion length is measured to the nearest tenth of mm at the end of each test. Figure 7b summarizes the invasion lengths for the 7 tests performed in the first part of the experimental program. Invasion lengths range from 3 mm up to greater than 50mm for applied stress ranges of 100 to approximately 156 kPa. A limitation is that the length of the syringe prevented any further increase in the applied stresses. Since the clay has a water content equal to the liquid limit, the undrained shear strength is approximately equal to 1.7kPa (Vardanega & Haigh, 2014). Results indicate that applied pressure and particle size are the most influential

parameters that affect the magnitude of the invasion. The increase in applied pressure and/or particle size of the granular packing result in higher invasion lengths.
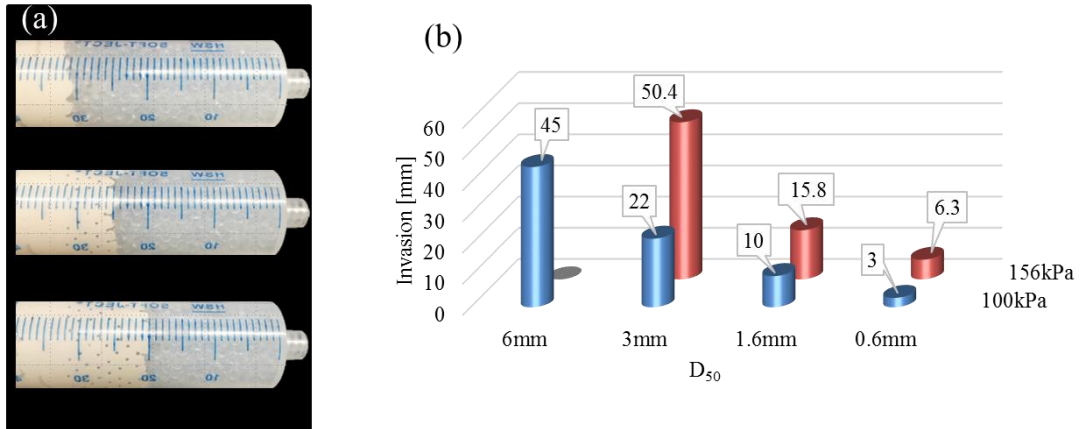


Figure 7. Invasion of high water content slurries into coarse-grained granular packings - Syringe tests. (a) Three stages of clay slurry invasion into a packing of 3mm glass beads – Notice the stable invasion. (b) Slurry invasion length vs. applied pressure for various particle diameter

### 2.4.2 Oedometer Tests

Figure 8 (a - c) displays the total vertical deformation versus the vertical effective stress for the nine oedometer tests. Each plot corresponds to tests with specific granular packing materials and contains three tests for the three adopted pre-consolidation stresses (12, 30, and 100kPa). The plots include the Kaolinite virgin compression and recompression lines obtained from separate tests on clay only specimens with the same thickness as the clay in the composite specimens. Figure 8a also shows a consolidation curve of the granular material. This curve represents the behavior of the three granular materials which exhibit a comparable stress-deformation behavior and have a relatively small contribution with respect to the total vertical deformation of the composite specimen. The maximum total vertical displacements ranged from 2mm to 4mm measured from the start of loading of the composite

19

specimens. Similar to the syringe test results, we noticed that as the grain diameter and applied stress increases the magnitude of the invasion rises. In addition, clays pre-consolidated to lower stresses have higher invasion lengths. Coarser particle sizes (Ottawa 10/20 and 3mm glass beads) provide a clearer demonstration of this effect.

The composite specimens follow the recompression curve when the applied vertical stress is less than the pre-consolidation pressure. This is an indication that no invasion takes place in the recompression zone. The curve then breaks to a steeper slope in comparison to the Kaolinite virgin compression slope after it exceeds the pre-consolidation pressure. However, we noticed that for coarser grain sizes, the stress at which the curve breaks is slightly less than the clay pre-consolidation pressure. The higher contact stresses induced by larger grain sizes may explain this behavior.
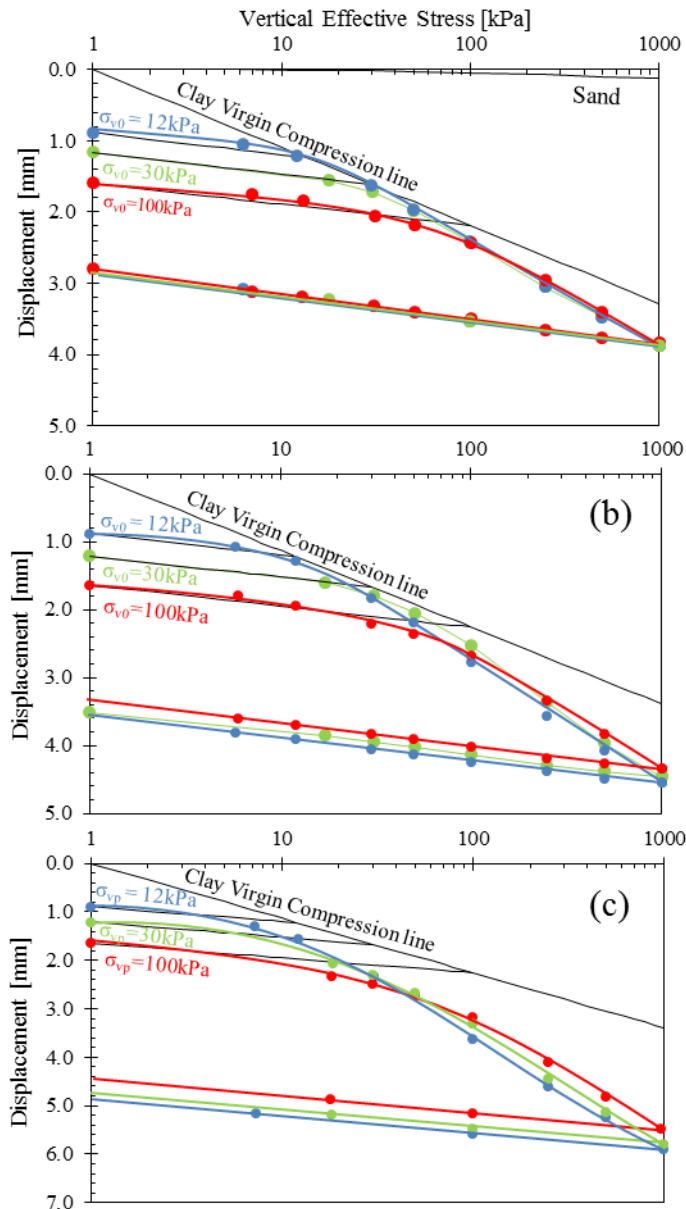
Figure 8. Soft-clay invasion into coarse-grained granular packings – Oedometer tests. The raw data shows the overall shortening of the composite specimen as a function of the applied vertical effective stress. The 9 cases shown correspond to clays preconsolidated to different preconsolidatgion pressures and granular packings.

The difference between the composite specimen and clay-only curves is approximately equal to the thickness of the clay that invaded the pores of the granular packing. The clay invasion thickness ($t_I$) relates to the invasion length ($I$) because the clay fills the voids by the porosity through the relationship below:

$$t_I = n \cdot I \tag{2}$$

At every stress increment $i$ the total measured displacement $(\delta_{t,i})$ is the summation of three contributors: (1) the deformation of the granular packing layer, (2) clay layer consolidation, and (3) the invasion of the clay into the granular packing:

$$\delta_{t,i} = \delta_{s,i} + \sum_{k=1}^{i} \delta_{c,k} + \sum_{k=1}^{i} t_{I,k} \tag{3}$$

where $\delta_{t,i}$ is the total vertical deformation of the composite specimen, $\delta_{s,i}$ is the vertical deformation in the sand at the end of the loading increment $i$:

$$\delta_{s,i} = \frac{C_{c,s}}{1 + e_{s,0}} \log\left(\frac{\sigma'_i}{\sigma'_0}\right) H_{s,0} \tag{4}$$

$\delta_{c,k}$ is the incremental vertical deformation in the clay due to stress increment $\Delta\sigma'_k = \sigma'_k - \sigma'_{k-1}$:

$$\delta_{c,k} = \frac{X}{1 + e_{c,k-1}} \log\left(\frac{\sigma'_k}{\sigma'_{k-1}}\right) H_{c,k-1} \tag{5}$$

$$X = C_{r,c} \text{ if } \sigma'_k \le \sigma'_p \text{ and } X = C_{c,c} \text{ if } \sigma'_k > \sigma'_p \tag{6}$$

$t_{I,k}$ is the thickness of the clay that invaded into the granular packing due to stress increment $\Delta\sigma'_k$. The presence of the summation signs in equation 3 indicates that these terms were calculated incrementally (i.e. for each stress increment $\Delta\sigma'_k$). Thus to calculate the accumulated clay consolidation from the start of the test to a stress increment $i$ requires the summation of all deformations which correspond to the previous $k$ increments.

To extract the invasion length from total measured deformation, we assume: (1) clay that invades into the granular packing will not contribute to consolidation in subsequent loading increments. Consequently, the calculation of clay consolidation requires incremental shifts in the reference stress and void ratio at every load increment

22

as shown in equation 5. (2) The height of the clean clay layer decreases after each

increment due to the invasion of a portion of the clay into the granular packing.

Therefore this height decreases at every load increment $i$ by the deduction of the

invasion thickness at the previous increment in addition to the deformation due to

consolidation:

$$H_{c,k-1} = H_{c,k-2} - t_{I,k-1} - \delta_{c,k} \tag{7}$$

In order to investigate the invasion of Ashrafieh soil into Ottawa sand,

additional Oedometer tests were performed using these material. However, we noticed

that no invasion took place. This outcome resulted from the fact that the Ashrafieh clay

contains fine sand particles that block the pores of the Ottawa sand and inhibit

penetration. A laser scan of the clay surface after the test is presented in Figure 9. This

scan covers a 5mm by 5mm area as can be seen from the axes. The colored legend

describes the elevation of the surface from the mean value in μm.
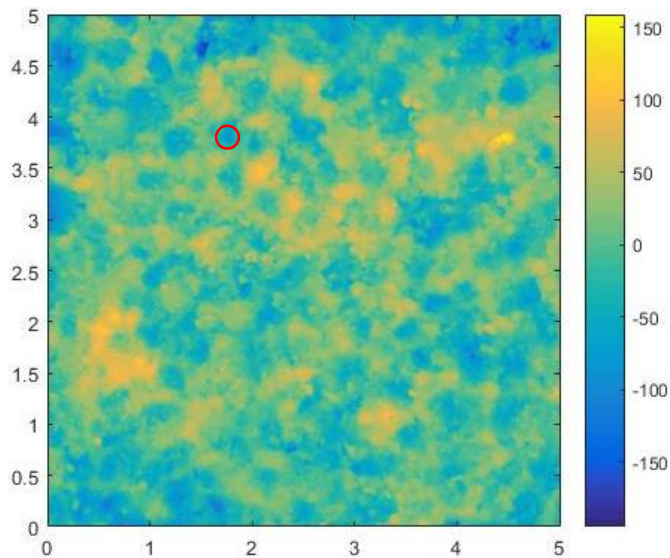


Figure 9. Laser scan of the surface of clay after the oedometer test.

The surface scan shown in Figure 10 shows the imprints of the Ottawa sand

particle on the clay surface, which supports the observation that no invasion has taken

place. The red circle on the same figure represents an average size of Ottawa sand particle for reference. This observation is important for the cyclic triaxial tests performed using Ashrafieh soil and presented in Chapter 4 of this thesis, as it implies/confirms that the lateral deformation of the specimen is solely related to the radial and shear strains developed from loading and not due the invasion of the clay into the sand pores within the granular column.

## 2.5    Dimensional Analysis and Model Development

### 2.5.1    *Dimensional Analysis*

Dimensional analysis is an important tool that can link the field and laboratory scales. First we define the phenomenon of interest which best describes the process modeled in our experiment. The phenomenon in this study is the ultimate invasion length of clay into a coarser granular packing as a result of an external applied stress.

Table 2 shows the list of influential parameters with their dimensions and the resulting pie terms. The number of dimensionless pie terms is the total number of parameters minus the number of dimensions as per Buckingham's pie theorem (Buckingham, 1915).

The function below relates the dimensionless parameters:

$$\frac{l}{r} = f(n, \Delta\sigma/s_u\,) \tag{8}$$

Let's assume a linear relationship between $l/r$ and $\Delta\sigma/s_u$ for a given porosity equation 8 becomes:

$$\frac{l}{r} = f(n) \cdot \Delta\sigma/s_u \tag{9}$$

Table 2. Dimensional analysis: parameters, dimensions, and pie terms.

| Parameters | Dimensions | Dimensionless Parameters |
|:---:|:---:|:---:|
| $I$ | $L$ | $\dfrac{I}{r}$ |
| $r$ | $L$ | |
| $s_u$ | $\dfrac{M}{LT^2}$ | $\dfrac{\Delta\sigma}{s_u}$ |
| $\Delta\sigma$ | $\dfrac{M}{LT^2}$ | |
| $A_t$ | $L^2$ | $\dfrac{A_v}{A_t} = n$ |
| $A_v$ | $L^2$ | |

Figure 10 shows the dimensionless plot for the nine oedometer tests. The normalized invasion has a linear trend with the normalized stress. The slope of this trend in tests were comparably similar. Tests with KAUST 20/30 as a granular packing showed a break in the linear trend as the applied stress increases. This break is clear for the case where the clay was pre-consolidated to 100kPa. Notice the break at a normalized stress increment ($\Delta\sigma/s_u$) of around 2.
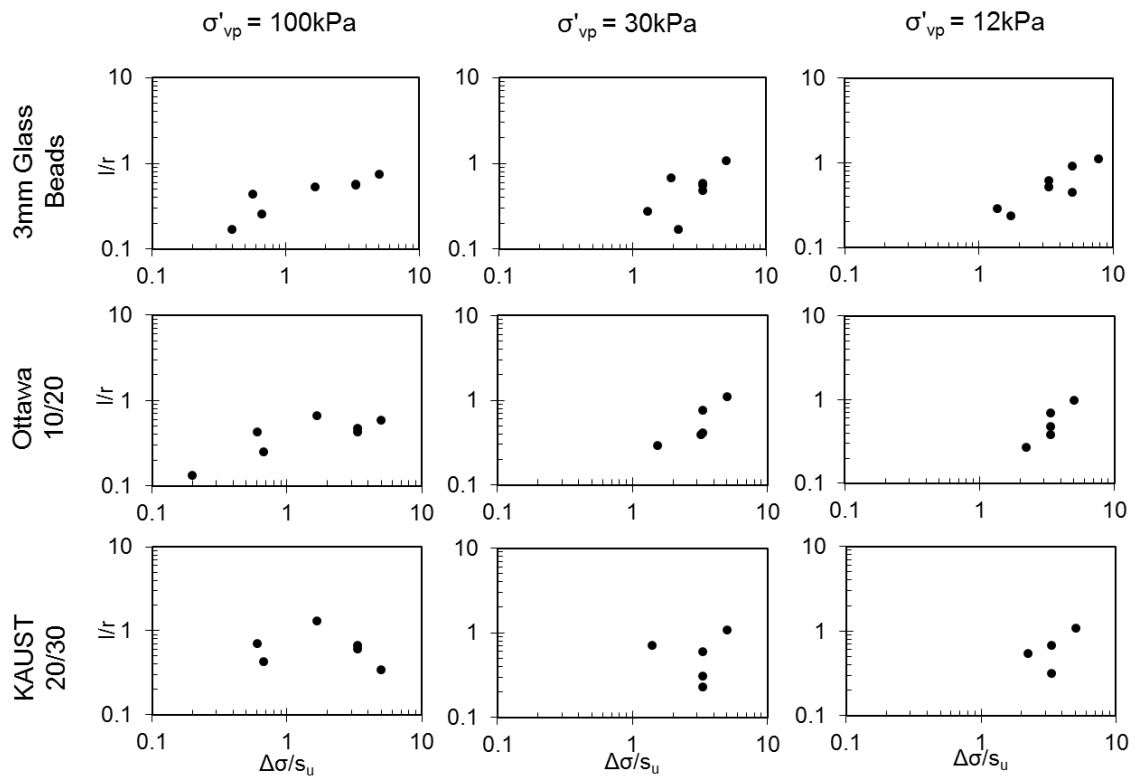
Figure 10. Dimensionless plot for the nine Oedometer tests: notice the comparable trend in tests with Ottawa10/20 and 3mm GB. For tests with KAUST 20/30 (bottom row), this trend is not clear for the tests with clay pre-consolidated to 100 and 30kPa.

This behavior is also reflected in the microscopic section (Figure 11) which shows that the clay invaded only the first monolayer of the sand packing. This points at the importance of the tortuous path for fine grained granular packing.

26

Figure 11. Microscopic view of a section across the oedometer sample showing the clay (σ'p=30kPa) invasion into KAUST 20/30. Notice that invasion only reached one monolayer.

Figure 12 shows the dimensionless plot for both the oedometer (Ottawa 10/20 and 3mm-GB) and the syringe tests results. Linear regression analysis resulted in a simple linear relationship for all data shown in the plot. The scatter around the trend line can be a result of three factors: variations in the targeted granular packing porosity, the representation of the particle radius by a nominal value ($D_{50}/2$), and micro-scale variations due to the particulate nature of soils. Since the model scale is equal to the field scale, the scaling factor is 1 and there is no need to check for distortions.
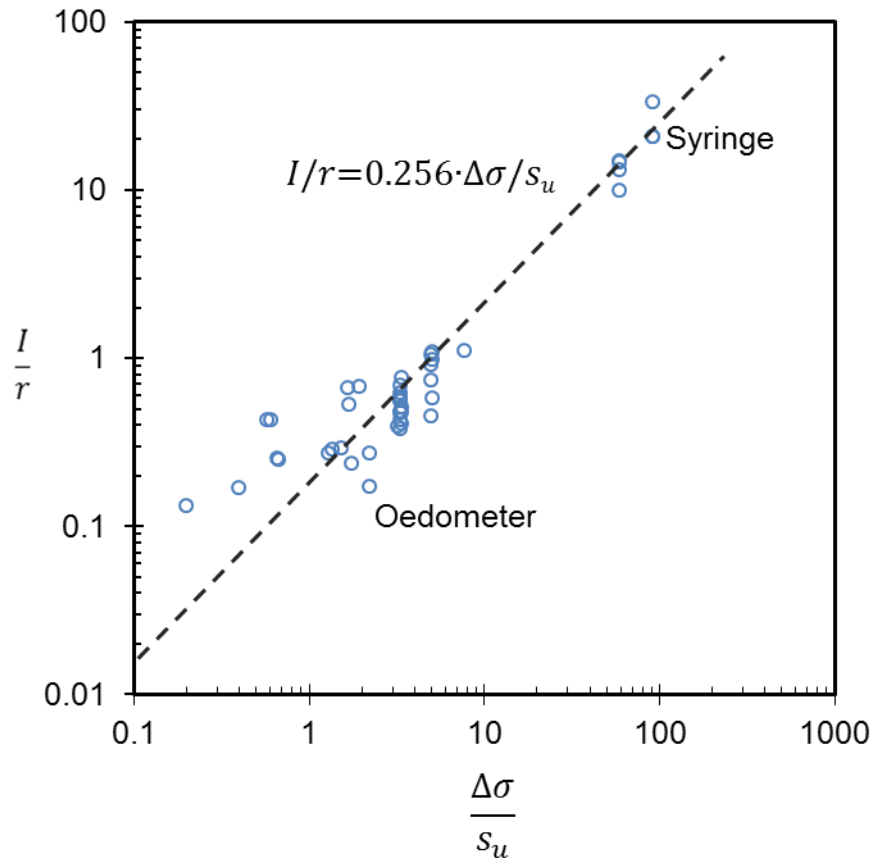
Figure 12. Dimensionless plot for the results of the syringe and the oedometer (with Ottawa 10/20 and 3mm-GB) with the fitted linear trend.

### 2.5.2 Prediction Models

This section presents three different approaches to develop predictive models that act as an upper bound estimation of the invasion length. The force equilibrium method underlies all models. We assumed that: (1) undrained conditions prevail as the soil is sheared into the pores of the granular packing, (2) no slippage takes place at the soil-particle interface which implies that the failure occurs within the soil, and (3) the clay behaves as a rigid-plastic material which implies that all measured displacements are due to soil invasion into the granular packing and not due to strains in the clay. Additional description follows:

*Model 1*: A group of tubes replaces the granular packing while the porosity of

28

the tube structure equates the estimated porosity of the granular packing. The cross-section of the pores is square in shape with a side length of $w$. Figure 13a depicts the geometry of the tubes and includes some important geometric parameters. The summation of forces along the horizontal direction equals zero when the invasion stops and results in:

$$n\Delta\sigma W^2 - s_u \times 4wNI = 0 \tag{12}$$

The multiplication of the driving force by the porosity accounts for the portion of stress resisted by the soil skeleton (tube walls in this case) and does not contribute to the invasion. The rearrangement of the equation to the dimensionless form results in:

$$\frac{I}{r} = \frac{1}{2\sqrt{2}} \cdot \frac{\Delta\sigma}{s_u} \tag{13}$$
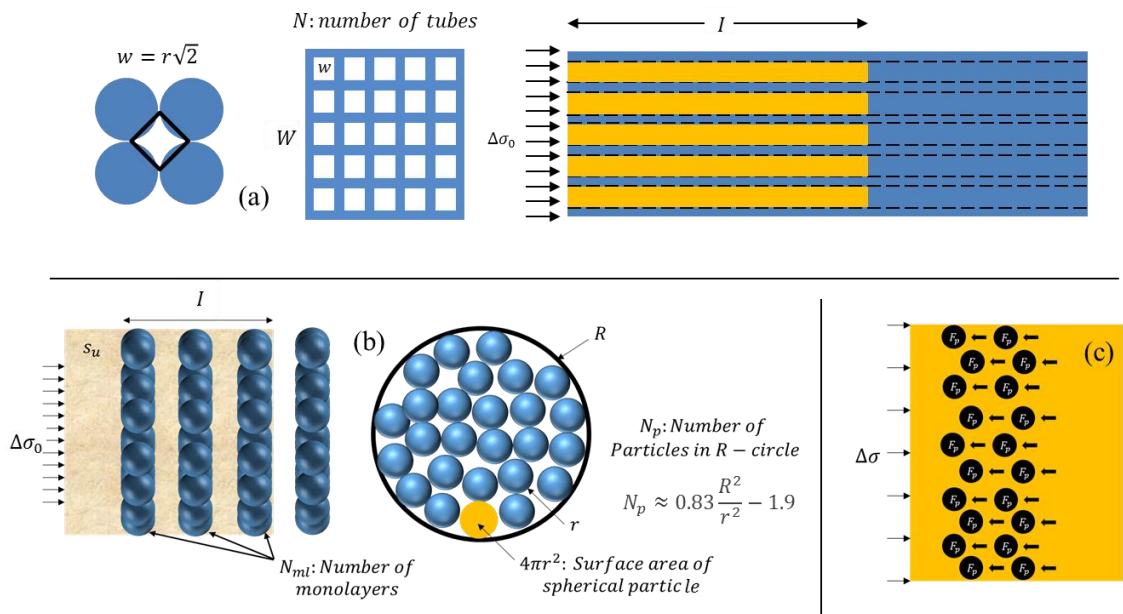


Figure 13. Illustrative plots for the three derived models: (a) square tubes approach: tube dimension, tube mesh: section and side view. (b) monolayers approach: side view and cross-section. (c) ball penetrometer approach: side view: driving and resisting forces.

*Model 2:* This model assumes a layered soil particle arrangement (with $N_p$ number of particles in each layer) that is perpendicular to the invasion length (Figure 13b). The invasion length is conservatively equal to the number of monolayers multiplied by the particle diameter. The shear area is the total surface area of the particles within the invasion zone. Balancing system forces will result in:

$$n\Delta\sigma A - s_u \times 4\pi r^2 \cdot N_p \cdot N_{ml} = 0 \tag{14}$$

The replacement of $N_{ml}$ by $I/2r$ and the rearrangement of equation 14 into the dimensionless form leads to:

$$\frac{I}{r} = \frac{n}{2} \cdot \frac{\pi \cdot R^2}{\pi \cdot r^2 \cdot N_p} \cdot \frac{\Delta\sigma}{s_u} \tag{15}$$

Since $\pi \cdot R^2$ equals the total cross-sectional area and $\pi \cdot r^2 \cdot N_p$ equals the area of the solids, equation 15 becomes:

$$\frac{I}{r} = \frac{n}{2} \cdot \frac{1}{1-n} \cdot \frac{\Delta\sigma}{s_u} \tag{16}$$

*Model 3*: The ball penetrometer is a field tool used to estimate the soil shear strength. This technique involves driving a spherical shaped metallic head into the soil layer while monitoring the resistance force. A wedge similar to a footing failure forms below the penetrometer. The undrained shear strength of the clay relates to the measured force ($F_p$) using the following relation:

$$s_u = \frac{F_p}{BCF \cdot A_c} \tag{17}$$

Where *BCF* is the bearing capacity factor and $A_c$ is half the surface area of the ball. The analogy between a ball penetrometer and a soil particle inserted into a clay layer can be a starting point for modelling the invasion of clay into sands. If the undrained shear strength of the clay is known, the driving force can be back-calculated

for one particle. The total resistance is the summation of all the particle resistance forces

estimated using equation 17 given the total number of particles within the invasion zone

(Figure 13c). This statement neglects the effect of the overlapping of the formed wedges

with each other and adjacent particles and can lead to conservative estimates of the

invasion lengths. The driving force equalizes the resisting forces and thus results in:

$$\Delta\sigma\pi R^2 - N_p \cdot N_{ml} \cdot BCF \cdot s_u \cdot 2\pi r^2 = 0 \tag{18}$$

$$\frac{I}{r} = \frac{1}{BCF \cdot (1-n)} \cdot \frac{\Delta\sigma}{s_u} \tag{19}$$

The $BCF$ for shallow foundation on cohesive soil is 5.14. This factor

approaches 9 for deep foundations. Particle resistance in the shallower zones of the

invasion length should theoretically better fit the 5.14 bearing capacity factor while

particles in deeper zones have higher resistance estimated using a higher bearing

capacity factor (closer to 9). Two separate models adopt these extremes.

Figure 14 and Figure 15 show the experimental and predicted results for the five

developed models. Unsurprisingly all models overestimate the invasion length

compared to the laboratory measurements. This reflects the underlying assumptions

adopted in the model derivations. In addition to these assumptions, none of these

models explicitly account for the effect of the tortuous path that the clay experienced.

Ball penetrometer models showed closer predictions to the laboratory measurements.

This model with a bearing capacity factor of 9 appeared to overestimate the small and

underestimate the larger invasions and suggests that the bearing capacity factor should

vary along the invasion length. This finding indicates that there is a need for future

research to more accurately define the trend of the bearing capacity factor.
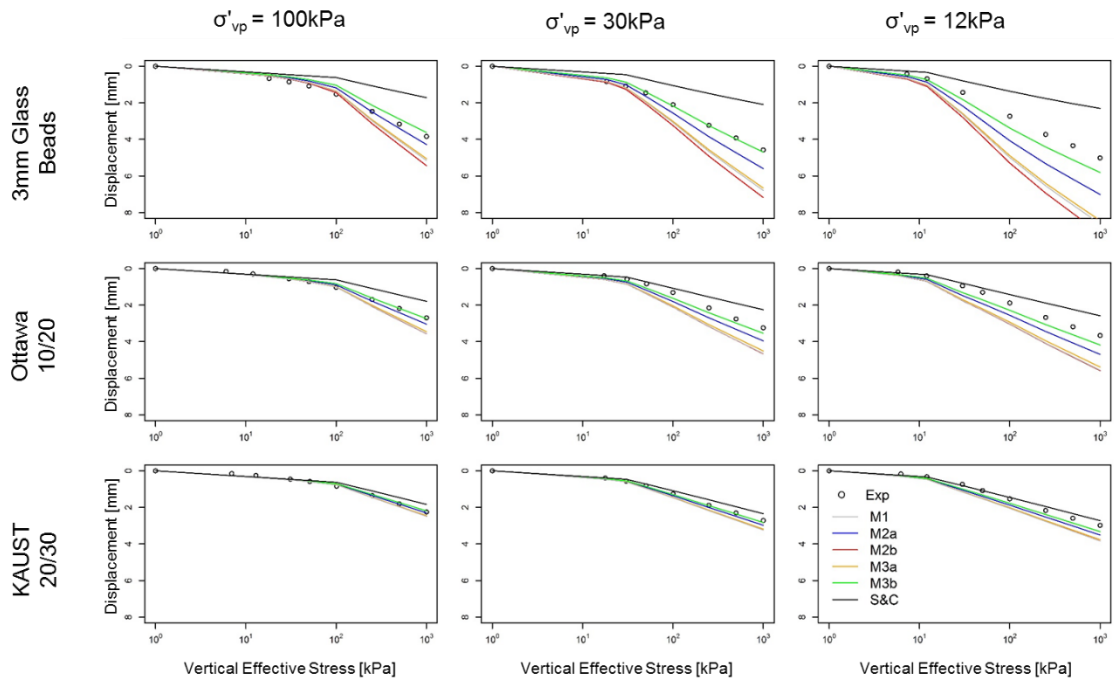
Figure 14. Measured and predicted shortening of the composite specimens versus vertical effective stress – Tests in oedometer cells . The 9 cases correspond to clays pre-consolidated to three effective stress levels σ'$_{vp}$= 12 kPa, 30 kPa and 100 kPa, and three differ
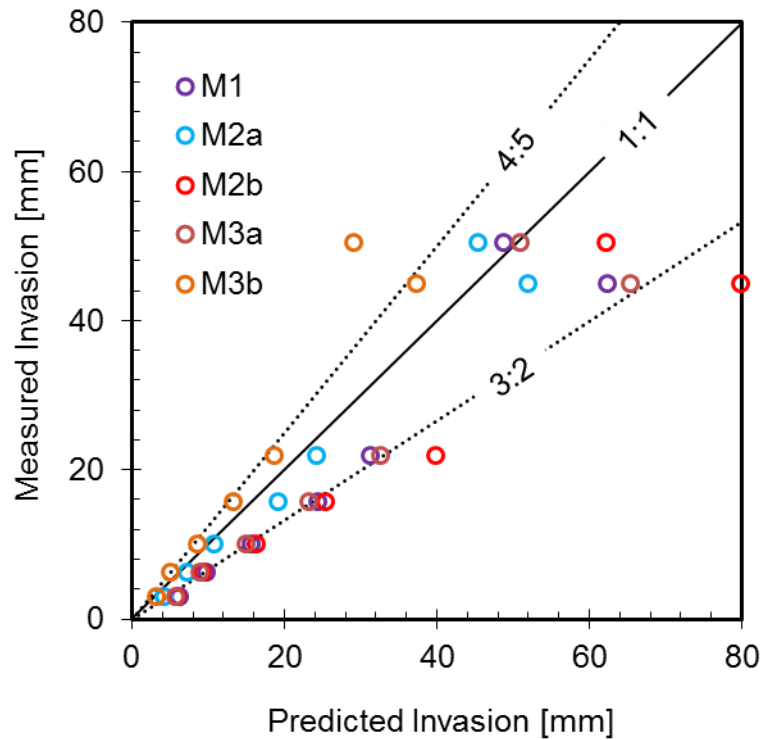


Figure 15. Measured and predicted invasion length for the 7 syringe tests. M1: equation 13, M2a: equation 15, M2b: equation 16, M3a and M3b: equation 19 with BCF of 5.14 and 9 respectively.

## 2.6    Engineering Implications

Various engineering applications include interfaces between clays and coarser porous material. Stone columns installed in clayey soil, drilling mud in wellbores, and gravel blankets over clayey soil are examples where a potential invasion can take place. The models derived in this paper are useful for estimates of the invasion magnitudes on the system response.

### 2.6.1    Stone Columns in Clay

Vibroflotation and tamping are major methods used to install stone columns. In vibroflotation, a motor with an eccentric weight contained in a torpedo-shaped body is inserted into the soil layer with the aid of jetted air or water. The vibratory action of the vibrofloat, its weight, and the tamping induce radial stresses which push the gravel into the surrounding clay. The models presented in this paper are useful for estimates of the invasion length that takes place at the interface between the gravel and clay. Knowledge of the induced stress, gravel particle size, and the undrained shear strength of the clay, can provide predictions of the magnitude of invasion. However, these models were developed for static loading conditions and thus should be used with caution for cyclic loading applications. The injected water during the column installation alters the water content of the clay and resulting in lower shear strengths.

Furthermore, the invasion of the clay into the gravel can affect the bearing capacity of the improved ground if the induced structural loads exceeds the locked in stresses at the clay/gravel interface induced by the column installation process.

### 2.6.2    Drilling Mud in Wellbores

During the wellbore drilling process, drilling muds act as a cleaning agent for cuttings, a lubricant between the drilling pipe and wellbore, and a coolant for drilling

bits. Although the pores of the formation could be very small, the high injection pressures could lead to the invasion of the drilling mud into the pores of the formation (Liu & Santamarina, 2018). Quantifying the extent of this invasion could affect the predictions of mudcake thickness and changes in the permeability of the formation.

### 2.6.3 *Gravel Blanket Overlying a Clay Layer*

In stone-column-improved clayey sites, engineers place a gravel blanket between the raft and supporting soil to aid in drainage. The settlement calculations under service loads neglect the contribution of the invasion. However, rough calculations based on the developed models for typical loading scenarios ($\Delta\sigma = 100kPa, r = 10mm, s_u = 30kPa, n = 0.5$) show significant contributions ranging from 3 to 10mm given the fact that the allowable settlement is 25mm.

## 2.7 Conclusions

The invasion of clays into coarser granular packing is an important phenomenon that engineers encounter in different field applications. This phenomenon could have a major effect on the overall response of engineering mechanisms. The experimental program presented in this manuscript investigated the invasion of clay with water contents which range from one to half of the liquid limit into granular packings with different grain sizes. The magnitude of the invasion is proportional to the stress increment and particle size and is inversely proportional to the undrained shear strength of the invading clay. The developed model results in acceptable estimations of the invasion with low uncertainty for a wide range of four logarithmic intervals of invasion thickness normalized by the particle diameter and stress increment to the undrained shear strength ratio.

# CHAPTER 3
# CKC TRIAXIAL MACHINE AND UPGRADES

## 3.1    Description

The CKC triaxial machine developed by Clarence Chan/UC Berkeley was used to perform the cyclic tests. The basic machine assembly includes five sensors: a linear variable differential transducer (LVDT) to measure the vertical displacement of the tested specimen, an external load cell to measure the deviatoric stress the specimen is subjected to, and three differential pressure sensors. The first sensor measures the differential pressure between the cell (air) and the atmospheric pressure (air) resulting in the net applied cell pressure. The second differential sensor is connected to the cell pressure from one side (air) and to the back pressure (water) from the other side resulting in the effective stress sensed by the specimen. The third differential sensor measures the column height connected to the pore water of the specimen indicating the change in the volume of saturated specimens. The third sensor obviously has a smaller range of pressures than the other two. Figure 16 shows a schematic plot of the triaxial setup with the main mechanical connections.

## 3.2    Upgrades

Given the composite nature of the specimens tested in this research effort (clay matrix with granular columnar inclusions) two major modifications/upgrade were introduced to the existing CKC machine to best collect/leverage the data obtained from each test. First, a new top cap was designed to have one drainage path directed to the center of the specimen (location of the sand column) and another drainage path directed towards the peripheral zone (clay around the sand column). These two paths, which do not intersect will theoretically allow the separation between the pore water pressures

generated within the sand and the clay. The second modification is the inclusion of an additional differential pressure sensor. This sensor is connected to the cell pressure (air) from one side and the drainage line going into the sand column from the other side. This additional sensor provides the capability of measuring the generated pore pressures within the sand column separately from the pore water pressure generated within the clay (using the built-in sensor). Figure 17 shows the schematic plot of the updated triaxial system.
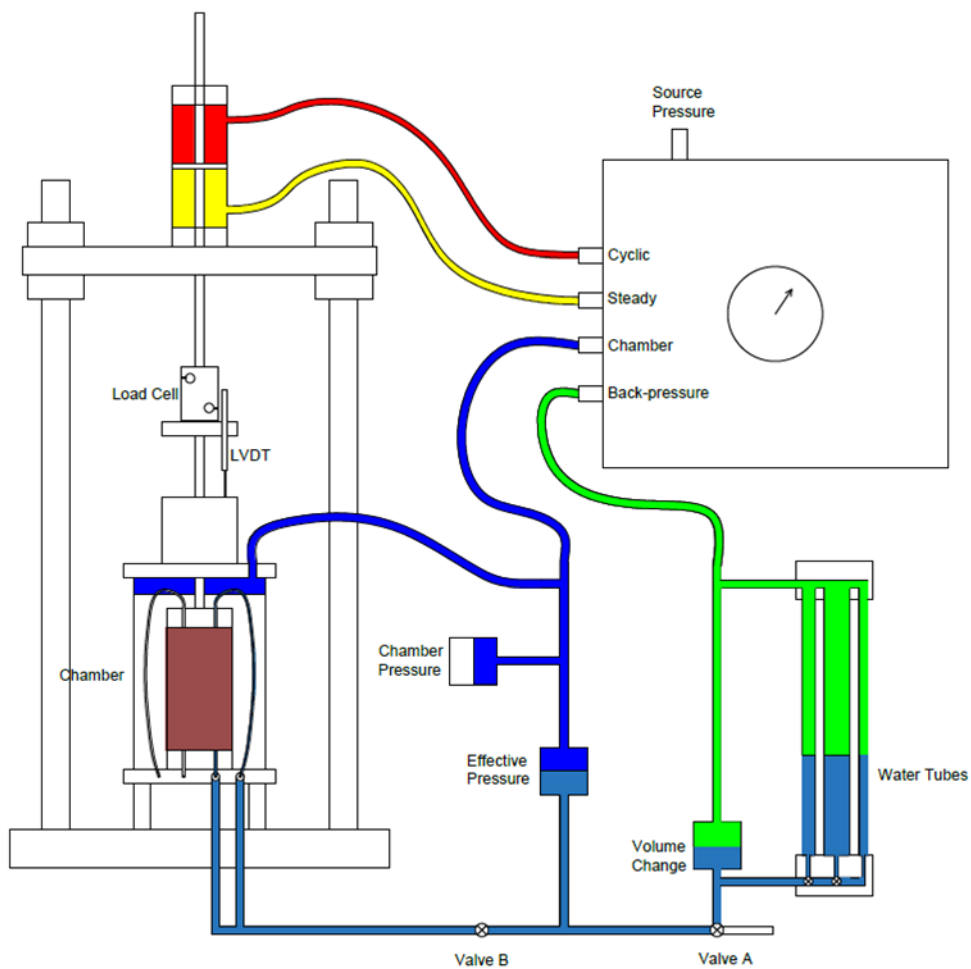


Figure 16. Schematic layout of the Standard CKC triaxial machine
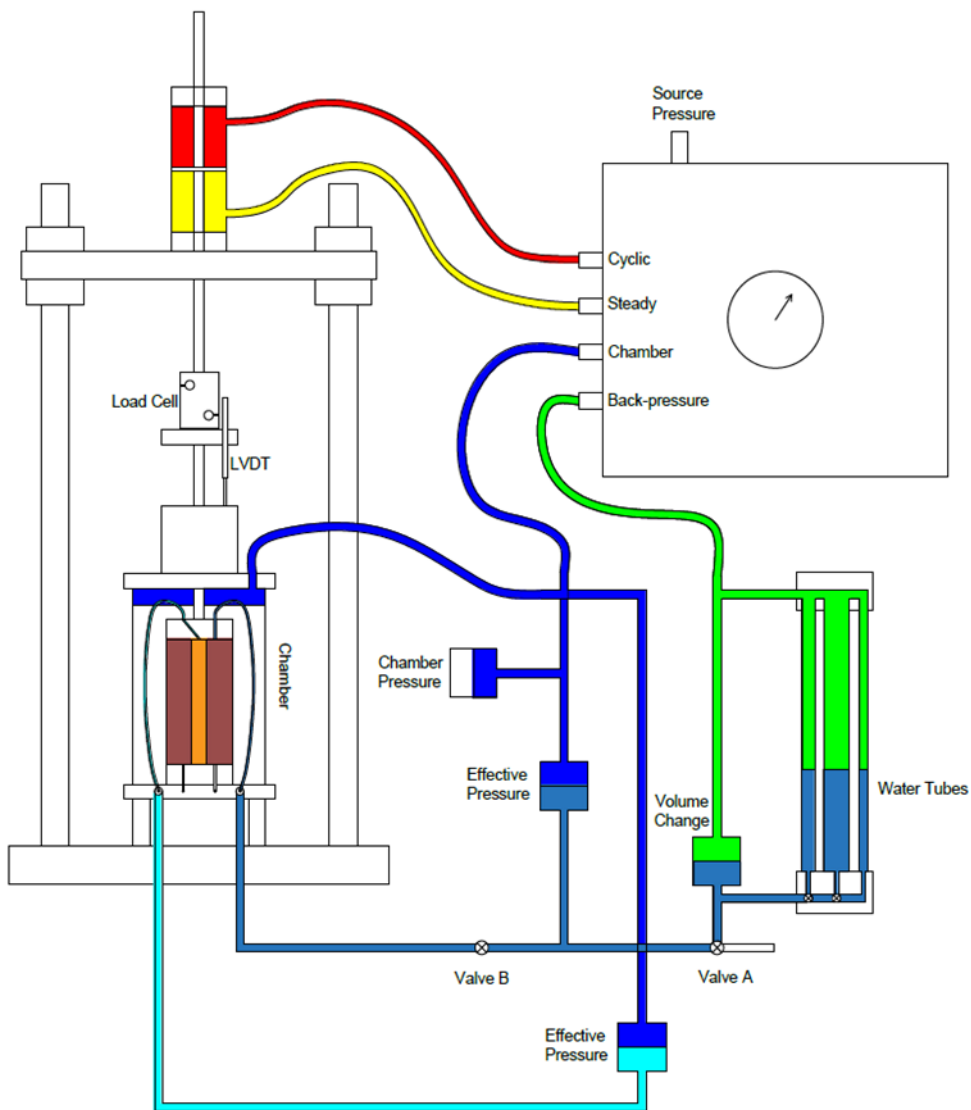
Figure 17. Schematic layout of the updated CKC triaixal machine showing the additonal pore water pressure differential sensor and the modifed cap

The additional differential pore water pressure requires an AC input excitation (5V at 3-5 kHz) and results in an AC output in the range of mV with an equivalent frequency equal to that of the excitation voltage (3-5 kHz). The original data acquisition system of the CKC triaxial machine only accepts DC output from the sensors. Thus the additional sensor required a special electric circuit in order to read its output using the CKC data acquisition system. Figure 18 shows the circuit developed to amplify the AC

output voltage of the sensor and convert it into a DC signal.
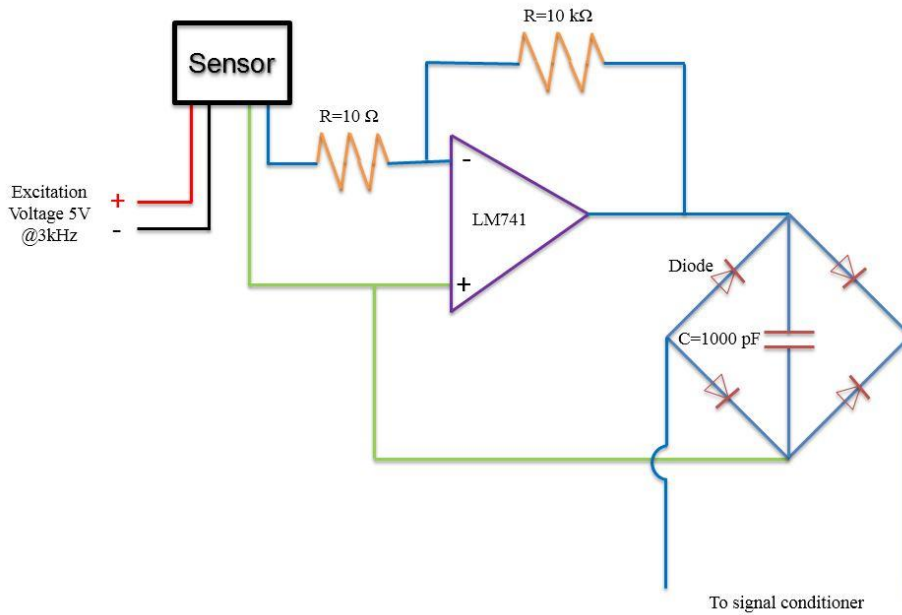


Figure 18. The electric circuit developed to amplify and transform AC sensor signal to a DC output

Additionally, the lower cap was equipped with a miniature load cell located under the clay zone to measure the stress experienced by the clay matrix. This arrangement, if successful, should give an estimate of the stress concentration factor and its evolution with the number of cycles. Unfortunately, we found that this sensor was not successful in reading reliable output because it was manufactured for applications where the interface is a liquid and not a soil, thus this feature was abandoned for the purpose of this testing program. Finally, two bender elements were installed in the top and bottom caps to measure the shear wave velocity through the sand column. The shear wave velocity measurements need to be performed at stable stress states, which is not possible during the cycled loading stages and measurements are restricted to states prior and subsequent to the cycled loading. Figure 19 shows the bottom cap with the location of the miniature load cell and the bender element.
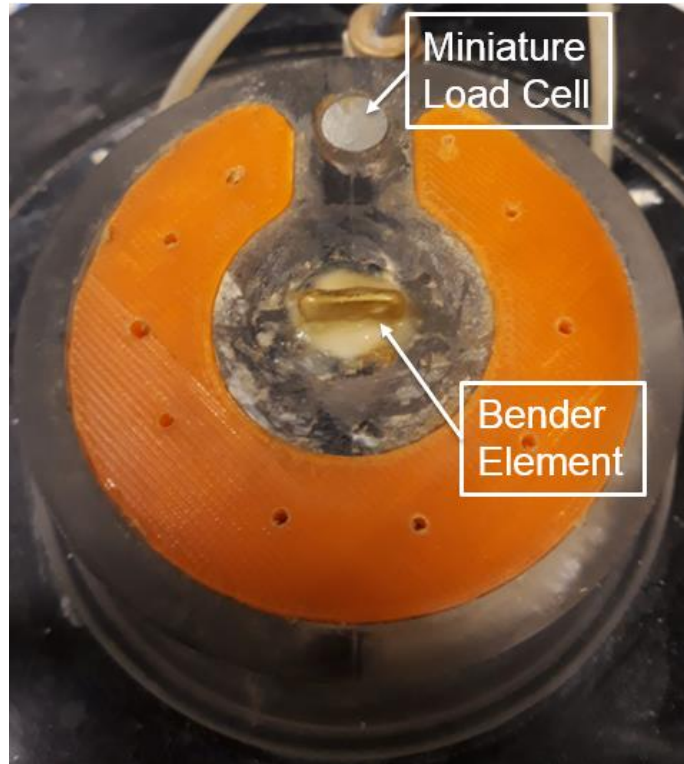
Figure 19. Bottom cap with the installed bender element and miniature load cell under the matrix clay zone.

# Chapter 4

# EFFECT OF COLUMNAR SAND INCLUSIONS ON THE CYCLIC RESISTANCE OF CLAY

## 4.1 Isotropically Consolidated Stress State

### 4.1.1 Abstract

Extensive research efforts aimed at studying the static performance of stone columns have proven that this improvement technique results in a significant increase in bearing capacity and a decrease in total and differential settlements. However, in some applications/situations repeated loading/unloading cycles could be the dominant form of solicitation and may thus govern actual behavior and associated design considerations. Earthquakes, wind, waves, filling and emptying of water/oil tanks and/or silos, and vibrating machines induce repeated loading patterns on the soil, at various levels of amplitudes and with different frequencies. Given that dense sands tend to dilate and generate negative pore pressures when sheared while normally consolidated clays generate positive pore water pressures, an interchange of pore water pressure takes place between the sand column and the surrounding clay. In order to investigate the interchange of pore water pressure between the sand and the clay, small scale cyclic triaxial tests are performed on cylindrical natural clay specimens reinforced with a central sand column. The top cap of the triaxial testing setup is modified to allow for the monitoring the evolution of the pore water pressure in the sand and the clay separately. The effect of varying the loading frequency is investigated as it influences the rate of pore pressure generation and dissipation.

### 4.1.2    - Introduction

4.1.2.1    <u>Behavior of clays under cyclic loading</u>

Significant research efforts have been directed at investigating the response of clays subjected to cycled/repeated loading patterns. The main areas of exploration were related to (1) the effect of clay plasticity and overconsolidation ratio on modulus degradation, damping and cyclic strength, (2) pore water pressure build-up due to cyclic loading, (3) loading rate and initial stress effects, (4) threshold cyclic shear stresses and (5) post-cyclic strength.

(Andersen, 1980; Procter & Khaffaf, 1984) investigated the effect of the overconsolidation ratio on the cyclic strength of undisturbed clays. They concluded that overconsolidated clays required fewer load cycles to reach failure when compared to normally consolidated clays. (A. M. Ansal & Erken, 1989; Procter & Khaffaf, 1984) showed that as the frequency of cyclic loading increases, the cyclic strength of the clay increases. (A. M. Ansal & Erken, 1989) studied the presence of a threshold cyclic shear stress below which no excess pore water pressure is generated. (Hyodo, Sugiyama, & Yamamoto, 1996) investigated the effect of initial shear stresses on the response of highly plastic clay. They found that the cyclic strength decreases as the initial shear stress increased. (Hanna & Javed, 2008) showed that partially drained samples required larger number of cycles to failure when compared to undrained conditions. (J. Wang, Cai, & Yang, 2013) performed monotonic and cyclic triaxial tests on clay soil from Zigingang (PL=26, LL=53, PI=26.5) in an attempt to solve the contradiction present in the literature regarding the effect of initial shear (drained) on the response of clays. Based on different initial shear stresses adopted in an experimental program, the authors noted that when the initial shear stress was smaller than the cyclic stress, S-shaped

hysteretic loops appear secant modulus degrades with cycles while when whereas when initial shear stress is higher than the cyclic stress, no S-shaped loops were noticed and little to negligible modulus degradation was noticed. Results from monotonic tests with initial shear stress showed that as the initial shear stress increases, the soil will have lower additional deviatoric stress but higher total deviatoric stress. The authors stated that in the analysis of slope problems, ignoring initial driving shear stress results in non-conservative estimate of strengths. More recently, (Beroya, Aydin, & Katzenbach, 2009) investigated the influence of clay mineral type on the cyclic resistance. They observed that for the same plasticity index (PI), Montmorillonite had the largest strength when compared to Illite and Kaolinite. A more extensive literature about the response of clays to cyclic loading can be found in (Nieto-Leal & Kaliakin, 2013).

Major concepts/observations related to the behavior of clay under cyclic loading are listed below:

1. For one-directional cyclic loading, a threshold cyclic shear stress exists, below which limited excess pore water pressure, limited strain development, and the post-cyclic strength is equal to the monotonic static undrained shear strength (around 2/3 static strength).

2. Two-directional cyclic loading is more detrimental on the clay behavior and leads to higher pore pressures and larger strains for the same number of cycles, when compared with one-directional loading.

3. Cyclic loading on normally consolidated clay samples leads to an apparent overconsolidated behavior in the post-cyclic loading.

4. Samples with higher overconsolidation ratio have higher cyclic strengths given that they have the same initial stress state (same confinement).

5. Highly overconsolidated clay samples produce less positive pore water pressures under cyclic loading when compared to normally consolidated clay samples.

6. Highly plastic clays develop lower strains under cyclic loading as compared with clays having low plasticity. Consequently, cyclic strength increases with increasing plasticity.

7. The cyclic strength of clays decreases with increasing initial drained shear stress.

8. Lower frequency of loading (slow loading rate) results in lower cyclic strength.

9. Cyclic strength deterioration is best explained as a strain-dependent phenomenon.

10. Flat-topped loading cycles lead to lowest cyclic strength.

11. Increasing clay content up to 15-20 % in a sand will increase its cyclic strength.

## 4.1.2.2 <u>Stone columns and seismic loading</u>

The use of granular piles/inclusions as part of an overall soil improvement scheme has been adopted in practice to mitigate the potential failures due to seismic excitations. The effectiveness of granular/stone columns has been the subject of substantial research. Laboratorial experiments, analytical models, and finite element approaches were utilized in predicting the load redistribution due the presence of

43

granular inclusions.

(J. Baez & Martin, 1993) assumed shear strain compatibility between the native soil and the stone column and developed a procedure to quantify the improvement taking into consideration the densification, drainage and stress redistribution effects. A stress reduction factor was suggested/defined to estimate the decrease in the stress on the soil for a reinforced site as compared to the original/reference unreinforced site:

$$K_G = \frac{1}{1 + a_r(G_{sc}/G_s - 1)} \qquad (20)$$

(Goughnour & Pestana, 1998) suggested that stress reduction is over-estimated by the available design approaches (J. Baez & Martin, 1993; S. J. Baez, 1997). This over-estimation emerges from the fact that the stone column deforms in flexure and shear rather than simply in pure shear as assumed in the approach adopted by (J. Baez & Martin, 1993; S. J. Baez, 1997) as shown in Figure 20.

In their simplified approach, the authors used basic elasticity theory to derive an equivalent shear modulus which accounts for flexural bending of the column.

$$G_{sc_{eq}} = 6.4 \times G_{sc} \times \left(\frac{d_{sc}}{\lambda}\right)^2 \qquad (21)$$

Where, $G_{sc}$ is the shear modulus of the stone column, $d_{sc}$ is the column diameter, and $\lambda$ is the wavelength of the shear wave in the column. This equivalent shear modulus was found to be much less than the shear modulus of the surrounding soil for typical diameters (0.6m ~ 1.2m) and wavelengths (100m ~ 1000m) available in practice. This means that the soil will be subjected to higher shear stresses when the site is reinforced with stone columns compared to the unreinforced site. However, the authors clarified that this counter-intuitive result is due to the neglecting of the interface shear stresses

between the soil and the column. They speculated that the soil should be subjected to comparable magnitudes of stresses in either case (reinforced or non-reinforced).
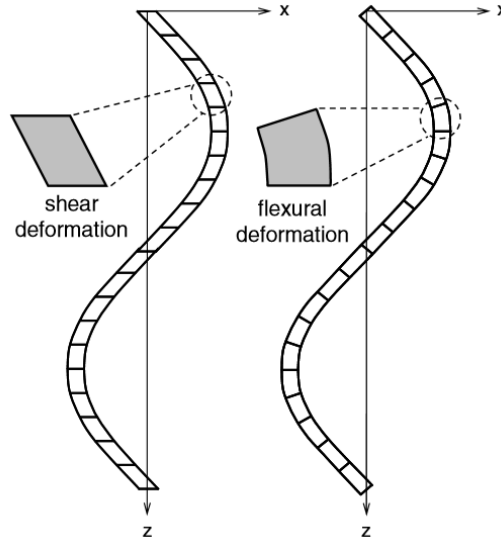


Figure 20. Shear vs. flexural deformation of a slender element

The authors modified the reduction factor proposed by (J. Baez & Martin, 1993) to include the effect of the variation of vertical effective stress in the soil due to the installation of the column.

$$K_G = \frac{1 + A_r(n-1)}{1 + A_r(\frac{G_{sc}}{G_s} - 1)} \tag{22}$$

Where, $n$ is the ratio of vertical effective stress in the column to that in the soil, $A_r$ is the area replacement ratio (decimal), and $G_s$ is the shear modulus of the soil. (Olgun & Martin, 2008) investigated available procedures for the design of stiff columnar reinforcements that assume shear strain compatibility using 3-D dynamic finite element modeling. Their results showed that the mode of deformation of the column has a significant influence on the degree of stress reduction obtained. Columns were found to deform in both flexure and shear (Figure 21). The greater the flexural

deformation, the less reduction in shear stress carried by the soil is achieved. Linear elastic models for soil and column were assumed sufficient to capture the effect of column mode of deformation. Although results show that the shear deformation contribution increases with depth, the authors state that even small values of flexural deformations have significant effects in decreasing the stress carried by the columns. Based on a parametric investigation on the effect of the ratio of column to soil stiffness, it was found that the stiffer the column, the more it will behave as a flexural beam.
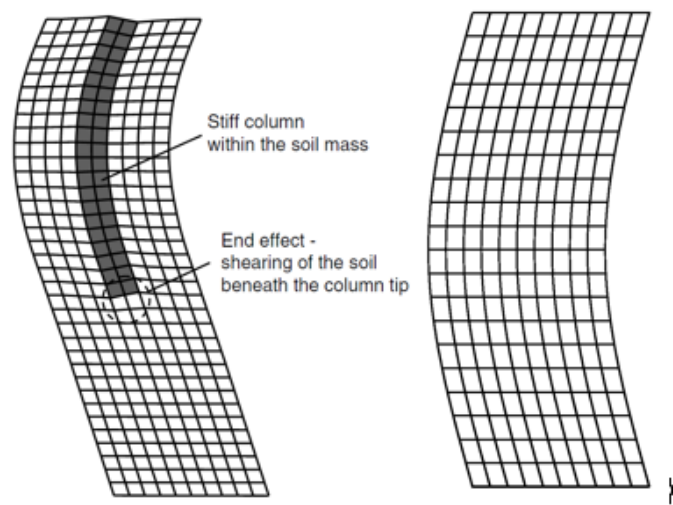


Figure 21. Column deforming in flexure and soil deforming in shear ((Olgun & Martin, 2008)

It was noticed that the column has a more prevalent shear deformation mode as the confinement increases. Therefore, it can be speculated that the presence of a surcharge load (structure) supported by the reinforced ground will diminish the flexural deformation that is dominant at shallow depths. However, more research is required to confirm this behavior.

(Engelhardt & Golding, 1975) performed large-scale vertical and shear tests on stone columns for the construction of a sewage treatment plant supported on clays with

interbedded lenses of sand. It was found that vibro-replacement is a useful technique in densifying sand lenses and that the shear strength of the combined column and soil is significantly higher than in-situ soils alone.

(Rayamajhi et al., 2012; Rayamajhi et al., 2013; Rayamajhi, 2016a; Rayamajhi, 2016b) performed an extensive numerical investigation to study the effect of the presence of stone/cemented columns in liquefiable soil in a unit cell modeling approach. 3-D Linear elastic model pseudo-static and dynamic excitations were first used to investigate the shear stress distribution mechanism and the reinforcing effect. The researchers reported that the assumption of compatible shear strains lead to an overestimation in the shear stress reduction. Parametric studies were performed for different area replacement ratios, relative stiffnesses, and dynamic loadings. An empirically-modified equation was proposed that accounts to the non-compatible shear strains in the soil-column system.

$$R_{rd} = \frac{1}{\frac{G_{sc}}{G_s}\left[A_r\gamma_r + \frac{G_s}{G_{sc}}(1 - A_r)\right]}$$

(23)

Where, $G_r$ is the shear moduli ratio of the column and soil and $\gamma_r$ is the ratio of shear strains in the column to that in the soil which was found to be a function of shear moduli ratio and defined by:

$$\gamma_r = 1.04\left(\frac{G_{sc}}{G_s}\right)^{-0.65} - 0.04$$

(24)

The $R_{rd}$ is equivalent to the $K_G$ if the convoluted peak ground accelerations were equal for the improved and unimproved sites. The authors extended their work by performing non-linear 3-D finite element analyses on dry and saturated soil models. The results obtained were consistent with those from linear elastic analyses. In the dry model, ground amplifications were noticed, while in the saturated model, less

amplification occurred since liquefaction developed in the natural soil. More

amplification was noticed in the improved model as compared to the unimproved one.

The stress reduction factor was found to decrease with increasing area replacement

ratio and ratio of shear moduli. Moreover, the stress reduction factor was not

significantly affected by applied surface pressure, column slenderness, and in-situ soil

relative density for typical area replacement ratios and ratio of moduli.

Finally, the effects of increasing various contributing parameters (area replacement

ratio, ratio of shear moduli, slope angle, column diameter) is summarized in Table 3

Table 3. Influence of design parameters on lateral displacement

| Parameter | lateral displacement |
|---|---|
| Area Replacement Ratio | Decreases |
| Shear Modulus Ratio | Insensitive |
| Slope Angle | Increases |
| Column Diameter | Decrease |

(Adalier, Elgamal, Meneses, & Baez, 2003) conducted a centrifuge testing program to

study the effectiveness of stone columns in mitigating liquefaction in non-plastic silty

deposits. Four models were shaken and are as follows (dimensions are for the

equivalent prototype):

1. Benchmark model of a 7.8m thick (prototype) placed in a laminar box was

   spun at 50g.

2. Reinforced model of a 7.8m thick prototype with 45 stone columns ($a_r$=20%) in

   the laminar box was spun at 50g. Stone columns were encased with latex

   membranes to eliminate/cancel the effect of drainage.

3. 10m thick silty layer with a rigid surcharge covering the central zone (144kPa)

placed in a rigid-wall box and spun at 63g.

4. Reinforced 10m thick silty layer with 36 stone columns ($a_r$=36%) placed in the rigid-wall box and spun at 63g.

The stone columns (Nevada No. 120) were 600 times more permeable than the adjacent matrix silty soil (100% silt size/Sil-Co-Sil 120) and had shear modulus that is 5 to 6 times higher than that of the silt. Stone columns with relative densities of 65% to 70% were prepared. Models 1 and 2 were shaken twice each with 20 cycles of increasing amplitude (maximum= 0.3g) at a frequency of 1.8Hz. While models 3 and 4 were shaken three times with a uniform harmonic motion at a frequency of 1Hz. The first loading/shake consisted of 10 cycles at an amplitude of 0.08g and second and third "shakes" were 30 cycles each, with peak acceleration of 0.18 and 0.2g, respectively.

When comparing models 1 and 2, it was noticed that the decay of accelerations in model 1 was faster than that in model 2. Generated pore water pressures within the top half of both models were comparable however in the bottom half it was slower in model 2. Twelve cycles of loading lead to liquefaction in model 1 while after 20 cycles, the upper half of model 2 liquefied. This was attributed to the low effective stress at shallow depths.

In model 3 and during shakes 2 and 3, asymmetric accelerations were noticed at locations near the edge of the surcharge which is an indication of lateral deformation. Negative pore water pressures were generated at the central zone (under the surcharge) while positive pore water pressures were noticed away. Large settlements took place in this model. These settlements were attributed to the migration of soil from the central zone to the free field. The installation of stone columns (model 4) reduced settlement into half, lead to reduced negative pore pressures in the central zone, and lowered the

free field positive pore water pressures. It is worthy to note that the presence of stone columns preserved the stiffness of the layer and lead to amplification of the transferred of acceleration from bottom to top.

(Adalier & Elgamal, 2004) presented a state of art summary for stone column improvement techniques as liquefaction counter-measures. The authors listed methods for the verification of improvement levels during and after the construction of the columns. These methods include: monitoring of the surface ground movement, volume of backfill, required energy and other typical in situ tests such as SPT, CPT, pressure-meter, dilatometer, and shear wave velocity tests. The authors also pointed to the difficulty of quantifying the permeability of installed columns. This is because of the mixing that takes place between column and native soil material. Different studies shows that around 20% of the material within the final column geometry are actually from in situ soils. Case studies reported that including stone columns as mitigation measures was effective and resulted in little to no damage during seismic events.

(Rollins, Quimby, Johnson, & Price, 2009) compared the performance of sites with variable fines and clay contents improved with stone columns to other sites improved with both stone columns and wick drains. The soil profile under consideration consisted of two main layers: An upper silty sand layer (0 – 4m) with average fines content of 26% and clay content of 6% and a lower sandy silt layer (6 – 12m) with average fines and clay contents of 45% and 14%, respectively. An intermediate layer (4 – 6m) lies between the above layers and consists mainly of silty sand and sandy silt. Pre-treatment SPT measurements ranged from 5 to 40 blow counts, while the targeted SPT to prevent liquefaction was specified as 23. The site was divided into four quadrants where 2 of them were reinforced only with stone columns while the

remaining 2 were reinforced with stones columns and wick drains. Post-treatment tests were performed after different intervals of time. The first tests (1 -3days) showed that all quadrants had a post-treatment SPT of 23 and above except for layers with lower permeability (high fines content) in the quadrants where no wick drains where installed. 2 weeks later, remarkable increases in the SPT was noticed in quadrants with wick drains while little increase took place in other quadrants. The authors pointed at the importance of wick drains since improvement was found to be time-dependent in soils containing fines content. The results from a similar research effort/program were presented in Rollins et al. (2006).

(Okamura, Ishihara, & Oshita, 2003) investigated the use of sand compaction piles (vibratory and non-vibratory) in densifying sandy profiles in 3 sites in Japan (Niigata, Izumo, and Yasugi) which classified as liquefiable. Comparing pre- and post-treatment SPT and RRS (rotary ram sounding) tests, post-treatment tests showed increased resistance is attained along the depth of the profile except the upper 3-4 meters and the improvement between columns was not found to be correlated with distance. The authors also pointed to the importance of accurately estimating the degree of saturation in the field in order to have a reliable comparison with lab tests.

(Rudolph, Serna, & Farrell, 2011) reported a case study of a site in California that was reinforced with rammed aggregate piers. The densification effect was evaluated with pre- and post-treatment CPT. Improvement was maximum for layers with low fines content.

(Kumar, 2001) presented the results of improving a site using deep dynamic compaction aided by the presence of stone columns. It was noticed that the upper 2 meters did not show any improvement.

(Bray, Sancio, Riemer, & Durgunoglu, 2004) assessed the reliability of the Chinese criteria for determining the susceptibility of fine-grained soils to liquefaction using cyclic triaxial tests on undisturbed samples from Adapazari, Turkey. The authors noted that the soil in this area do not meet the Chinese criteria as being liquefiable, though, liquefaction was observed during the Kokaeli earthquake of 1999. The authors investigated the effects of soil plasticity and initial confining pressure. They found that the cyclic resistance increases as the soil plasticity increases and the confining pressure decreases.

More recently, (Ashour, 2016) studied the effect of loading frequency and cyclic stress on soft clays reinforced with stone columns for railway track foundation applications. The author reported that the inclusion of stone columns at an area replacement ratio of 7% only slightly increased the cyclic resistance of the composite mass, but had the positive effect of reducing permanent strains.

### 4.1.2.3   Stone columns and consolidation

(Barron, 1900) presented a solution for radial and vertical flow for a consolidation problem in a site with drain wells. The author investigated the effects of well resistance and smear zone on the rate of consolidation. Both equal and free strain conditions were analyzed. Since the sought improvement aspect was only accelerating consolidation, wells were assumed to have a stiffness similar to that of the native soil, and small well diameters compared to stone column applications.

(Alamgir et al., 1996) proposed a theoretical approach to estimate distribution of shear and normal stresses and settlements in a soft ground reinforced with columnar inclusions. The authors assumed free strain conditions with elastic material properties.

52

Deformation compatibility was imposed on the deformations of the column and the soil at their interface and radial deformation was assumed to be negligible. A parametric study was conducted for different column spacing, moduli ratio, and Poisson's ratio. It was found that the stress concentration ratio starts from unity at the top of the unit cell and increases asymptotically with depth. It increases as spacing decreases and as the column to soil moduli ratio increases. Poisson's ratio had a negligible effect on the results. Finally the authors compared their solution to with finite element results which should acceptable comparability.

(Han & Ye, 2001) presented a solution for computing the rate of consolidation for stone column-reinforced saturated sites. The authors assumed free drainage in the columns (no well resistance), and that columns have higher stiffness than surrounding soil and considered only 1-dimensional deformation. Equal strain with no smear zone conditions were adopted in developing their approach. The main difference from Barron's approach is that the stresses are shared between the column and soil. Major findings were that the stress on the column increases while that on the soil decreases as consolidation progresses (stress concentration ratio increases with time). The difference between this solution and Barron's solution is the modified time factor which is a function of an adjusted coefficient of consolidation that accounts for load shearing between the soil and the column.

(Han & Ye, 2002) updated his previous work by including the effect of well resistance due the contamination of the column material with surrounding soil and the presence of a smear zone around the column as a product of the installation process. 1-dimensional deformation was again considered in their theoretical approach. Only radial flow was assumed in the analysis. Parametric study on influential design factors showed

that (1) as diameter ratio ($D_{unit\ cell}/D_{column}$) increases the rate of consolidation decreases, (2) as the permeability of the column or smeared zone decreases, the rate of consolidation decreases, (3) as the moduli ratio ($E_{column}/E_{soil}$) increases, consolidation rate increases, (4) as the thickness of smeared zone increases, the rate of consolidation decreases, and finally as the thickness of the soil layer increases, the rate of consolidation increases. The latter point is attributed to increased drainage path within the column since in the soil only radial drainage is assumed taking place. The authors plotted the change in total and effective stresses with time and showed that the relief of pore pressures is due to two mechanisms namely the dissipation of excess pore water pressure and stress reduction on the soil (redistribution of stresses between column and soil).

(Castro & Sagaseta, 2009) refined analytical models by taking into account the effect of radial deformation of the column on the radial consolidation of soil around stone columns incorporating elastic-elastic and elastic-elasto-plastic models for the soil and column respectively. The lateral deformation was neglected in previous approaches. However the authors didn't consider well resistance and smear zone in their analysis. Lower stress concentration factors were obtained particularly when adopting an elasto-plastic behavior of the column (1-5).

All the previously mentioned solutions are applicable to instantaneous loading that is kept constant during the consolidation stage. (G. Wang, 2009) presented an analytical solution for weak soils reinforced with stone columns subjected to time-dependent loading patterns. Solutions for typical loading such as step, ramp and periodic trapezoidal are obtained. Smear zone and well resistance are also included in the analysis.

(Xie, Lu, Hu, & Chen, 2009) presented a theoretical study for equal-strain consolidation of composite foundation taking into consideration the following initial conditions: (1) linear variation in the permeability of the surrounding soil in the radial direction instead of including a smeared zone, (2) change in total average stress with depth, and (3) load varying with time. Only vertical strains were considered in the analysis. Compared to (Han & Ye, 2002), this approach resulted in the fastest rate of consolidation.

In a following publication (Xie, Lu, & Liu, 2009) released the assumption of equal quantity of flow into the smeared zone and out of the column assuming that the net difference is attributed to the change in the volume of the column. The authors incorporated three patterns for the variation of permeability of the smeared zone. Results showed that incorporating a parabolic trend of variation of the permeability in the smeared zone results in the fastest rate of consolidation. Additionally, considering column volume change resulted in lower degree of consolidation though not significant.

### 4.1.3   Testing Program

The work presented in this Chapter stems from an extensive testing program conceived and designed to address areas of remaining uncertainty in reference to the response of native clayey ground reinforced within columnar granular inclusions, under varying conditions of initial placement and loading.

In a first phase, cyclic tests were performed separately on clay and sand specimens to characterize their respective response. The effects of the applied cyclic stress ratio and frequency of the loading cycles were studied. This initial sequence of tests was followed by a series of tests on sand-column-reinforced clay specimens. In

addition to the cyclic stress ratio and loading frequency, the effect of the area

replacement ratio, effective confining pressure, and drainage conditions were explored

in this second Phase of the program.

Table 4

 shows a comprehensive list of the tests performed. In this table, tests with area replace

ment ratio of 0 and 100% percent correspond to tests performed on homogeneous clay

and sand specimens, respectively.

Table 4. cyclic triaxial tests performed

| Test Number | $a_r$ [%] | CSR | T [sec] | Valves |
|---|---|---|---|---|
| 1 | 0 | 0.2 | 300 | C |
| 2 | 0 | 0.25 | 1 | C |
| 3 | 0 | 0.25 | 3 | C |
| 4 | 0 | 0.25 | 10 | C |
| 5 | 0 | 0.25 | 300 | C |
| 6 | 0 | 0.35 | 1 | C |
| 7 | 0 | 0.35 | 300 | C |
| 8 | 100 | 0.25 | 1 | C |
| 9 | 100 | 0.30 | 1 | C |
| 10 | 100 | 0.35 | 1 | C |
| 11 | 100 | 0.4 | 1 | O |
| 12 | 100 | 0.4 | 3 | O |
| 13 | 100 | 0.4 | 10 | O |
| 14 | 18 | 0.35 | 1 | C |
| 15 | 18 | 0.35 | 300 | C |
| 16 | 18 | 0.35 | 1 | O |
| 17 | 18 | 0.35 | 3 | O |
| 18 | 18 | 0.35 | 10 | O |
| 19 | 18 | 0.35 | 60 | O |
| 20 | 18 | 0.35 | 300 | O |
| 21 | 32 | 0.35 | 1 | C |
| 22 | 32 | 0.35 | 300 | C |
| 23 | 32 | 0.35 | 1 | O |
| 24 | 32 | 0.35 | 10 | O |
| 25 | 32 | 0.35 | 300 | O |

### 4.1.4 Apparatus

The updated CKC Automated Triaxial Testing System was used to conduct stress-controlled cyclic tests on anisotropically-consolidated specimens. A full description of the apparatus is presented in chapter 3.

### 4.1.5 Material

A local soil (Ashrafieh Clay) was used as the "native"/natural matrix material in all the tests. This soil was sourced from a construction site in Beirut, Lebanon. This clay has a c/p ratio of about 0.30; thus the undrained strength at 100kPa confinement is ~30kPa. Ottawa sand (C 109) was used as the reinforcing granular soil. The relevant geotechnical characteristics of the matrix clay and reinforcing sand are given in Table 5 and Table 6, respectively.

Table 5. Ashrafieh clay properties

| | |
|---|---|
| Liquid Limit (%) | 27 |
| Plastic Limit (%) | 16 |
| Specific Gravity ($G_s$) | 2.63 |

Table 6. Ottawa sand properties

| | | | |
|---|---|---|---|
| $D_{10}$ (mm) | 0.22 | Soil Classification (USCS) | SP |
| $D_{30}$ (mm) | 0.3 | Minimum Void Ratio ($e_{min}$) | 0.49 |
| $D_{60}$ (mm) | 0.5 | Maximum Void Ratio ($e_{max}$) | 0.75 |
| Coefficient of Uniformity | 2.3 | Specific Gravity ($G_s$) | 2.65 |
| Coefficient of Curvature | 0.82 | Drained Friction Angle (°) | 33 |

### 4.1.6 Testing Procedure and Program

A clay slurry prepared at a water content of 150% was poured into PVC split-

molds where it was 1-dimensionally consolidated under a confining pressure of around 75kPa. Control samples were then extracted from the split-mold and placed in the triaxial chamber.  Samples which were to be reinforced with a sand column were placed in a specifically fabricated setup (Najjar, 2013a) which allowed the precise augering of a central hole in which the sand column was then installed. Saturated sand columns were prepared via freezing at densities of 17.0kN/m$^3$ for dense (D) granular columns respectively. A thorough description of the specimen preparation can be found in (Rayess, 2015).

### *4.1.7    Results*

4.1.7.1   <u>Cyclic Triaxial Tests on Ashrafieh Clay</u>

Seven cyclic triaxial tests were performed on clay control specimens. Three cyclic stress ratios were selected (*CSR*=0.2, 0.25, and 0.35). Loading periods ranged from 1 second to 300 seconds.

Figure 22,Figure 23, Figure 24, and Figure 25 show the results of 4 cyclic tests performed under a CSR of 0.25 and loading periods of 1, 3, 10 and 300 seconds. For each test, the deviatoric stress, pore water pressure, and axial strains were plotted versus time. Additionally the deviatoric stress versus the axial strain are also shown.

As is clear from the respective figures and results presented, the response of the identical clay specimens under the same CSR of 0.25 is significantly affected by the loading frequency.  The smaller that value, i.e. the longer the period of the loading cycles, the "weaker" the response as demonstrated in number of cycles to failures (excessive strains). This observation is in line with expected behavior, as longer periods allow the clay to respond to the loading and develop higher pore water pressure and plastic strains during each loading cycle.

The quality and consistency of the results as shown in the respective figures referenced earlier indicates that the modified testing apparatus and data acquisition and analyses perform as desired/designed.
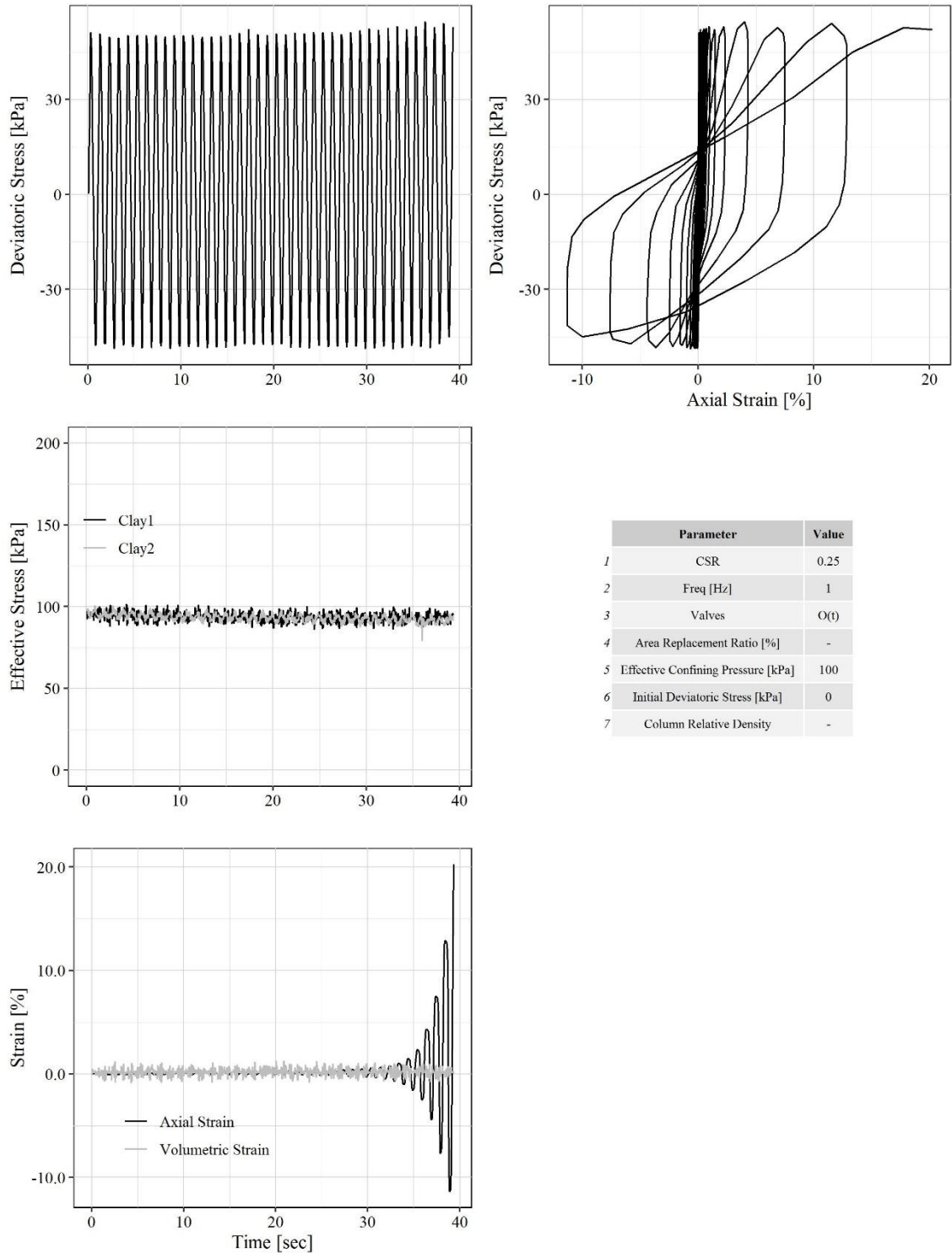


Figure 22. Cyclic triaxial test on Ashrafieh clay specimen: CSR=0.25, T=1sec

| | Parameter | Value |
|---|---|---|
| 1 | CSR | 0.25 |
| 2 | Freq [Hz] | 1/3 |
| 3 | Valves | C |
| 4 | Area Replacement Ratio [%] | - |
| 5 | Effective Confining Pressure [kPa] | 100 |
| 6 | Initial Deviatoric Stress [kPa] | 0 |
| 7 | Column Relative Density | - |
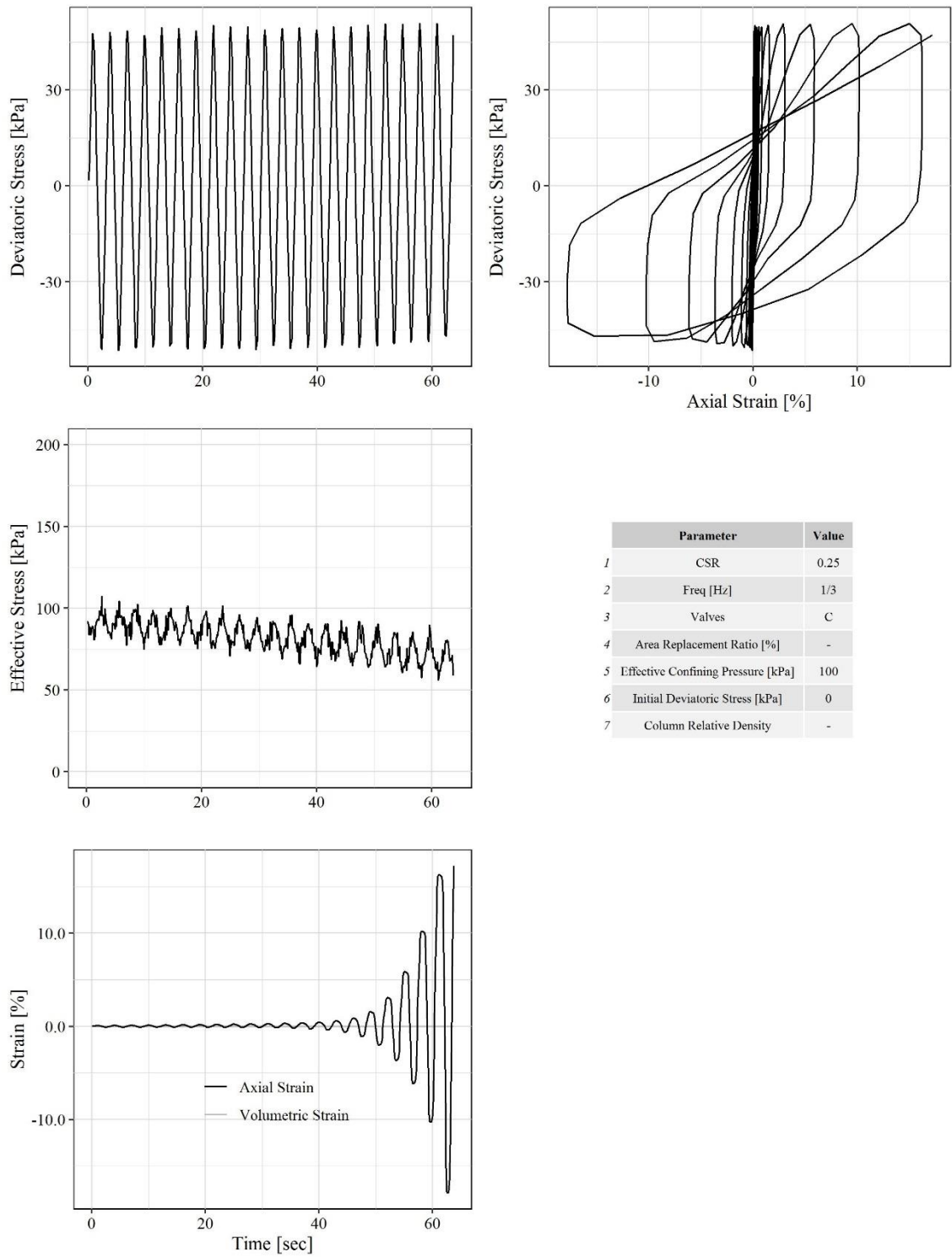
Figure 23. Cyclic triaxial test on Ashrafieh clay specimen: CSR=0.25, T=3sec
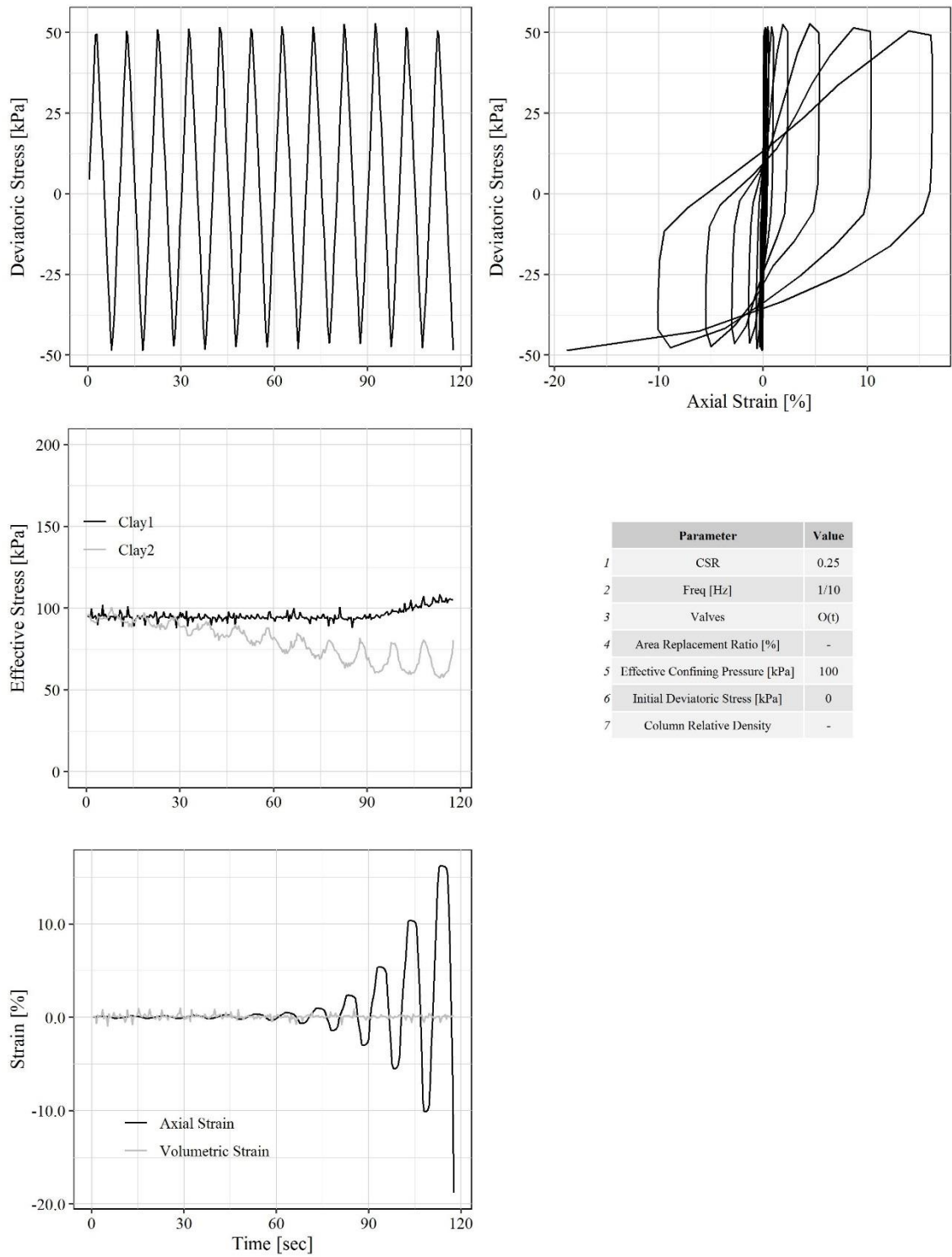
Figure 24. Cyclic triaxial test on Ashrafieh clay specimen: CSR=0.25, T=10sec

| | Parameter | Value |
|---|---|---|
| 1 | CSR | 0.25 |
| 2 | Freq [Hz] | 1/10 |
| 3 | Valves | O(t) |
| 4 | Area Replacement Ratio [%] | - |
| 5 | Effective Confining Pressure [kPa] | 100 |
| 6 | Initial Deviatoric Stress [kPa] | 0 |
| 7 | Column Relative Density | - |
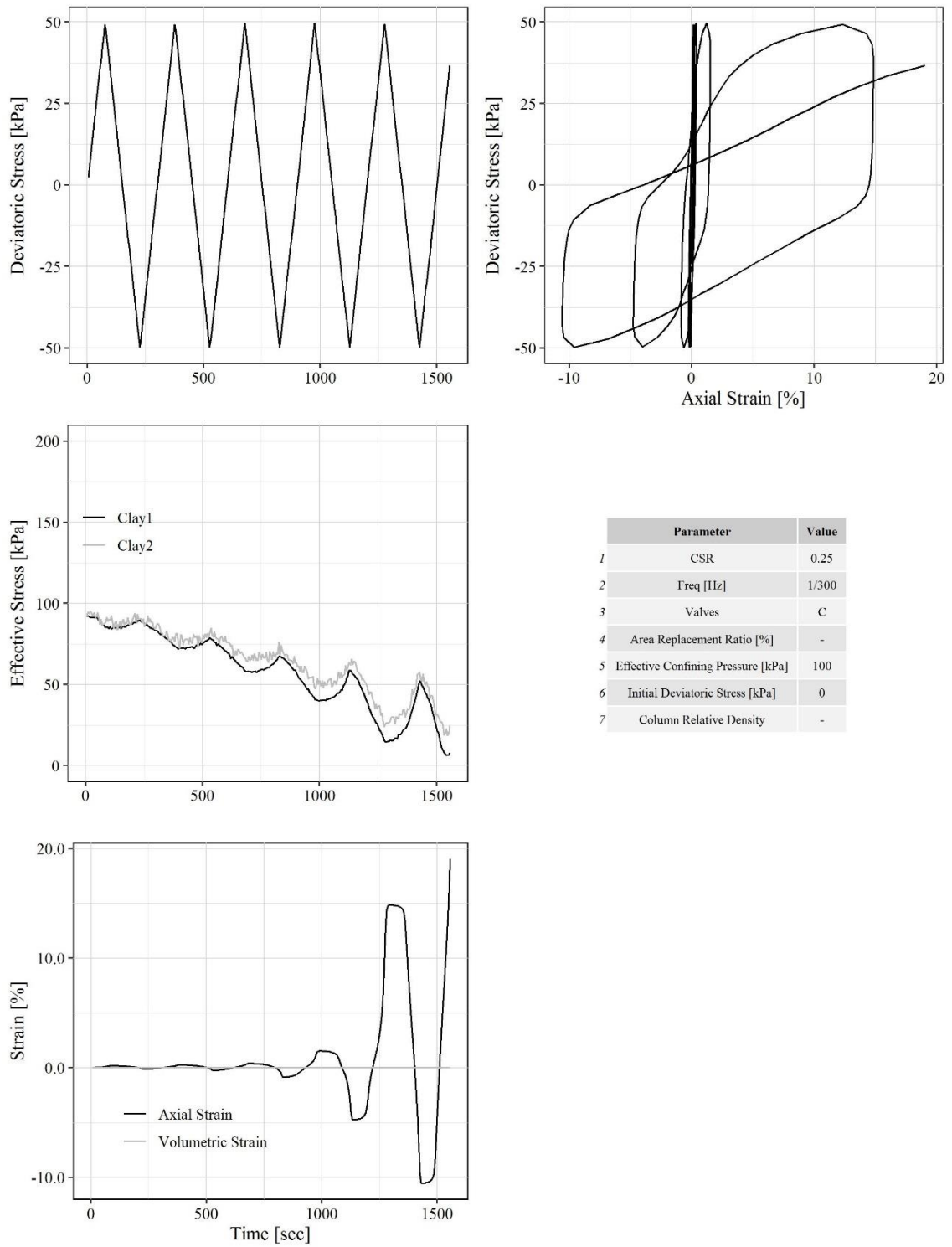
Figure 25. Cyclic triaxial test on Ashrafieh clay specimen: CSR=0.25, T=300sec

For reference and completion/comparison, two tests were performed on the
same Ashrafieh clay specimens however this time, under a CSR of 0.35 with loading

periods at the extreme of the range explored earlier of 1 and 300 seconds. The results of these tests are presented in Figure 26 andFigure 27.

As anticipated, the higher CSR resulted in a response which indicated "failure" reached at a lower number of cycles. Loading with a CSR of 0.35 at a period of 1 second led to excessive straining after 3 to 4 cycles, which the same loading with a longer period of 300 seconds resulted in sample failure within the first cycle.

Finally, an Ashrafieh clay control sample was prepared to the same initial conditions as all the precedent specimens tested and then cyclically loaded with a CSR of 0.2. A loading period of 300 seconds was used for that test, as a shorter loading period would have not resulted in excessive straining/failure at the CSR used. The results of that test are shown in Figure 28. They show that excessive straining/cyclic mobility was only reached after roughly 35 cycles of loading at the long period.

| | Parameter | Value |
|---|---|---|
| 1 | CSR | 0.35 |
| 2 | Freq [Hz] | 1 |
| 3 | Valves | C |
| 4 | Area Replacement Ratio [%] | 0 |
| 5 | Effective Confining Pressure [kPa] | 100 |
| 6 | Initial Deviatoric Stress [kPa] | 0 |
| 7 | Column Relative Density | - |
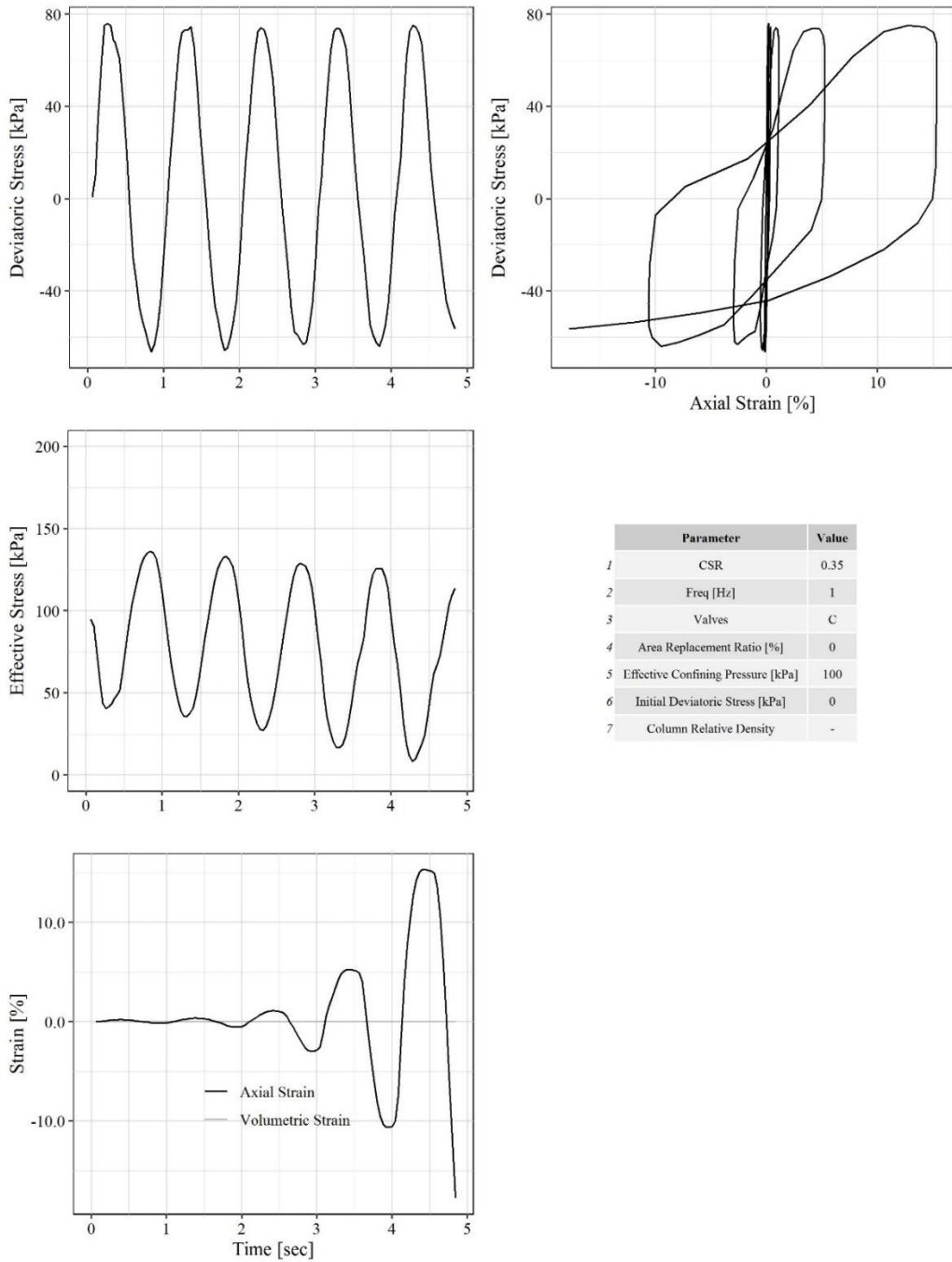
Figure 26. Cyclic triaxial test on Ashrafieh clay specimen: CSR=0.35, T=1sec

| | Parameter | Value |
|---|---|---|
| 1 | CSR | 0.35 |
| 2 | Freq [Hz] | 1/300 |
| 3 | Valves | O(t) |
| 4 | Area Replacement Ratio [%] | - |
| 5 | Effective Confining Pressure [kPa] | 100 |
| 6 | Initial Deviatoric Stress [kPa] | 0 |
| 7 | Column Relative Density | - |
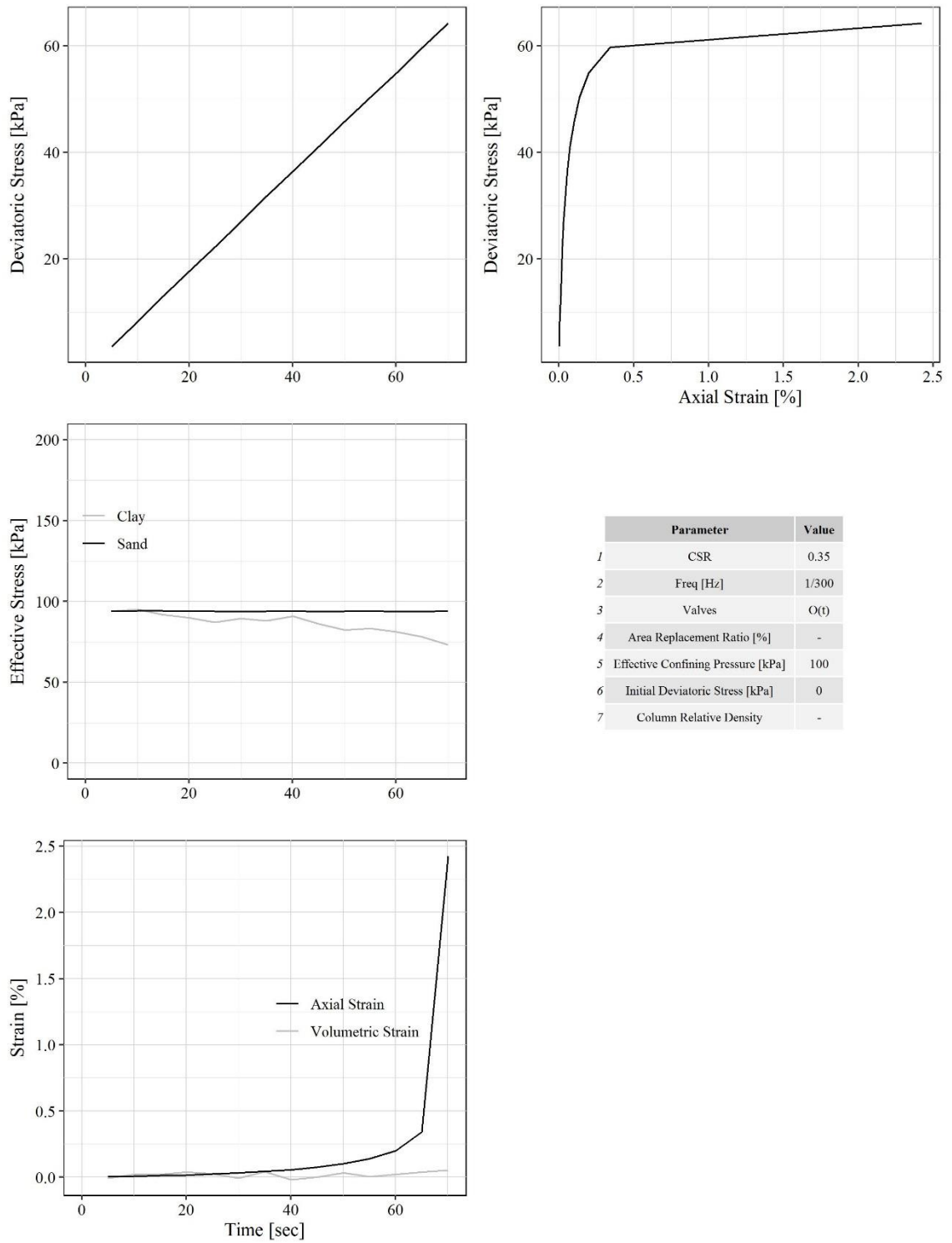
Figure 27. Cyclic triaxial test on Ashrafieh clay specimen: CSR=0.35, T=300sec

The table in the figure:

| | Parameter | Value |
|---|---|---|
| 1 | CSR | 0.20 |
| 2 | Freq [Hz] | 1/300 |
| 3 | Valves | C |
| 4 | Area Replacement Ratio [%] | - |
| 5 | Effective Confining Pressure [kPa] | 100 |
| 6 | Initial Deviatoric Stress [kPa] | 0 |
| 7 | Column Relative Density | - |
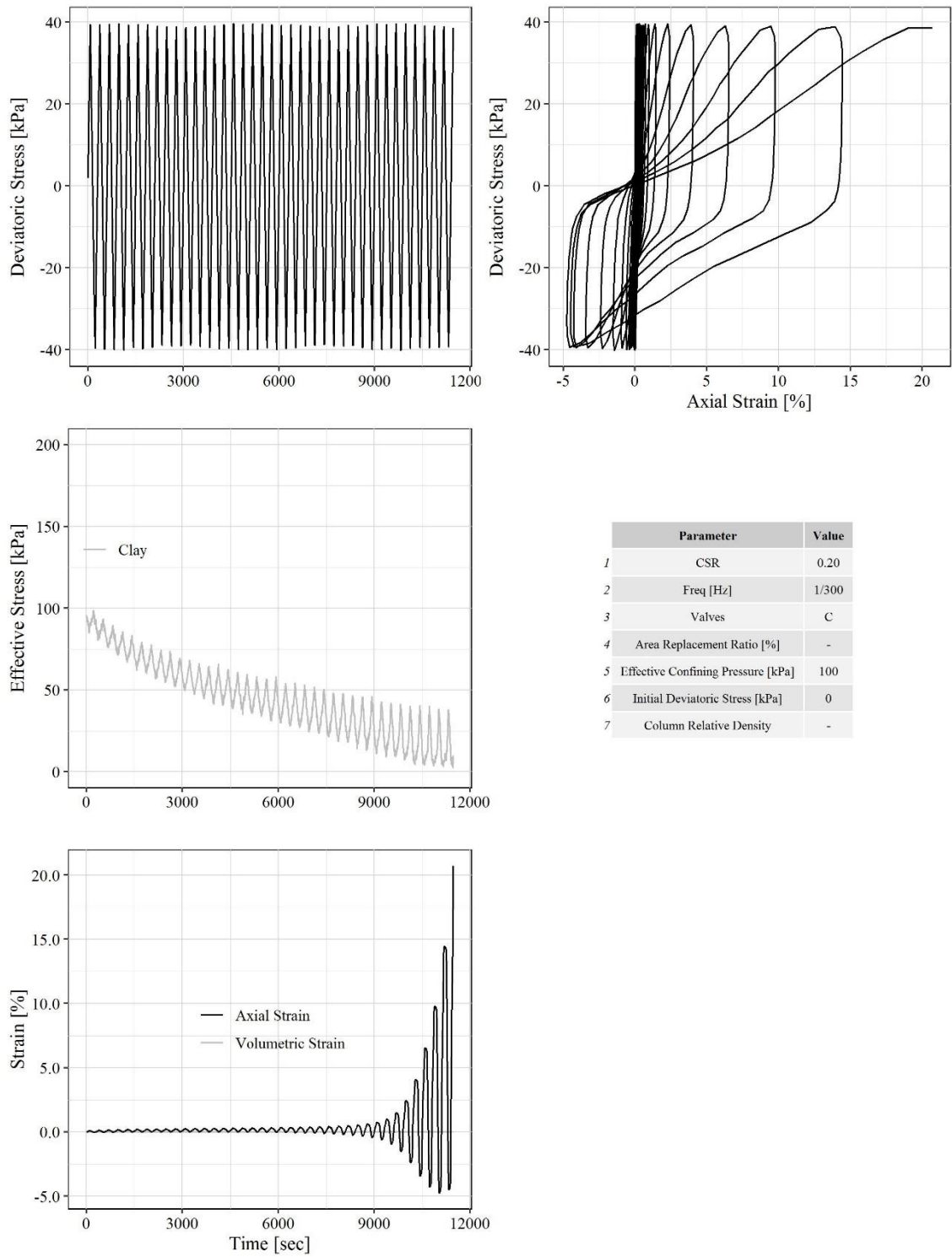
Figure 28. Cyclic triaxial test on Ashrafieh clay specimen: CSR=0.2, T=300sec

4.1.7.2  <u>Cyclic Triaxial Tests on Ottawa Sand</u>

A total of six cyclic triaxial tests were performed on Ottawa sand specimens. Since loading periods were relative fast, three tests were done when valves are closed (undrained conditions) and three other tests were performed while valves are left open during the cyclic loading phase. This testing approach for the sand was adopted to query/establish the effect of potential partial drainage which may still occur even at the lowest periods of testing cycles.

The tests conducted on the Ottawa Sand samples were done at periods of loading of 1 second and CSRs of 0.25, 0.3, 0.35 with drainage valves closed. As is clearly apparent in the respective results shown in Figures 30, 31 and 32. It is notable that under the loading frequency of 1Hz (period of 1 sec) for these tests, the sand samples held their own even at the higher values of CSR.

For completion, three additional Ottawa Samples were prepared at the same relative density as all the previous identical specimen, and tested at a very high CSR of 0.4 with valves open to allow "partial drainage" with periods of 1, 10 and 60 seconds. The results of these tests are shown in Figures 33, 34 and 35. It is notable here that the tests with open valves, even at such a high CSR did not show significant degradation.

| | Parameter | Value |
|---|---|---|
| 1 | CSR | 0.25 |
| 2 | Freq [Hz] | 1 |
| 3 | Valves | C |
| 4 | Area Replacement Ratio [%] | 100 |
| 5 | Effective Confining Pressure [kPa] | 100 |
| 6 | Initial Deviatoric Stress [kPa] | 0 |
| 7 | Column Relative Density | - |
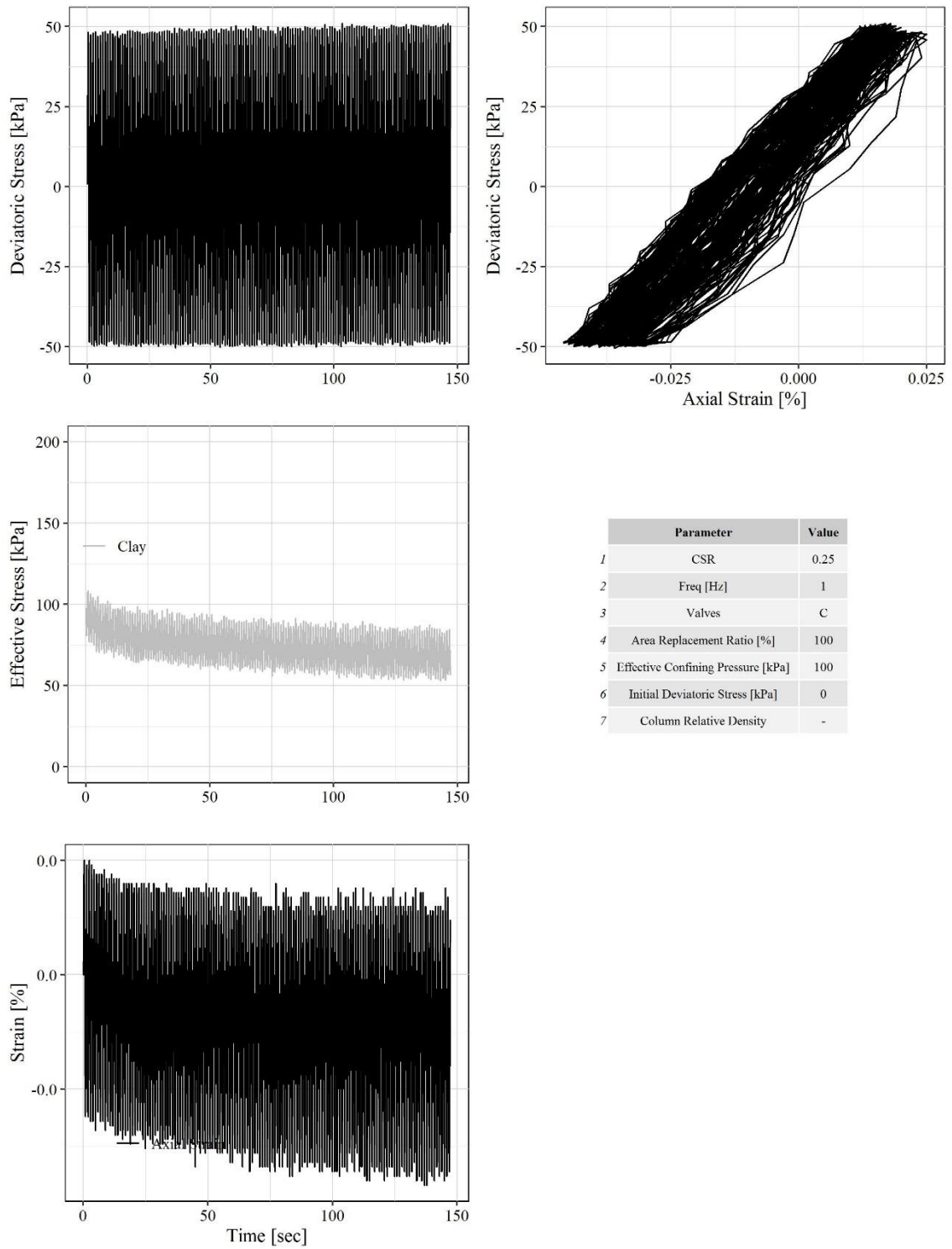
Figure 29. Cyclic triaxial test on Ottawa sand specimen: CSR=0.25, T=1sec, valves closed

| | Parameter | Value |
|---|---|---|
| 1 | CSR | 0.3 |
| 2 | Freq [Hz] | 1 |
| 3 | Valves | C |
| 4 | Area Replacement Ratio [%] | 100 |
| 5 | Effective Confining Pressure [kPa] | 100 |
| 6 | Initial Deviatoric Stress [kPa] | 0 |
| 7 | Column Relative Density | - |
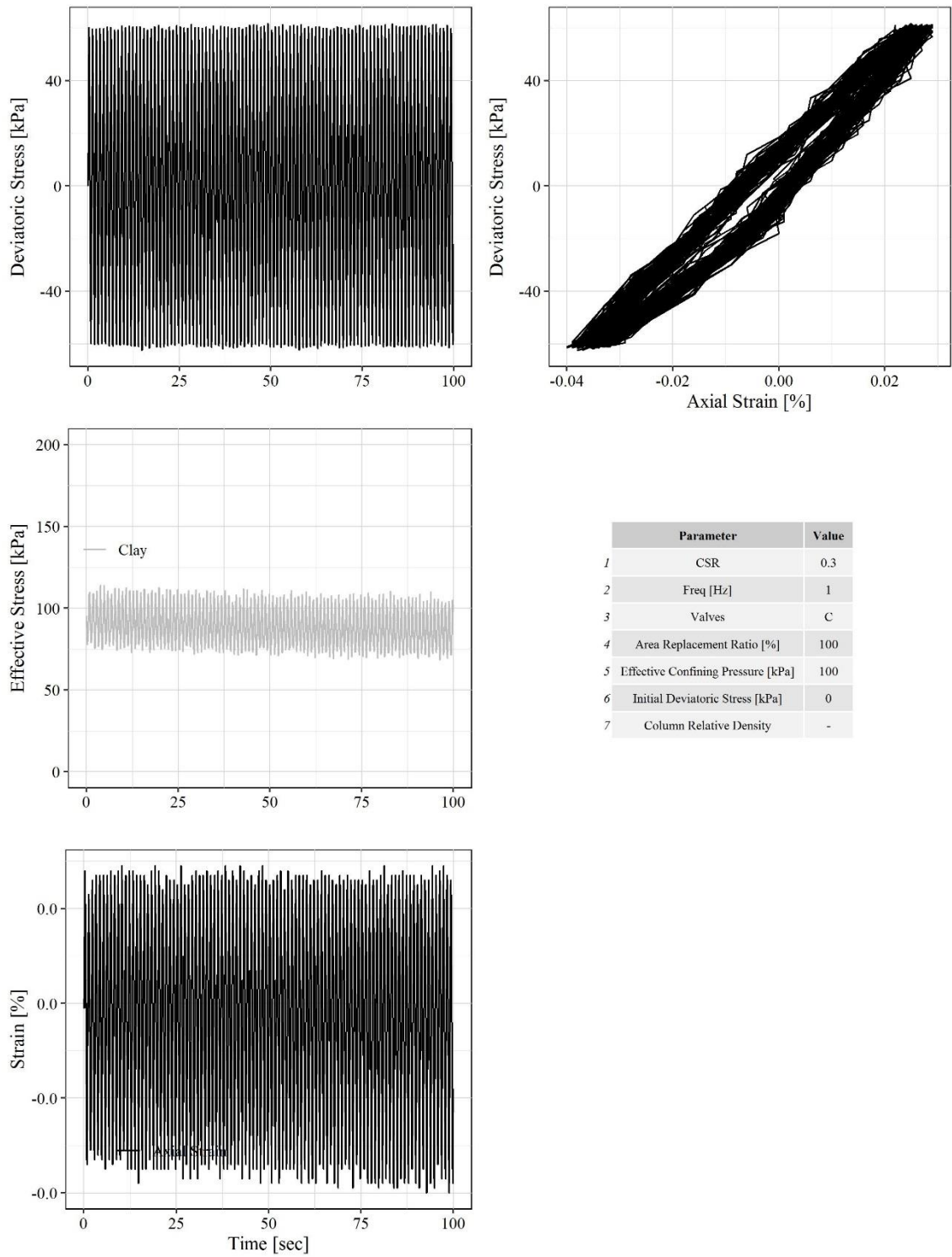
Figure 30. Cyclic triaxial test on Ottawa sand specimen: CSR=0.3, T=1sec, valves closed
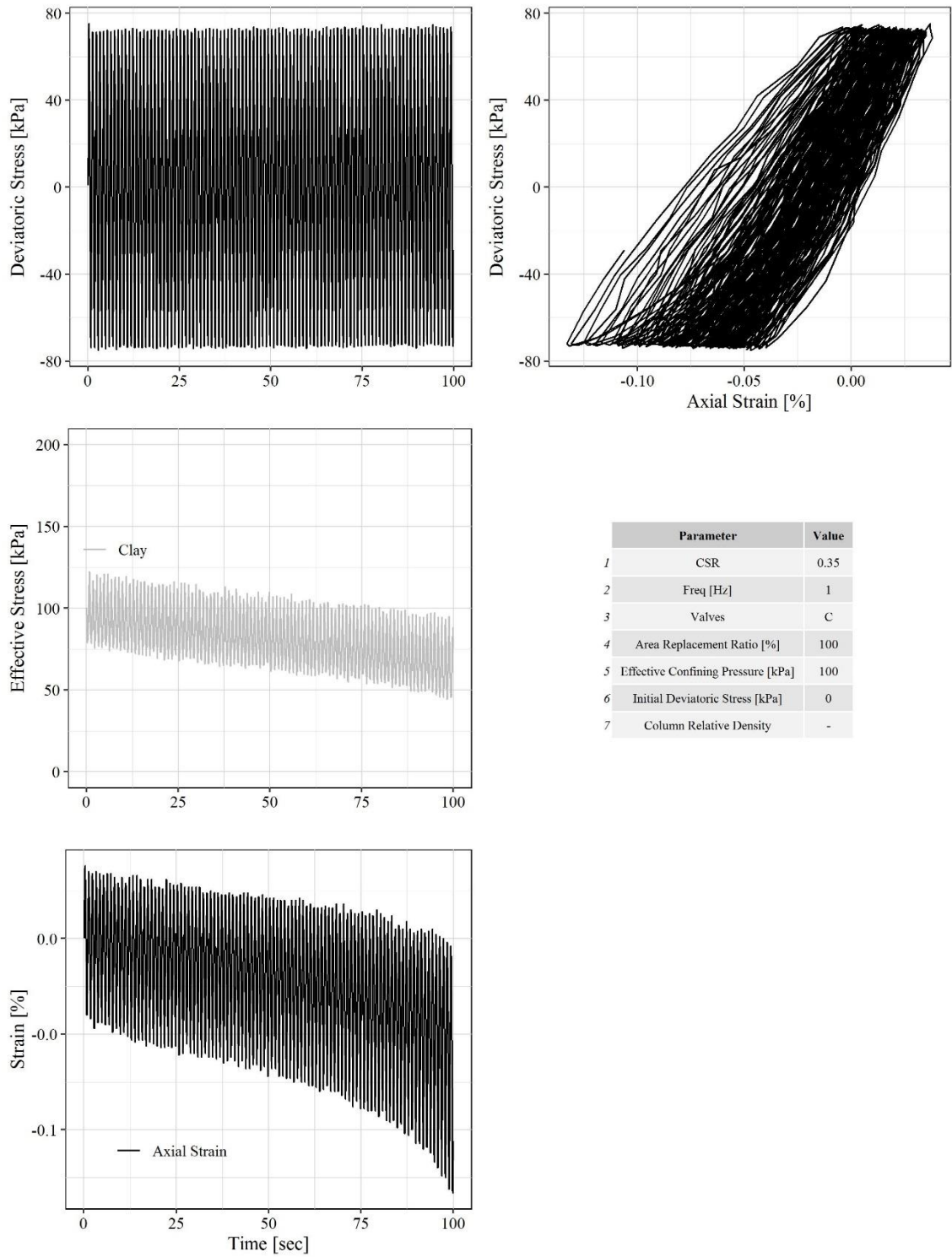
Figure 31. Cyclic triaxial test on Ottawa sand specimen: CSR=0.35, T=1sec, valves closed

| | Parameter | Value |
|---|---|---|
| 1 | CSR | 0.4 |
| 2 | Freq [Hz] | 1 |
| 3 | Valves | O |
| 4 | Area Replacement Ratio [%] | - |
| 5 | Effective Confining Pressure [kPa] | 100 |
| 6 | Initial Deviatoric Stress [kPa] | 0 |
| 7 | Column Relative Density | 86 |
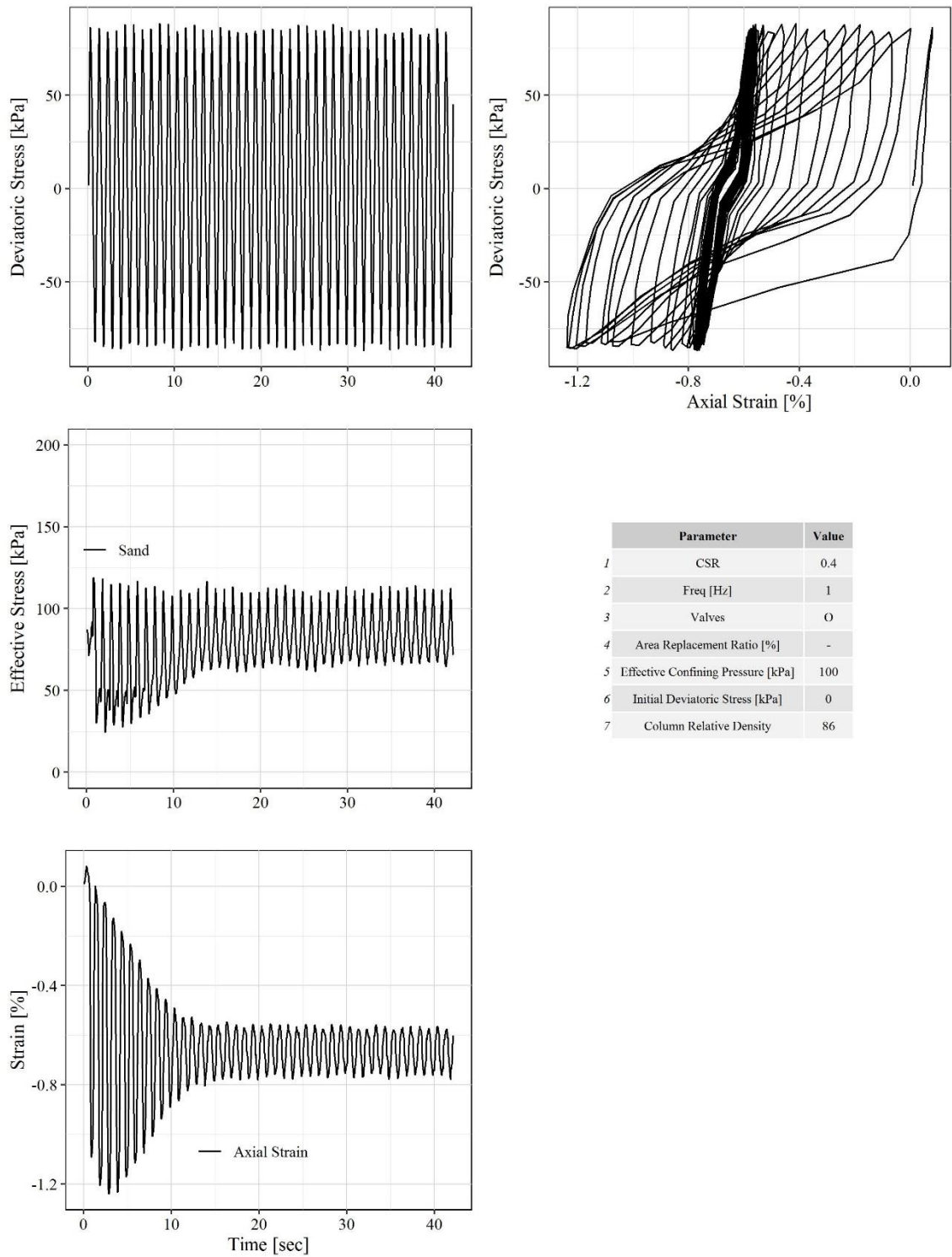
Figure 32 Cyclic triaxial test on Ottawa sand specimen: CSR=0.4, T=1sec, valves opened

| | Parameter | Value |
|---|---|---|
| 1 | CSR | 0.4 |
| 2 | Freq [Hz] | 1/10 |
| 3 | Valves | O |
| 4 | Area Replacement Ratio [%] | 100 |
| 5 | Effective Confining Pressure [kPa] | 100 |
| 6 | Initial Deviatoric Stress [kPa] | 0 |
| 7 | Column Relative Density | - |
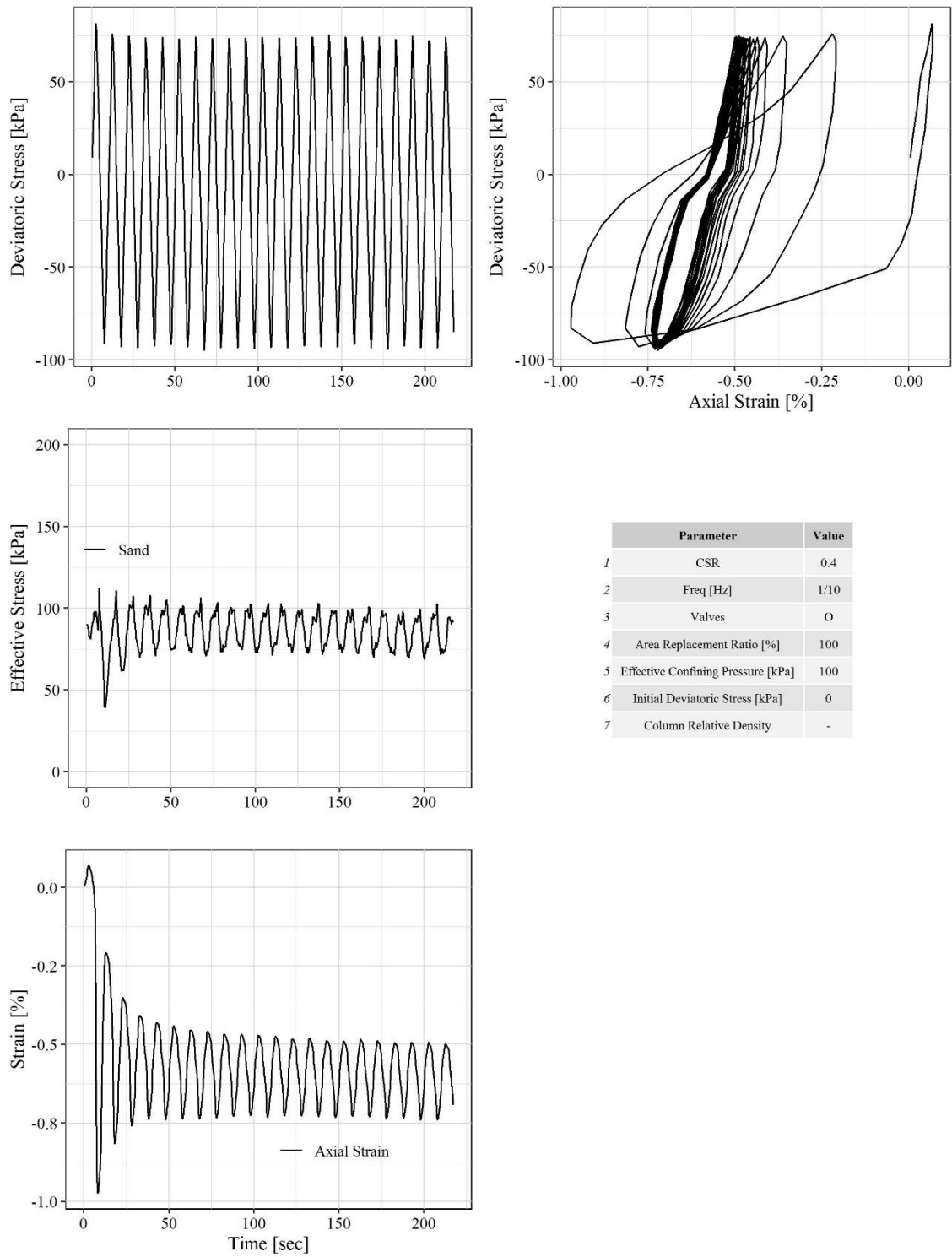
Figure 33. Cyclic triaxial test on Ottawa sand specimen: CSR=0.4, T=10sec, valves opened

| | Parameter | Value |
|---|---|---|
| 1 | CSR | 0.4 |
| 2 | Freq [Hz] | 1/60 |
| 3 | Valves | O |
| 4 | Area Replacement Ratio [%] | 100 |
| 5 | Effective Confining Pressure [kPa] | 100 |
| 6 | Initial Deviatoric Stress [kPa] | 0 |
| 7 | Column Relative Density | - |
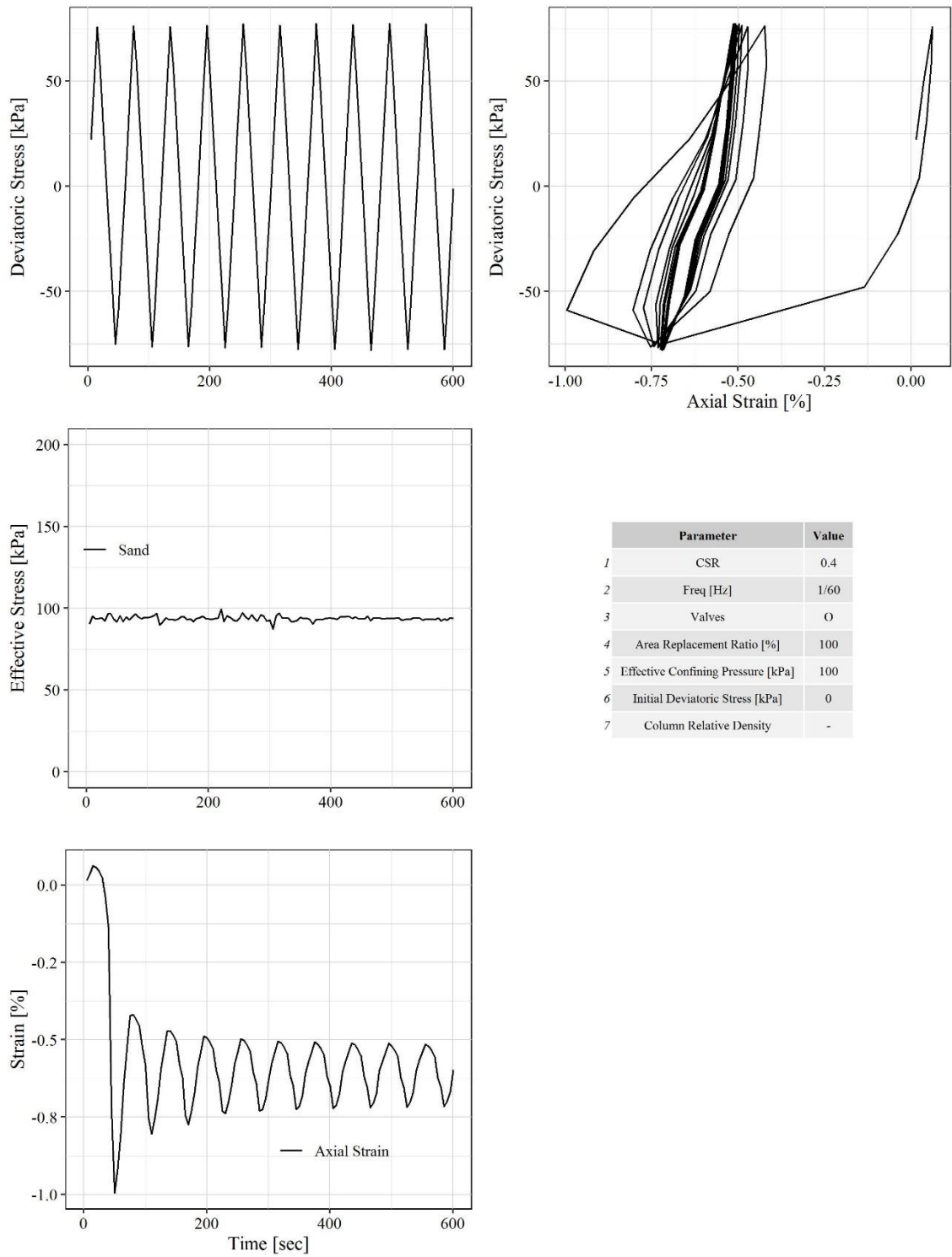
Figure 34. Cyclic triaxial test on Ottawa sand specimen: CSR=0.4, T=60sec, valves opened

### 4.1.7.3  Cyclic Triaxial Tests on Reinforced Specimens

- Area replacement ratio of 18%

   Two cyclic triaxial tests with closed drainage valves and four tests with opened
drainage valves were performed on 3cm-sand column reinforced clay specimens. A
cyclic stress ratio of 0.35 and loading periods ranging from 1 to 300sec were adopted in
the testing program.

| | Parameter | Value |
|---|---|---|
| 1 | CSR | 0.35 |
| 2 | Freq [Hz] | 1 |
| 3 | Valves | C |
| 4 | Area Replacement Ratio [%] | 18 |
| 5 | Effective Confining Pressure [kPa] | 100 |
| 6 | Initial Deviatoric Stress [kPa] | 0 |
| 7 | Column Relative Density | 86 |
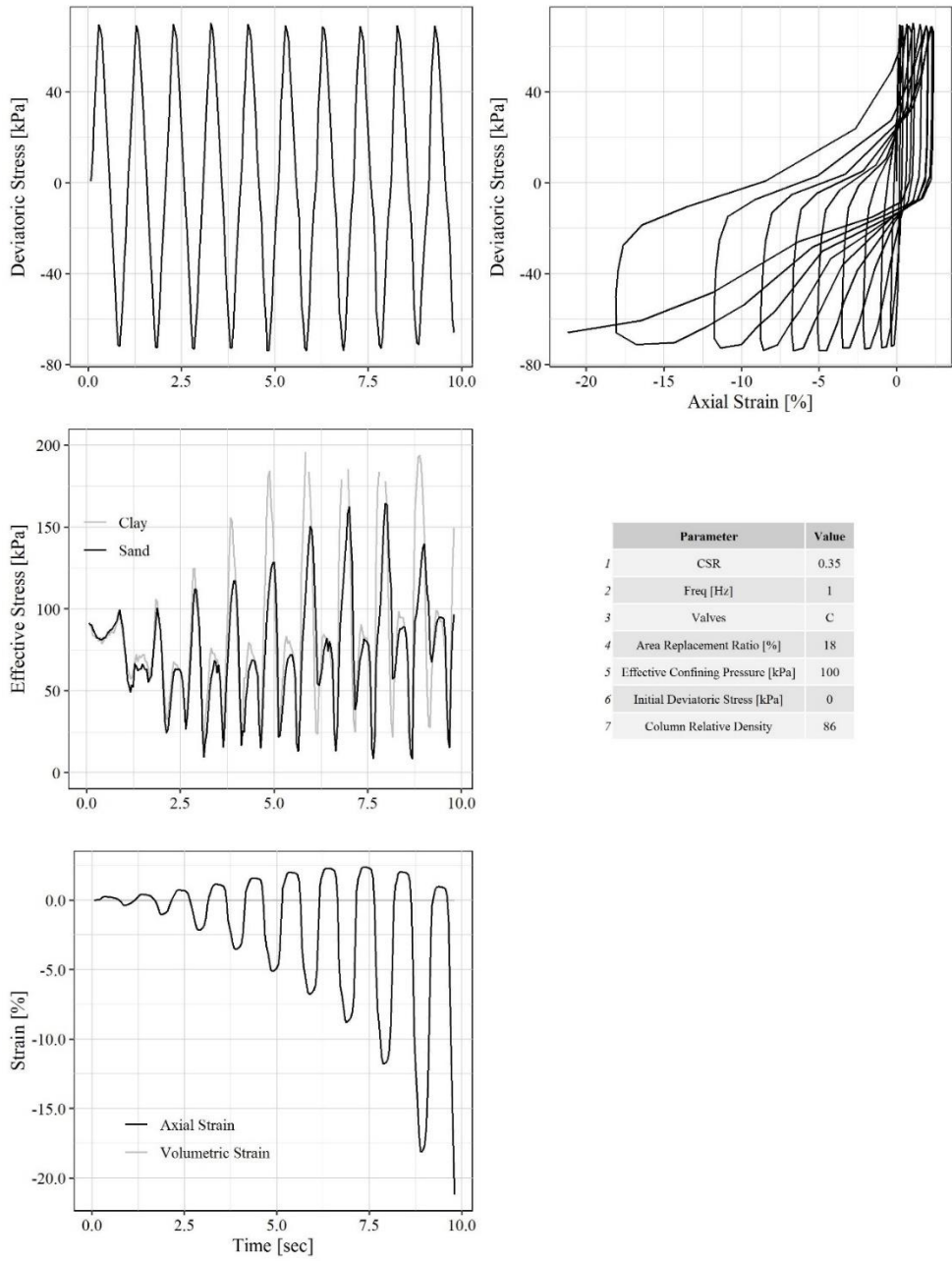
Figure 35. Cyclic triaxial test on reinforced clay specimen: CSR=0.35, T=1sec, valves closed

| | Parameter | Value |
|---|---|---|
| 1 | CSR | 0.35 |
| 2 | Freq [Hz] | 1/300 |
| 3 | Valves | C |
| 4 | Area Replacement Ratio [%] | 18 |
| 5 | Effective Confining Pressure [kPa] | 100 |
| 6 | Initial Deviatoric Stress [kPa] | 0 |
| 7 | Column Relative Density | - |
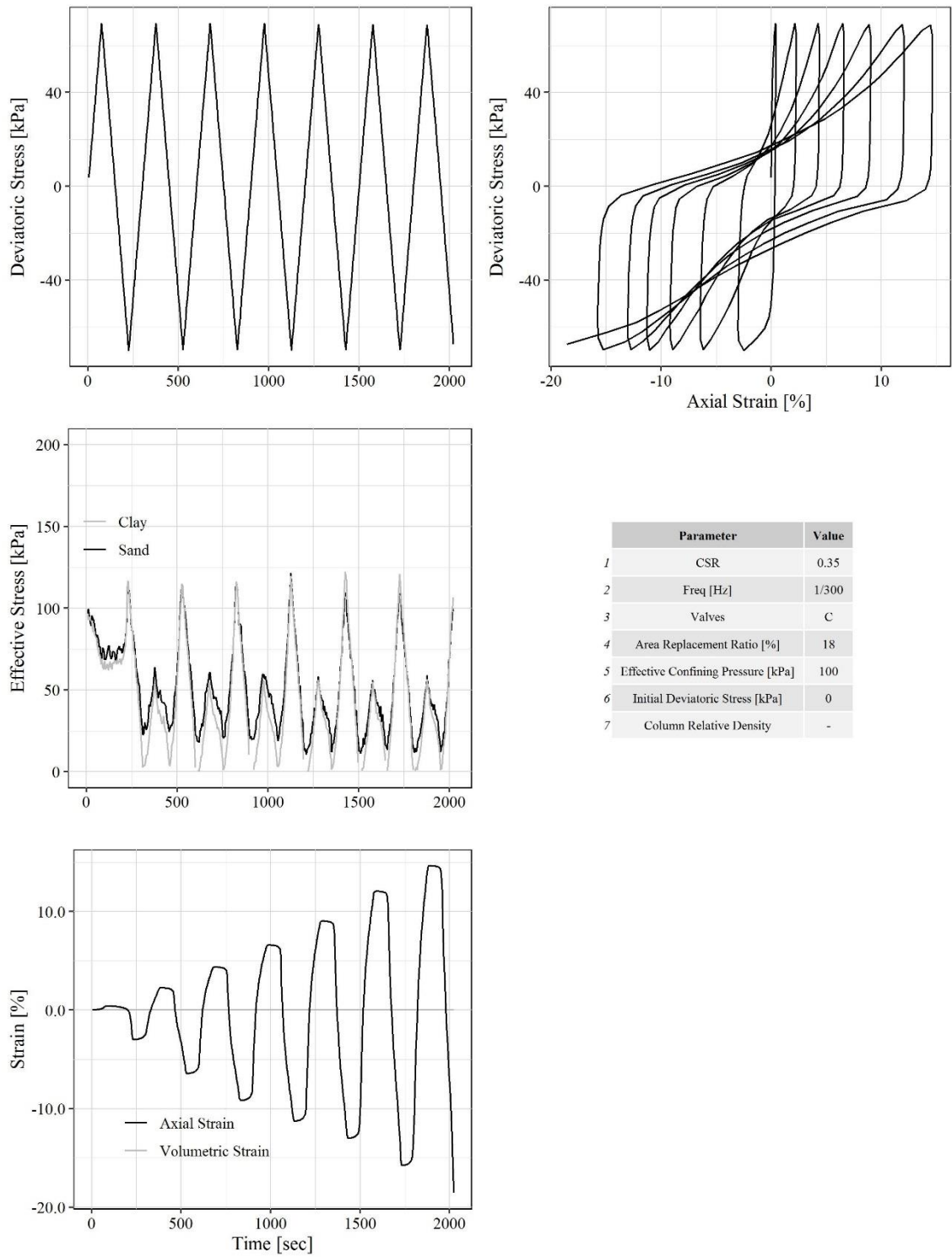
Figure 36. Cyclic triaxial test on reinforced clay specimen: CSR=0.35, T=1sec, valves closed

The table in the figure contains:

| | Parameter | Value |
|---|---|---|
| 1 | CSR | 0.35 |
| 2 | Freq [Hz] | 1 |
| 3 | Valves | O |
| 4 | Area Replacement Ratio [%] | 18 |
| 5 | Effective Confining Pressure [kPa] | 100 |
| 6 | Initial Deviatoric Stress [kPa] | 0 |
| 7 | Column Relative Density | 86 |
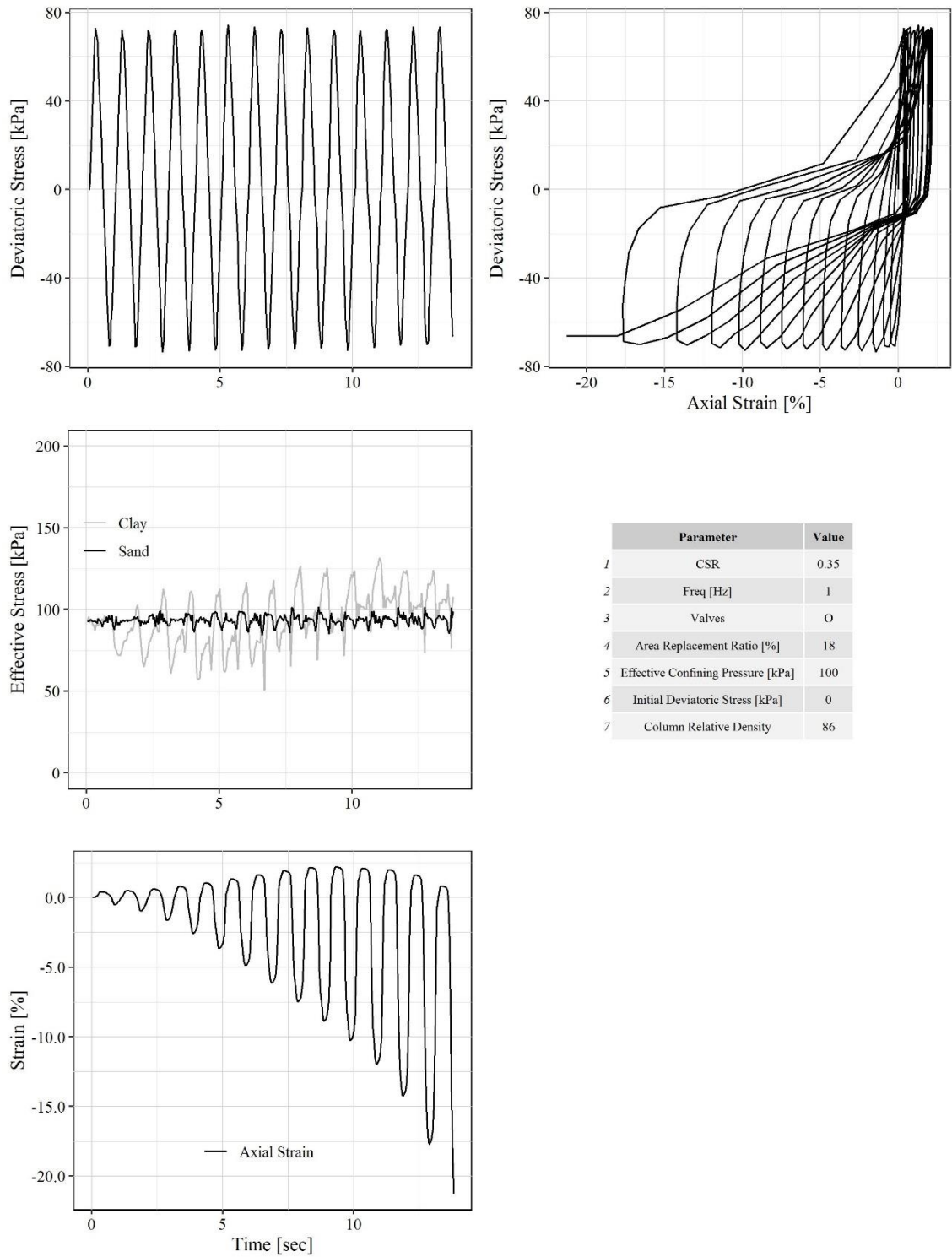
Figure 37. Cyclic triaxial test on reinforced clay specimen: CSR=0.35, T=1sec, valves opened

| | Parameter | Value |
|---|---|---|
| 1 | CSR | 0.35 |
| 2 | Freq [Hz] | 1/3 |
| 3 | Valves | O |
| 4 | Area Replacement Ratio [%] | 18 |
| 5 | Effective Confining Pressure [kPa] | 100 |
| 6 | Initial Deviatoric Stress [kPa] | 0 |
| 7 | Column Relative Density | - |
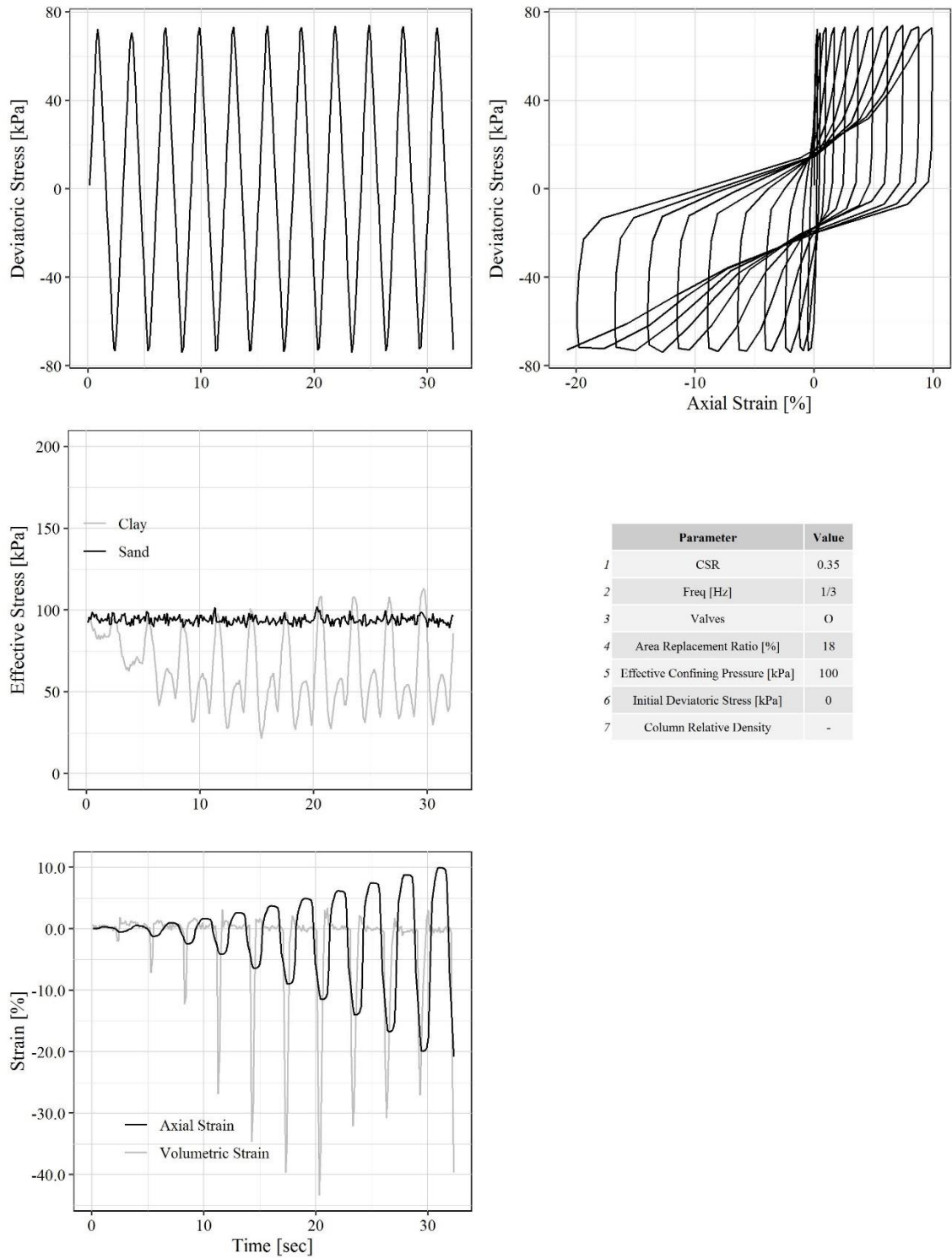
Figure 38. Cyclic triaxial test on reinforced clay specimen: CSR=0.35, T=3sec, valves opened

| | Parameter | Value |
|---|---|---|
| 1 | CSR | 0.35 |
| 2 | Freq [Hz] | 1/10 |
| 3 | Valves | C |
| 4 | Area Replacement Ratio [%] | 18 |
| 5 | Effective Confining Pressure [kPa] | 100 |
| 6 | Initial Deviatoric Stress [kPa] | 0 |
| 7 | Column Relative Density | – |
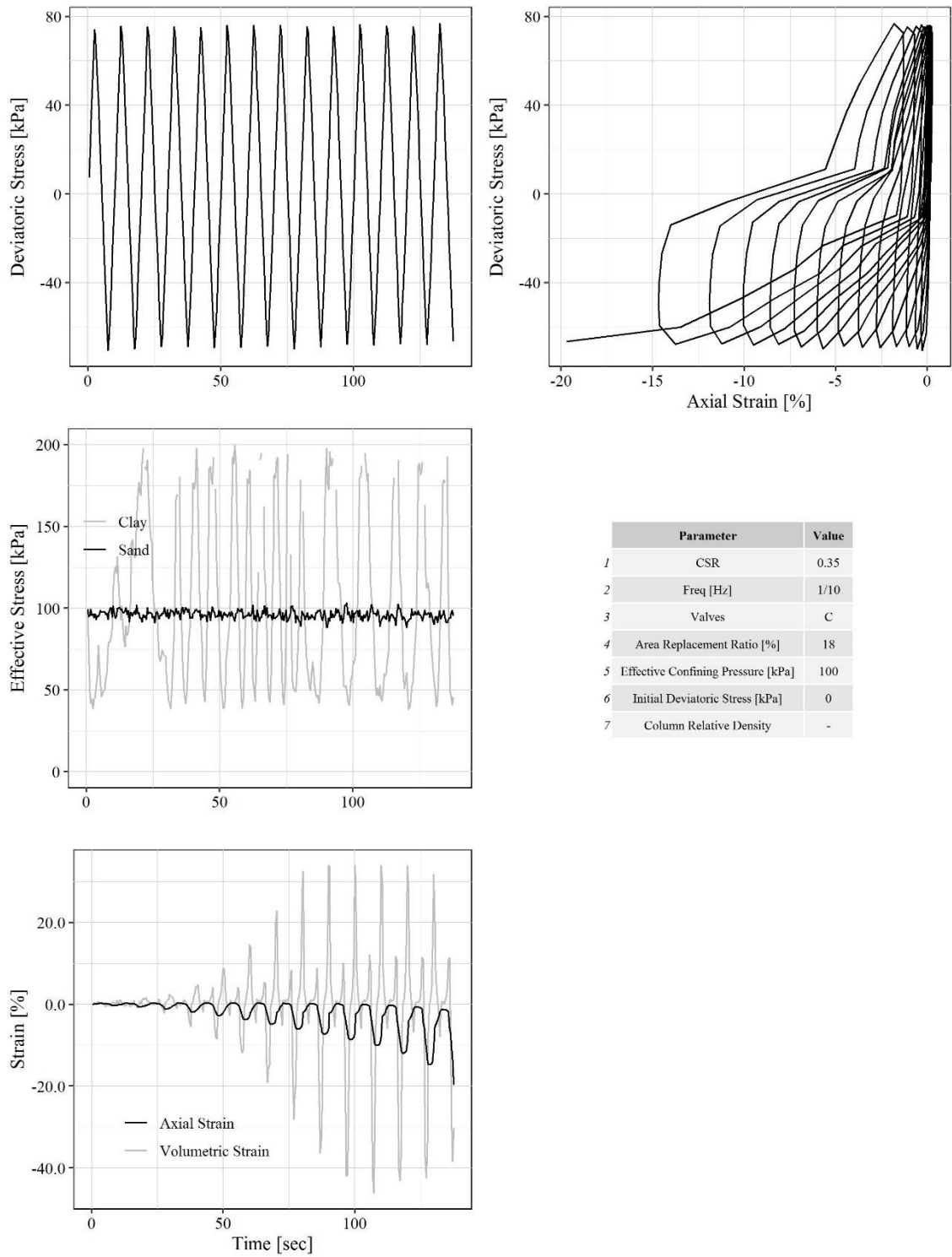
Figure 39. Cyclic triaxial test on reinforced clay specimen: CSR=0.35, T=10sec, valves opened

| | Parameter | Value |
|---|---|---|
| 1 | CSR | 0.35 |
| 2 | Freq [Hz] | 1/300 |
| 3 | Valves | O(t) |
| 4 | Area Replacement Ratio [%] | 18 |
| 5 | Effective Confining Pressure [kPa] | 100 |
| 6 | Initial Deviatoric Stress [kPa] | 0 |
| 7 | Column Relative Density | 86 |
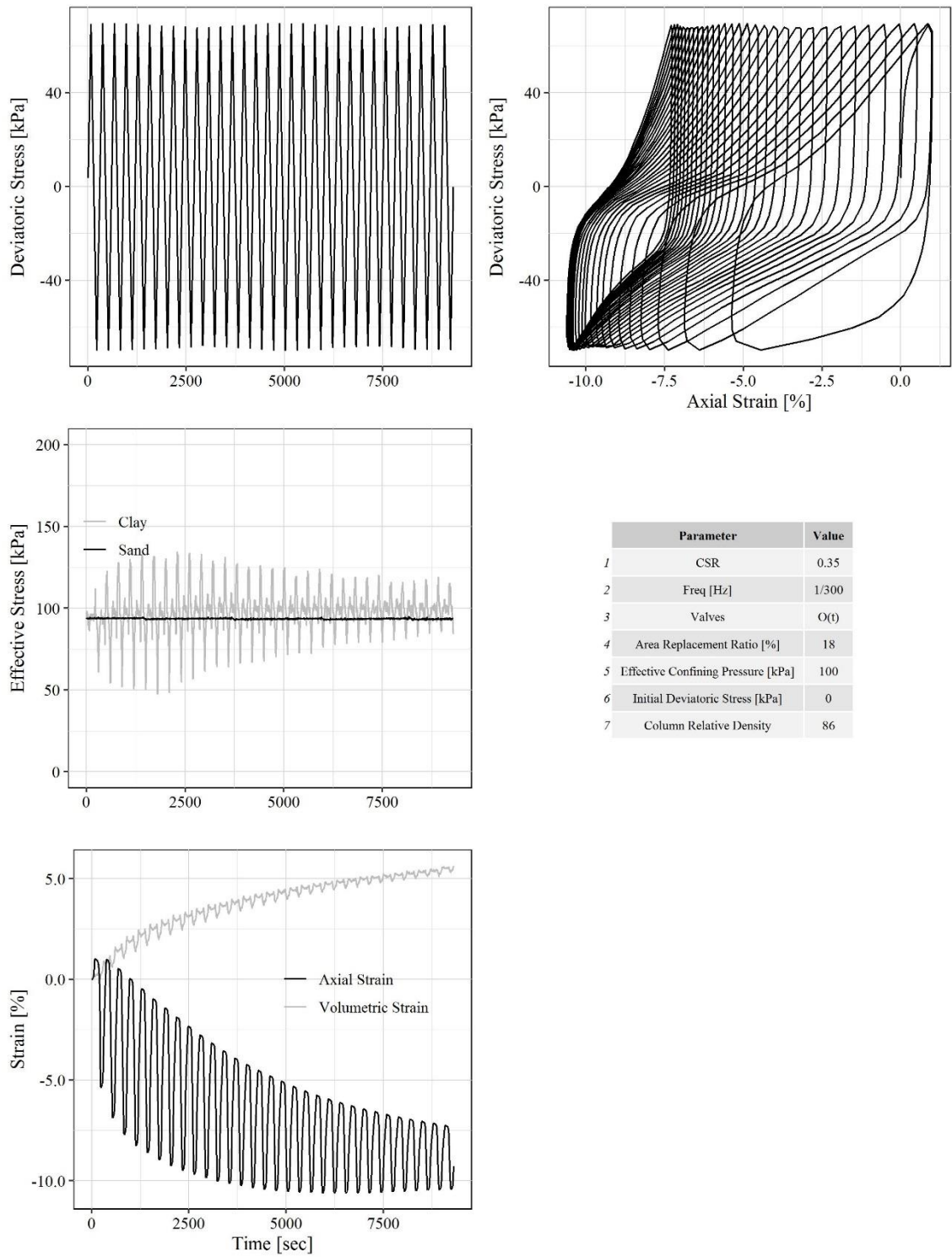
Figure 40. Cyclic triaxial test on reinforced clay specimen: CSR=0.35, T=300sec, valves opened

- Area replacement ratio of 32%

Two cyclic triaxial tests with closed drainage valves and four tests with opened drainage valves were performed on 3cm-sand column reinforced clay specimens. A cyclic stress ratio of 0.35 and loading periods ranging from 1 to 300sec were adopted in the testing program.

| | Parameter | Value |
|---|---|---|
| 1 | CSR | 0.35 |
| 2 | Freq [Hz] | 1 |
| 3 | Valves | C |
| 4 | Area Replacement Ratio [%] | 32 |
| 5 | Effective Confining Pressure [kPa] | 100 |
| 6 | Initial Deviatoric Stress [kPa] | 0 |
| 7 | Column Relative Density | 86 |
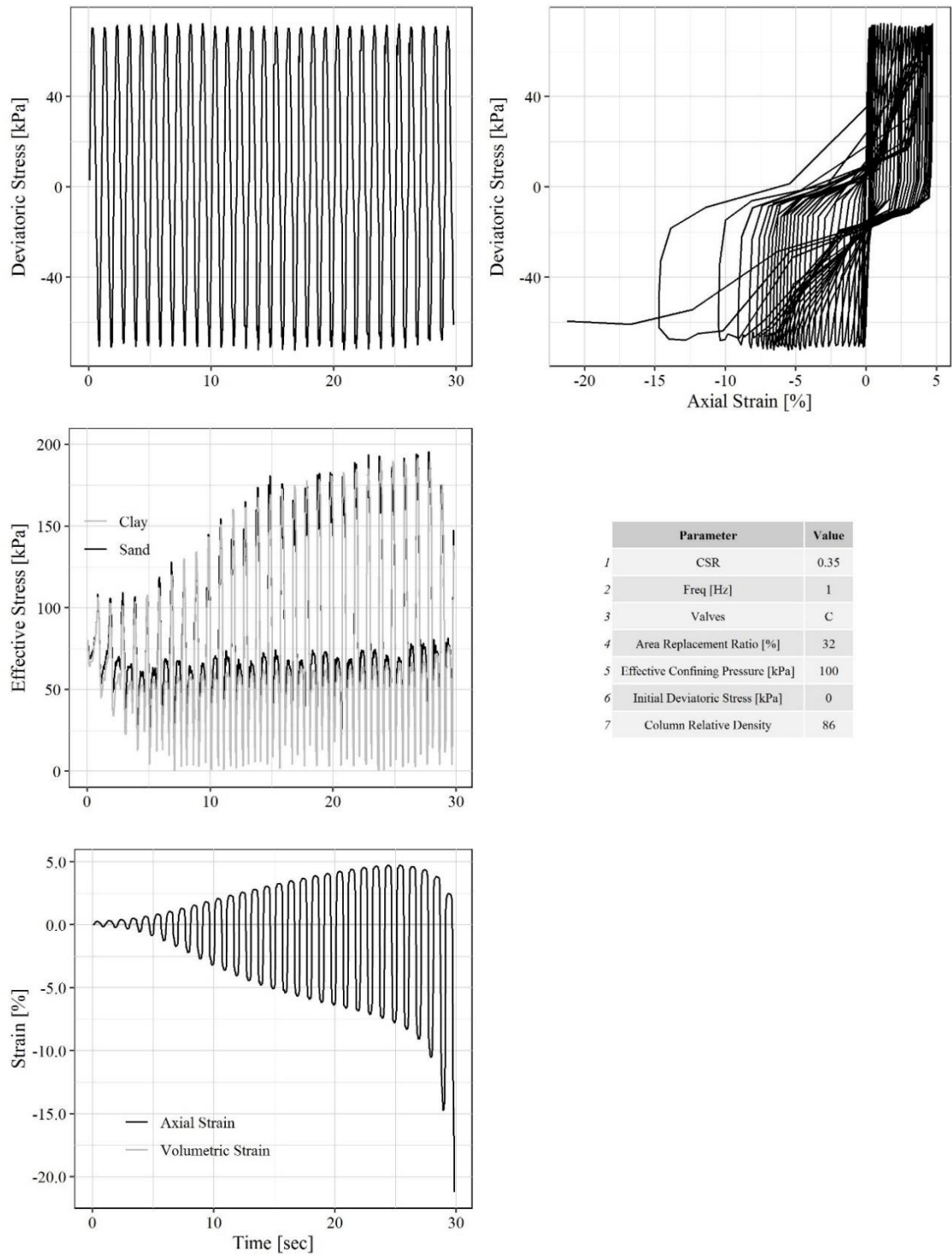
Figure 41. Cyclic triaxial test on reinforced clay specimen: CSR=0.35, T=1sec, valves closed

| | Parameter | Value |
|---|---|---|
| 1 | CSR | 0.35 |
| 2 | Freq [Hz] | 1/300 |
| 3 | Valves | C |
| 4 | Area Replacement Ratio [%] | 32 |
| 5 | Effective Confining Pressure [kPa] | 100 |
| 6 | Initial Deviatoric Stress [kPa] | 0 |
| 7 | Column Relative Density | – |
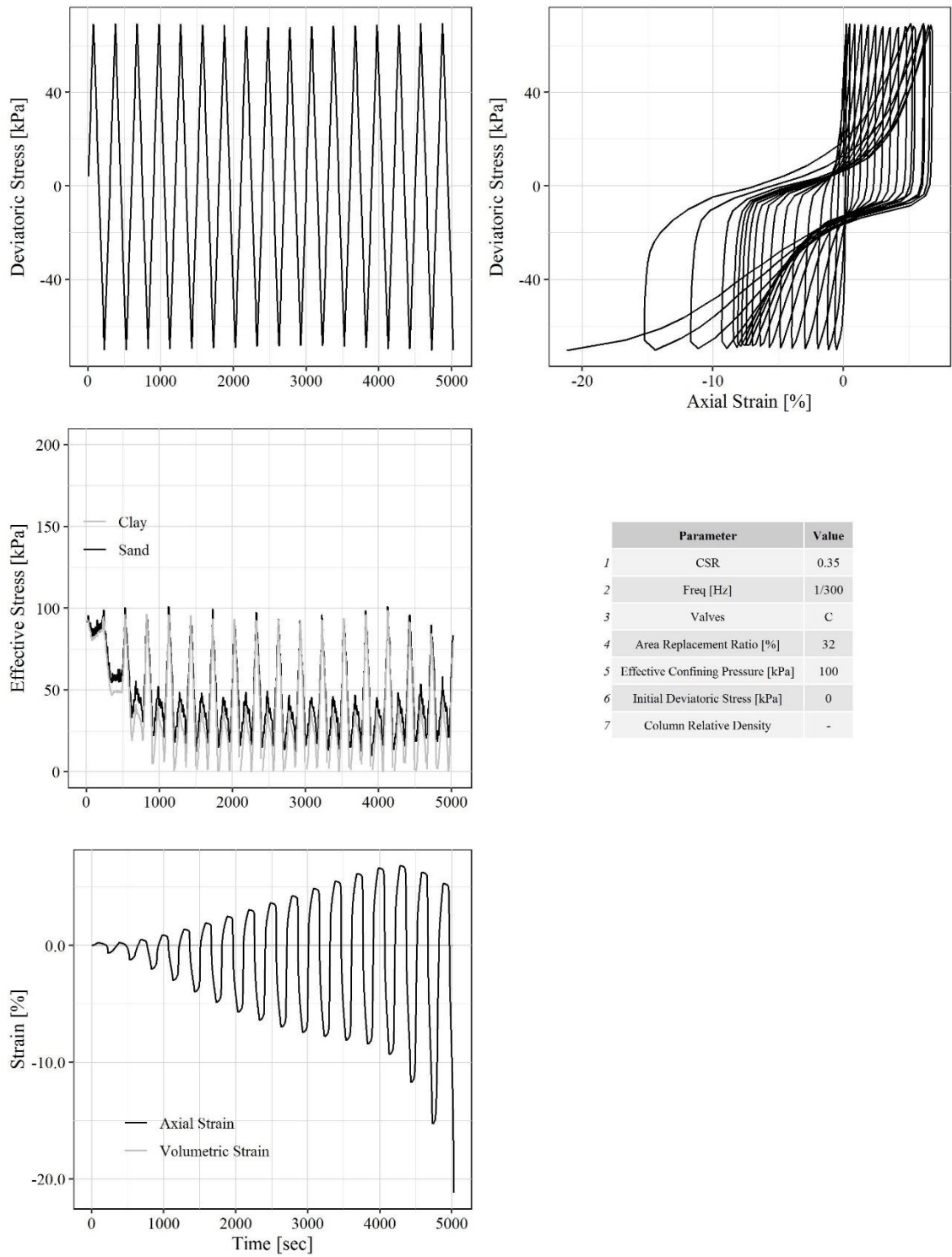
Figure 42. Cyclic triaxial test on reinforced clay specimen: CSR=0.35, T=300sec, valves closed

| | Parameter | Value |
|---|---|---|
| 1 | CSR | 0.35 |
| 2 | Freq [Hz] | 1 |
| 3 | Valves | O |
| 4 | Area Replacement Ratio [%] | 32 |
| 5 | Effective Confining Pressure [kPa] | 100 |
| 6 | Initial Deviatoric Stress [kPa] | 0 |
| 7 | Column Relative Density | - |
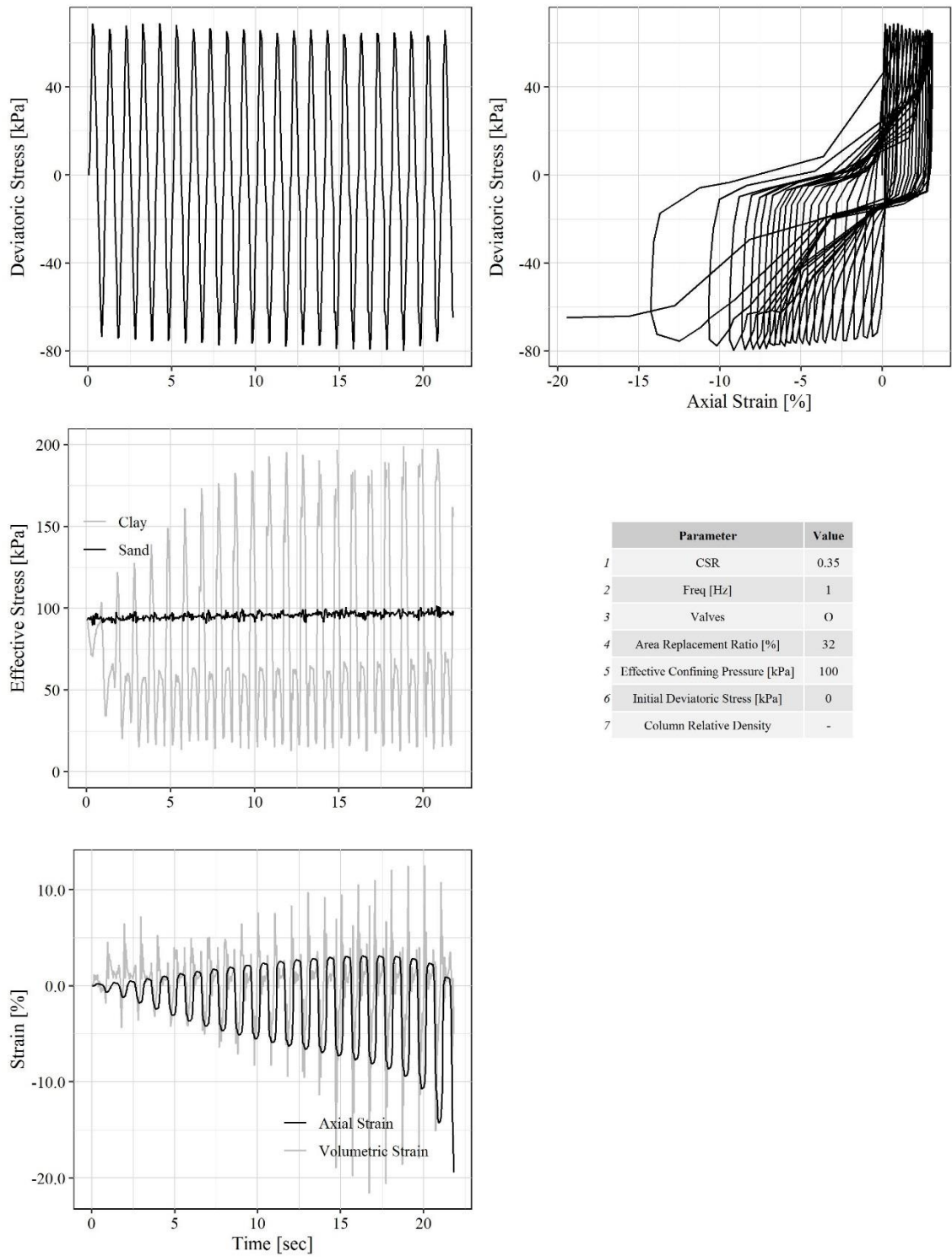
Figure 43. Cyclic triaxial test on reinforced clay specimen: CSR=0.35, T=1sec, valves opened

| | Parameter | Value |
|---|---|---|
| *1* | CSR | 0.35 |
| *2* | Freq [Hz] | 1/10 |
| *3* | Valves | O(t) |
| *4* | Area Replacement Ratio [%] | 32 |
| *5* | Effective Confining Pressure [kPa] | 100 |
| *6* | Initial Deviatoric Stress [kPa] | 0 |
| *7* | Column Relative Density | 86 |
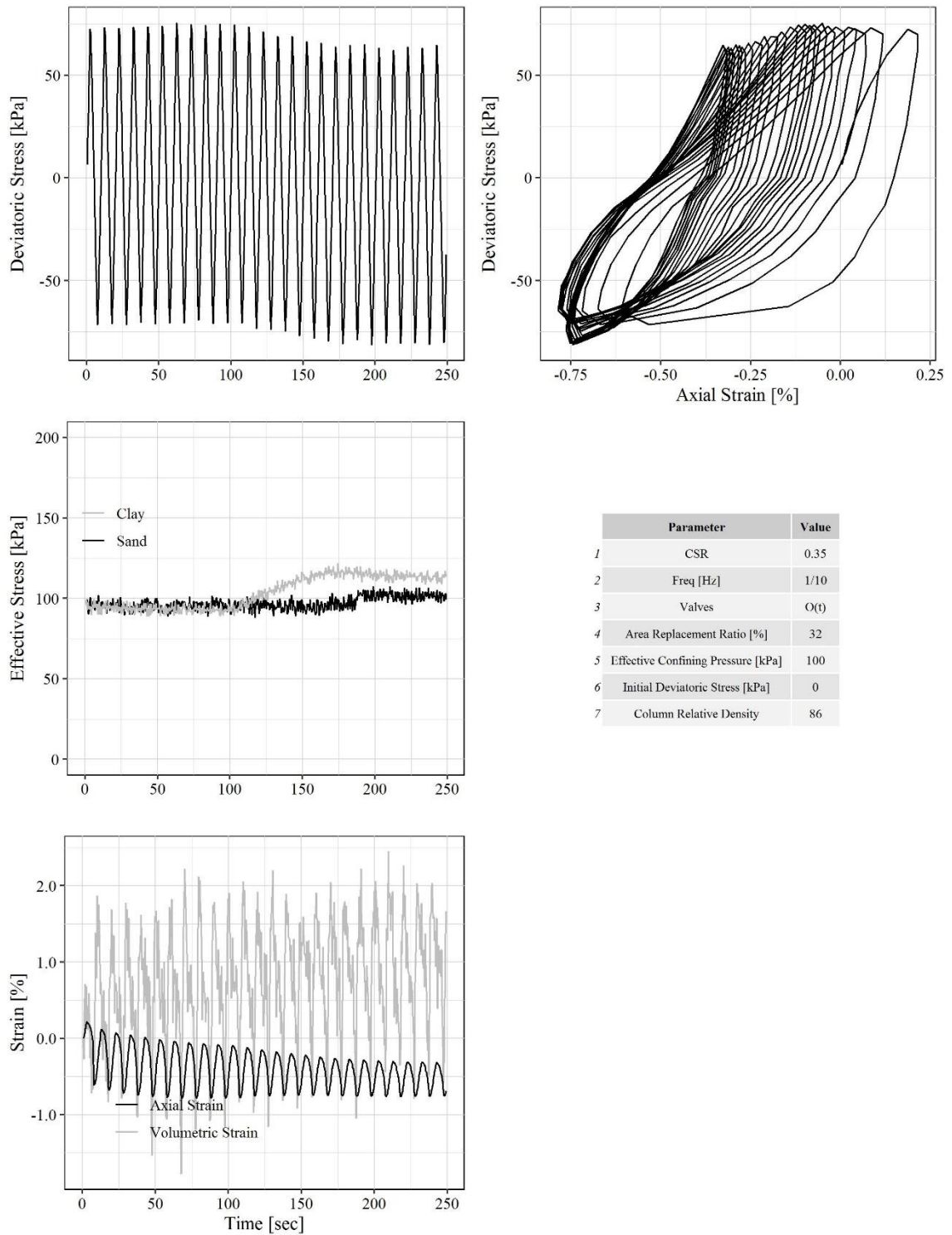
Figure 44. Cyclic triaxial test on reinforced clay specimen: CSR=0.35, T=10sec, valves opened

| | Parameter | Value |
|---|---|---|
| 1 | CSR | 0.35 |
| 2 | Freq [Hz] | 1/300 |
| 3 | Valves | O(t) |
| 4 | Area Replacement Ratio [%] | 32 |
| 5 | Effective Confining Pressure [kPa] | 100 |
| 6 | Initial Deviatoric Stress [kPa] | 0 |
| 7 | Column Relative Density | 86 |
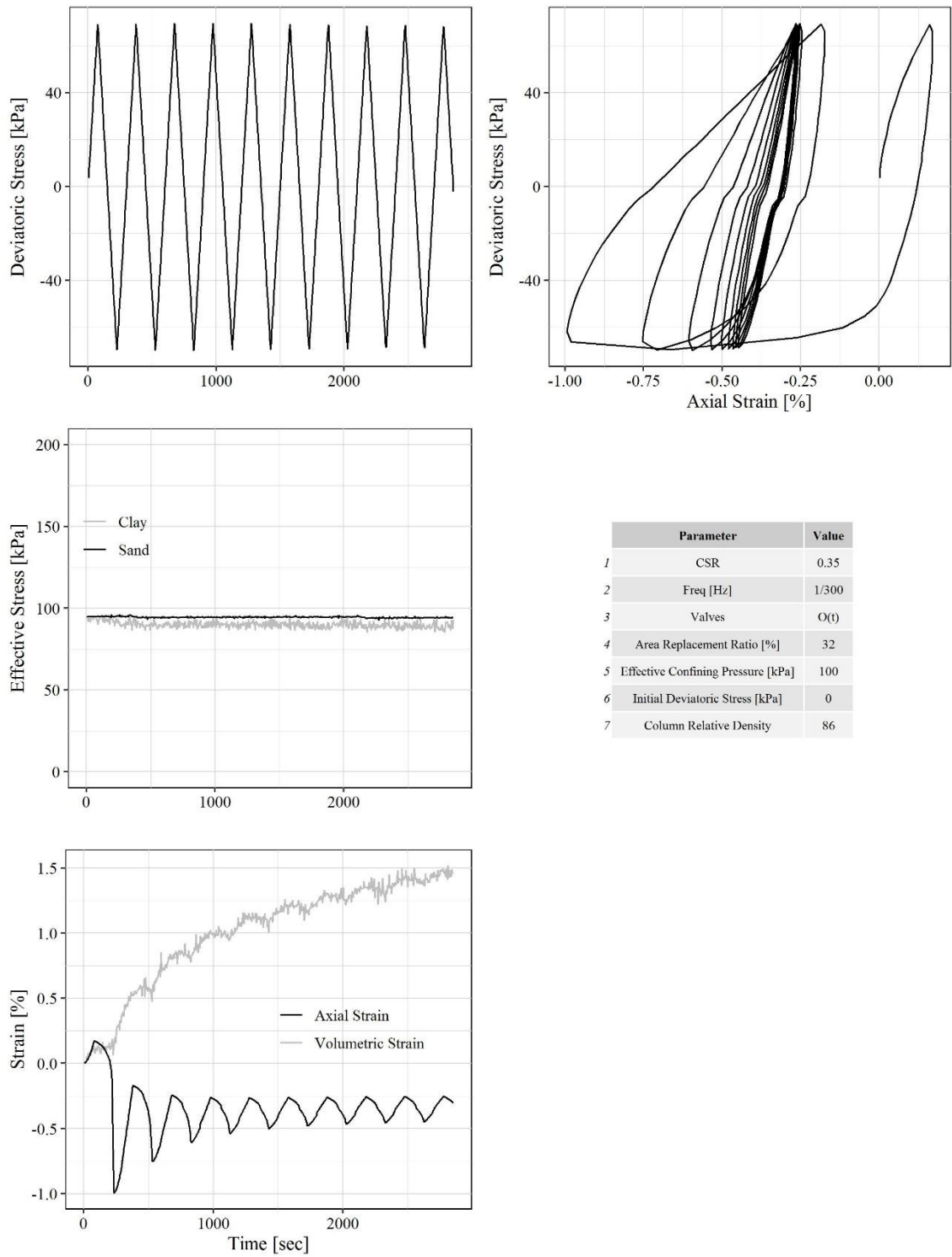
Figure 45. Cyclic triaxial test on reinforced clay specimen: CSR=0.35, T=300sec, valves opened

### 4.1.8 Analysis and Discussion

4.1.8.1 Response of the Ashrafieh clay

Seven cyclic tests were performed at different cyclic stress ratios (CSR=$\tau/\sigma'_{30}$). The cyclic stress ratio were selected based on the reference/corresponding static strength of the clay. From substantial static tests conducted on the Ashrafieh clay at the American University of Beirut (Rayess, 2015) it presents an $s_u/\sigma'_{30}$=0.3. This implies that the undrained shear strength of the clay is 30kPa when the confining pressure is 100kPa. Cyclic stress ratios of 0.2, 0.25, and 0.35 were adopted in the testing program. Figure 46 shows the number of cycles to reach failure versus the loading period (T) for the different cyclic stress ratios used. The number of cycles decreases drastically as the cyclic stress ratio increases from 0.2 to 0.35. This drop appears at all loading periods but with different magnitudes. When the cyclic stress ratio approaches the $s_u/\sigma'_{30}$ of the clay, the number of cycles to failure drops to 1 (CSR=0.35, T=300sec).
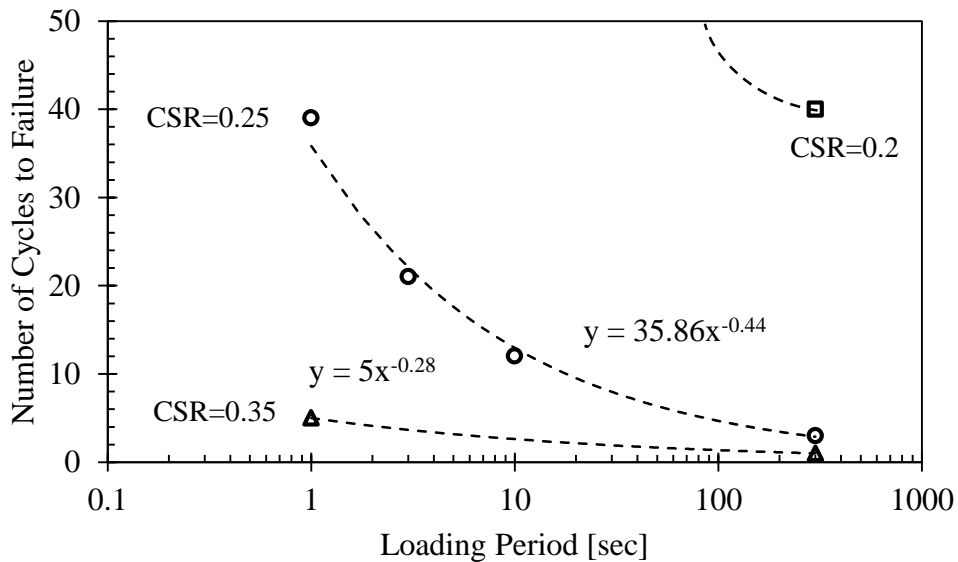


Figure 46. Number of cycles to reach 20% axial strain versus the loading period for the clay tests

The loading period was varied from 1sec to 300sec to investigate the time-dependent response of Ashrafieh clay. This effect can be observed in Figure 46. As can

87

be noticed, the number of cycles to reach failure decreases as the loading period increases. This particularly clear for the tests performed under a cyclic stress ratio of 0.25. The number of cycles decreased from 38 at a loading period of 1sec to only 4 cycles at a loading period of 300sec. Similar trend with a lighter slope is seen for clay tests performed under cyclic stress ratio of 0.35.This behavior is expected for the clay at these loading rates where viscous properties of the material control the behavior.

Practically speaking, this behavior shows that clayey sites can withstand cyclic loading with high frequencies such as earthquake, while it could fail under a lower number of cycles of a loading with similar amplitude but lower frequencies such as emptying and filling of water tanks or silos.

In reference to the generated pore water pressures during the cyclic phase, slow loading tests (loading period =300sec) showed that pore water pressure ratios reached 100% at failure. This is noticed in Figure 25 andFigure 28. However, in faster tests (shorter periods), pore water pressures reached much lower values. This observation is attributed to the unachieved pore water pressure equalization within the specimen during the cyclic phase while the pore pressure sensor measures the pore water pressure at the specimen boundary.

The hysteretic loops for the tests show the degradation of the stiffness modulus ($\sigma_d/\varepsilon_a$) with the number of cycles. An elastic behavior prevails at the initial/earlier cycles after which plastic strains start to develop. This is translated by the widening of the hysteretic loops as the cycles progress. In each cycle, at the beginning of the compression and extension half-cycles, the specimen has a very high stiffness. It degrades in between where the pore pressures show maximum values.

4.1.8.2   Response of the sand specimens

        Six cyclic tests were performed on dense sand specimens with a relative
density of 86% similar to the density of the sand columns used to reinforce clay
specimen. The first three tests (FiguresFigure 29, andFigure 30, andFigure 31) were
performed under cyclic stress ratios of 0.25, 0.3 and 0.35 and a loading period of 1sec
while imposing undrained conditions (closing the drainage valves). The axial strains
double amplitudes did not exceed 0.05, 0.1, and 0.2% under these cyclic stress ratios,
respectively. The development of relatively low pore water pressures was noticed during
early cycles and then reached a steady state. The test pore water pressure ratios did not
exceed 40% in any of the three tests. Hysteretic loops show that the tests under cyclic
stress ratio of 0.2 and 0.25 did not develop plastic strains, however, slight plastic strains
were developed for the tests under a cyclic stress ratio of 0.35.

        In order to investigate the effect of the loading frequency, three additional tests
(Figure 32,Figure 33, andFigure 34) were performed under a cyclic stress ratio of 0.4
and loading frequencies of 1, 10 and 60sec. In these tests, the drainage valves were left
open to check whether the sand will accumulate pore water pressure or will be able to
dissipate all the pore water pressures generated. This was done to replicate conditions in
some of the reinforced specimens which were performed while leaving drainage valves
open. It is noted that at a loading period of 1sec, somewhat larger strains develop at the
initial/early cycles (less than 25) and then oscillate within a narrow range of strains. As
the loading period increases, large strains develop at a lower number of cycles (3 and 1
cycles) and then oscillate within a narrow strain range. This shows that the sand is not
able to dissipate all developed pore water pressures during the cyclic phase at small
loading periods.

4.1.8.3   Response of reinforced specimens

Clay specimens reinforced with 3cm and 4cm sand columns (corresponding to 18% and 32% area replacement ratios, respectively) were tested under the same boundary conditions as the control clay specimens. The effect of the loading period was investigated while allowing or blocking drainage path to study the effect of the drainage on the response of the reinforced clay. Reinforced specimens with area replacement ratios of 18 and 32% for tests where drainage out of the sample is not allowed, have a shear strength of 40kPa and 75kPa respectively, under an initial confining pressure of 100kPa. A cyclic stress ratio of 0.35 which is equivalent to 35kPa shear stress at a confining pressure of 100kPa is adopted in the cyclic tests. Figure 47 shows the number of cycles to reach 20% axial strain with the loading period for reinforced clay specimens performed while closing drainage valves. The results for the clay specimens are also displayed for comparison.
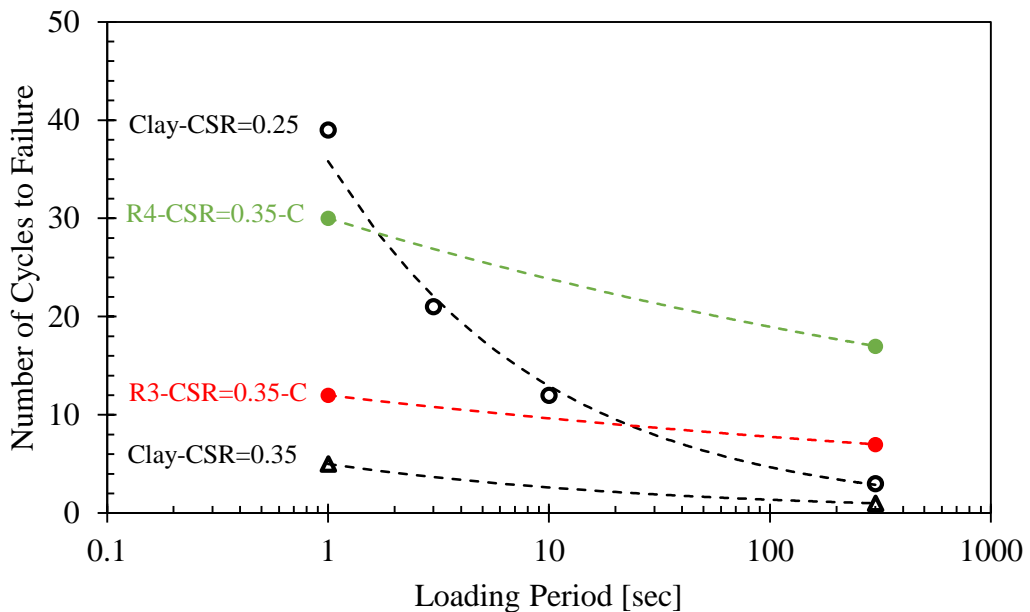


Figure 47. Number of cycles versus the loading period for clay and reinforced specimens performed while imposing global undiraned conditons.

A decreasing trend in the number of cycles is noticed as the loading period increases. For the specimens reinforced with 3cm and 4cm sand columns, the number of cycles decreased from 12 to 7 and from 31 to 20 respectively, as the loading period increased from 1 to 300sec. This drop is attributed to the decrease in the clay strength with loading period as a can be seen from the control clay behavior. Pore water pressures within the clay and the sand in the reinforced specimens were oscillating in phase, with slightly larger values in the sand zone than that in the clay zone. It is possible to have some homogenization of the pore water pressures taking place at the top cap interface with the specimen. This hypothesis is supported by the fact that in the control clay specimens, pore water pressures were only positive and no negative pore pressures were generated during the extension half cycle while in the reinforced specimens, the generated pore water pressure in the clay followed the pattern of pore pressure generated in the sand. The hysteretic loops for the reinforced specimens had an inverted "S" shape similar to what is typically encountered with sand specimen. This inverted "S" shape results from having the maximum positive pore water pressures taking place around zero deviatoric stress in both the extension and compression half cycles. The peaks in the inverted "U" shape in the effective stress versus time plot locates aligns with the zero deviatoric stress as shown in by the red lines in Figure 48.

Comparing the control clay and the reinforced clay results under a cyclic stress ratio of 0.35, we can notice that the reinforced specimens required larger number of cycles to reach 20% axial strain. At a loading period of 1sec, clay specimen required 4 cycle to reach failure however, 11 and 31 cycles are required for the specimens with area replacement ratio of 18 and 32% respectively.

| | Parameter | Value |
|---|---|---|
| 1 | CSR | 0.35 |
| 2 | Freq [Hz] | 1/300 |
| 3 | Valves | C |
| 4 | Area Replacement Ratio [%] | 32 |
| 5 | Effective Confining Pressure [kPa] | 100 |
| 6 | Initial Deviatoric Stress [kPa] | 0 |
| 7 | Column Relative Density | - |
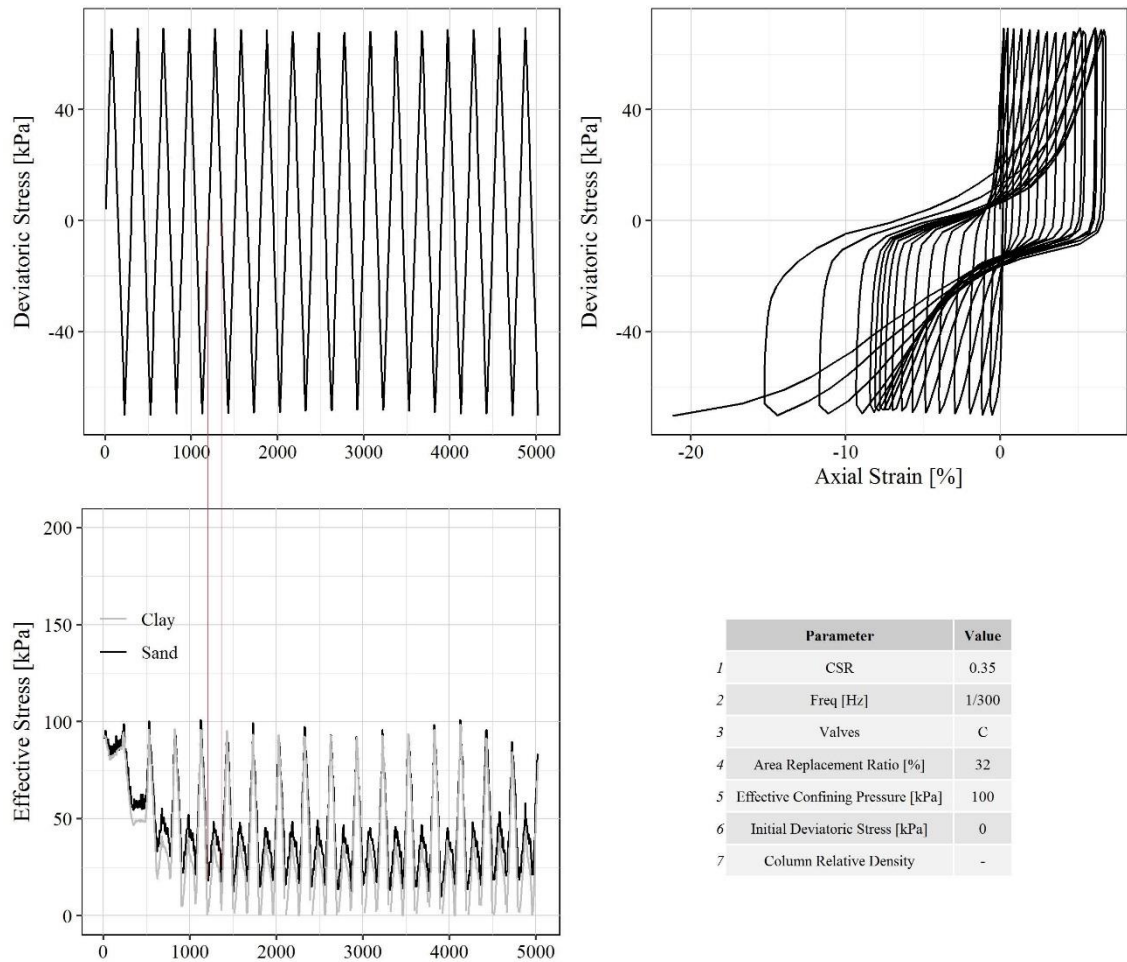
Figure 48. The location of the minimum effective stress (maximum pore water pressures) with respect to the deviatorc stress causing the inversted "S" shape in the hysteretic loops.

On the other hand, the results of the tests performed on reinforced specimens while keeping the drainage valves opened showed different behavior than when drainage vales were closed. Figure 49 shows the number of cycles required to reach 20% axial strain versus the loading period. For comparison, the figure contains the results of the previous tests (control clay and reinforced clay with closed drainage valves).

92
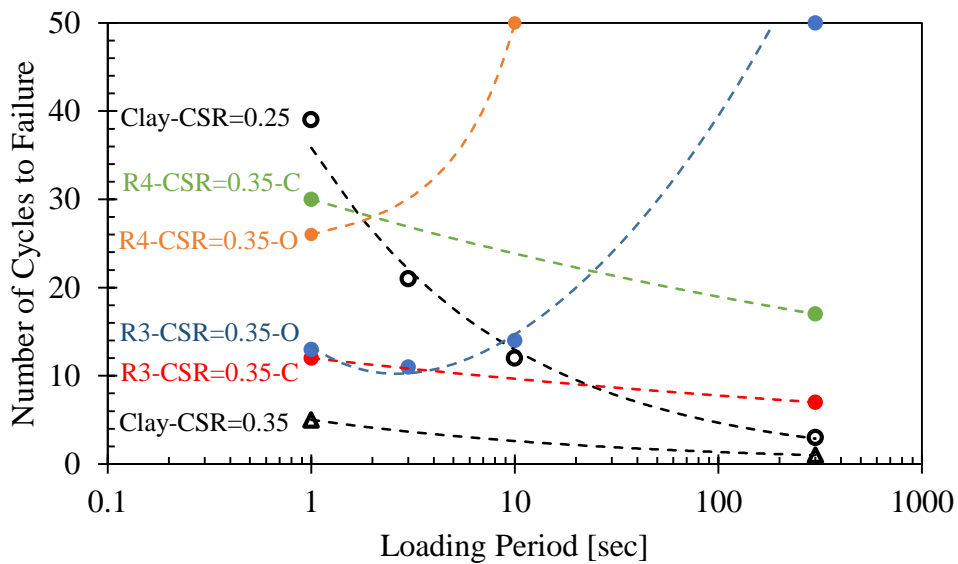
Figure 49. Number of cycles to reach 20% axial strain versus loading period for contorl clay and all reinforced clay tests.

The tests performed with opened drainage valves started at approximately the same number of cycles as the tests performed with closed valves at the loading period of 1sec. However, tests performed with both area replacement ratios have an increasing trend as the loading period increases. This is because the sand has a partially drained behavior at small loading periods (1sec) and as the loading period increases, it approaches the fully drained response. This is reinforced by the sand tests that were performed while keeping drainage vales opened at different loading periods. Additionally, the clay experienced different levels of partial drainage as the loading period increased. This is manifested by the increase in pore water pressure measured by the sensor connected to the clay zone. Barron 1948 approach (Figure 50), though developed for sand drains, it could explain the response of the clay in our case. The degree of consolidation for the 18% and 32% specimens are plotted versus time in Figure 51.

$U_r$ = Average Degree of Radial Consolidation

$$U_r = 1 - \exp\left(\frac{-8T_r}{m}\right) \quad \textbf{Barron (1948)}$$

$$m = \left(\frac{n^2}{n^2-1}\right)\ln(n) - \frac{3n^2-1}{4n^2}$$

$$n = \frac{d_e}{2r_w} \qquad \begin{array}{l} d_e = \text{Effective Diameter} \\ r_w = \text{Sand Drain Radius} \end{array}$$

$$T_r = \frac{c_{vr}t}{d_e^2} \qquad \begin{array}{l} c_{vr} = \text{Coefficient of Radial Consolidation} \\ T_r = \text{Time Factor for Radial Consolidation} \end{array}$$

$$c_{vr} = \frac{k_h}{\left[\dfrac{\Delta e}{\Delta\sigma'(1+e_o)}\right]\gamma_w}$$

$k_h$ = Coefficient of Horizontal Permeability
$T_r$ = Time Factor for Radial Consolidation
$e_o$ = Initial Void Ratio
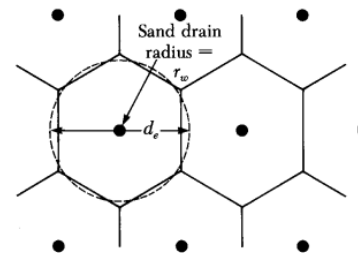
**Plan View – Sand Drain Triangular Spacing**
**Figure 7.30.** Das FGE (2006).

Figure 50. Barron 1948 radial drainage solution for a unit cell.
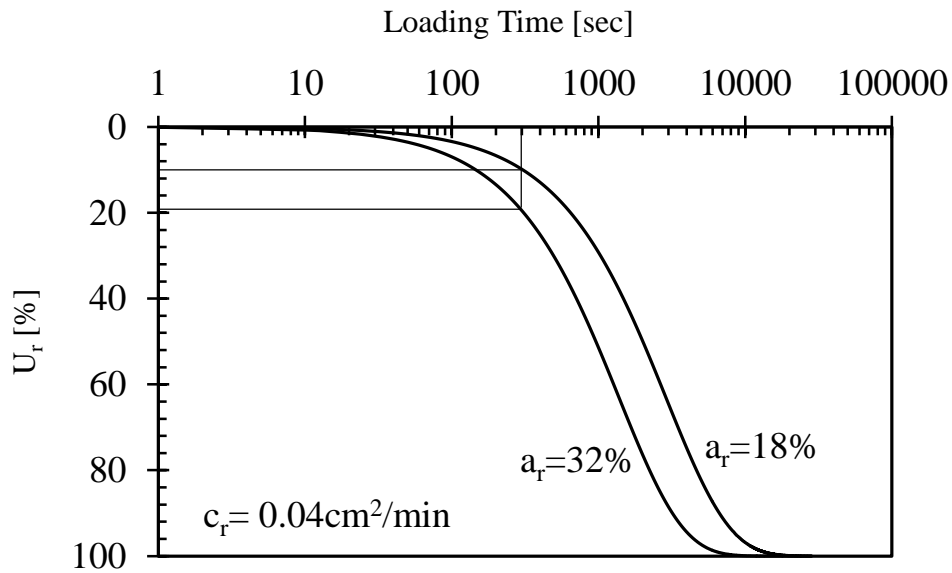


Figure 51. Degree of consolidation versus time for the 18% and 32% reinforced clay specimens.

It can be noticed that the specimens required more than 1000sec to reach 50% average degree of consolidation. This confirms that the clay never reach fully drained conditions at the loading periods adopted in the testing program.

94

### 4.1.9  *Conclusion*

The presence of sand columns improves the cyclic resistance of clays. This improvement depends on whether the sand column has the time to dissipate the load-induced pore water pressure. The loading period is an influential parameter to account for in the design of system that involve repeated loading patterns. At large loading periods, the clay will have lower cyclic resistance while the sand will have longer duration to dissipate pore pressure build-up. The viscous properties of the clay govern the cyclic behavior under fast loading rates. The behavior of the sand column as drained or undrained is important for quantifying the degree of improvement attained. The cyclic resistance increases for the composite specimens as the loading period increases if the sand is allowed to drain. However, if undrained conditions are imposed, the cyclic resistance will decrease as the loading period increases. This implies that the positive effect of drainage overcomes the negative effect of clay viscous behavior.

## 4.2 Anisotropically Consolidated stress State

### 4.2.1 Abstract

Soil elements located at the toe of natural slopes and/or embankments are subject to extension stresses. This initial stress state is critical particularly when the elements are exposed to cyclic loading due to a seismic event. Using granular columns as a ground reinforcement and improvement alternative for clayey subgrades/natural soils is considered as an effective mitigation option to improve short and long term static stability, and increase the resistance to seismically-induced stresses. This paper investigates the effect of columnar granular inclusions on the cyclic resistance of anisotropically consolidated clay samples. Stress-controlled triaxial tests were conducted on both "control" and sand-column reinforced samples at a range of cyclic stress ratios. The effect of varying the density of the sand column inclusions is also explored as part of the testing program. Test results are analyzed and presented showing significant improvement due to the presence of the reinforcing columns along with a pronounced effect of the density of the inclusions.

### 4.2.2 Introduction

The stability of natural and man-made slopes is one of the enduring challenges in geotechnical engineering. Different triggering mechanisms have been associated with slope instability and failures. The roots of instability can be broadly categorized in two main groups. The first is associated with a decrease in soil strength and the second with an increase in the applied load. The latter can be further sub-divided into increases in static, or cycled loading or combination of both. In fact, it is typical for slope failures to be the result of a combination of driving causes rather than be instigated by simply one factor.

In marginally-stable slopes, soil elements along a potential slip surface experience different states of stress. Soil elements at the top of the slope are loaded in compression while elements at the toe are subjected to extension forces. Figure 52 shows a section of a slope with schematics of stress states on elements at the crest and at the toe. These initial anisotropic stress states can be critical, particularly when the slope is subjected to a seismic event. For clayey slopes, (Duncan, Wright, & Brandon, 2014) differentiated between two types of anisotropy that affect clay strength. Inherent anisotropy which is due to the plate-shaped clay particles, and stress state-induced anisotropy which is a result of the geometry of the slope. In limit equilibrium analyses, failure is assumed to occur simultaneously along the totality of the slip surface; however, in reality failure initiates at the weakest points and then progresses due to redistributed stresses. This phenomenon was termed as "progressive failure" in (Kramer, 2005).

Significant research efforts have been directed at investigating the response of clays subjected to cycled/repeated loading patterns. The main areas of exploration were related to (1) the effect of clay plasticity and overconsolidation ratio on modulus degradation, damping and cyclic strength, (2) pore water pressure build-up due to cyclic loading, (3) loading rate and initial stress effects, (4) threshold cyclic shear stresses and (5) post-cyclic strength. (Andersen, 1980) investigated the effect of the overconsolidation ratio on the cyclic strength of undisturbed clays. They concluded that overconsolidated clays required fewer load cycles to reach failure when compared to normally consolidated clays. (Procter & Khaffaf, 1984) showed that as the frequency of cyclic loading increases, the cyclic strength of the clay increases. (A. Ansal, Iyisan, & Yıldırım, 2001) studied the presence of a threshold cyclic shear stress below which no

excess pore water pressure is generated. (Hyodo et al., 1996) investigated the effect of initial shear stresses on the response of highly plastic clay. They found that the cyclic strength decreases as the initial shear stress increased. (Hanna & Javed, 2008) showed that partially drained samples required larger number of cycles to failure when compared to undrained conditions. More recently, (Beroya et al., 2009) investigated the influence of clay mineral type on the cyclic resistance. They observed that for the same plasticity index (PI), Montmorillonite had the largest strength when compared to Illite and Kaolinite. A more extensive literature about the response of clays to cyclic loading can be found in (Nieto-Leal & Kaliakin, 2013).
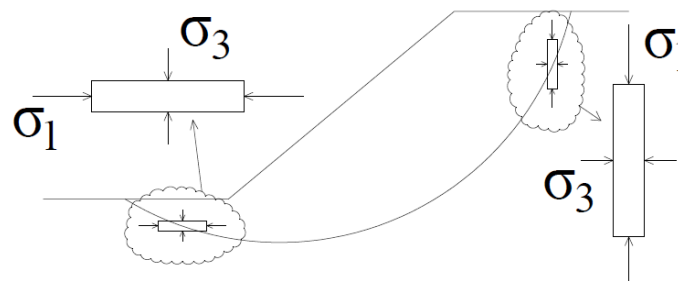


Figure 52. Stress state at the toe of a slope

The effectiveness of granular/stone columns has been the subject of substantial research. (J. Baez & Martin, 1993) assumed shear strain compatibility between the native soil and the stone column and developed a procedure to quantify the improvement taking into consideration the densification, drainage and stress redistribution effects. (Goughnour & Pestana, 1998) suggested that stress reduction is over-estimated by the available design approaches and included the effect of slenderness of the column in calculating the stress redistribution/reduction factor. (Adalier et al., 2003) relied on centrifuge testing to study the influence of stone columns on the liquefaction resistance of non-plastic silts. (M. Madhav & Krishna, 2008) investigated

various mechanisms of improvement resulting from the inclusion of stone columns in granular soils. More recently, (Ashour, 2016) studied the effect of loading frequency and cyclic stress on soft clays reinforced with stone columns for railway track foundation applications. It was found that the inclusion of stone columns at an area replacement ratio of 7% only slightly increased the cyclic resistance of the composite mass, but had the positive effect of reducing permanent strains. Rayamajhi et al. (2016) used non-linear three-dimensional finite element analyses to investigate the effect of stone columns as shear reinforcing elements in liquefiable ground. Their results showed that the columns had a non-compatible mode of deformation with the surrounding soil and as a result, the reduction in cyclic stress ratio (CSR) was much less than that estimated from conventional design approaches.

In this section, the effect of columnar sand inclusions on the cyclic response of mildly anisotropically-consolidated clay samples is investigated in a laboratory set-up. The initial stress state adopted in the testing program represents conditions at the toe of a marginally-stable slope. In order to demonstrate the significance of the initial stress state on the cyclic strength of clays, results from the current study of two cyclic triaxial tests on clays with a CSR of 0.25 are shown in Figure 53. In test (a), the sample was isotropically-consolidated while in test (b), the sample was anisotropically-consolidated to reproduce a stress state typical of an element at the toe of a slope. It is clear from the response shown that the anisotropically-consolidated sample required a lower number of load cycles to reach failure when compared to that needed by the isotropically-consolidated specimen. Furthermore, the sample in test (a) failed in compression while in test (b), the sample failed in extension. It should be noted that the particular initial anisotropic stress state used in our study, in which the major principal plane is the

vertical plane, can be best reproduced in a triaxial setup.

In the balance of the work presented in this section, the effects of the presence of columnar granular inclusions of different densities in a saturated clay soil, consolidated under anisotropic initial conditions are explored. To this end, eleven cyclic stress-controlled undrained triaxial tests were performed on "control" and "sand-column reinforced" clay samples loaded at different cyclic stress ratios. The degree of the improvement observed in the response of the composite system was found to be closely correlated with the density of the sand column inclusion.
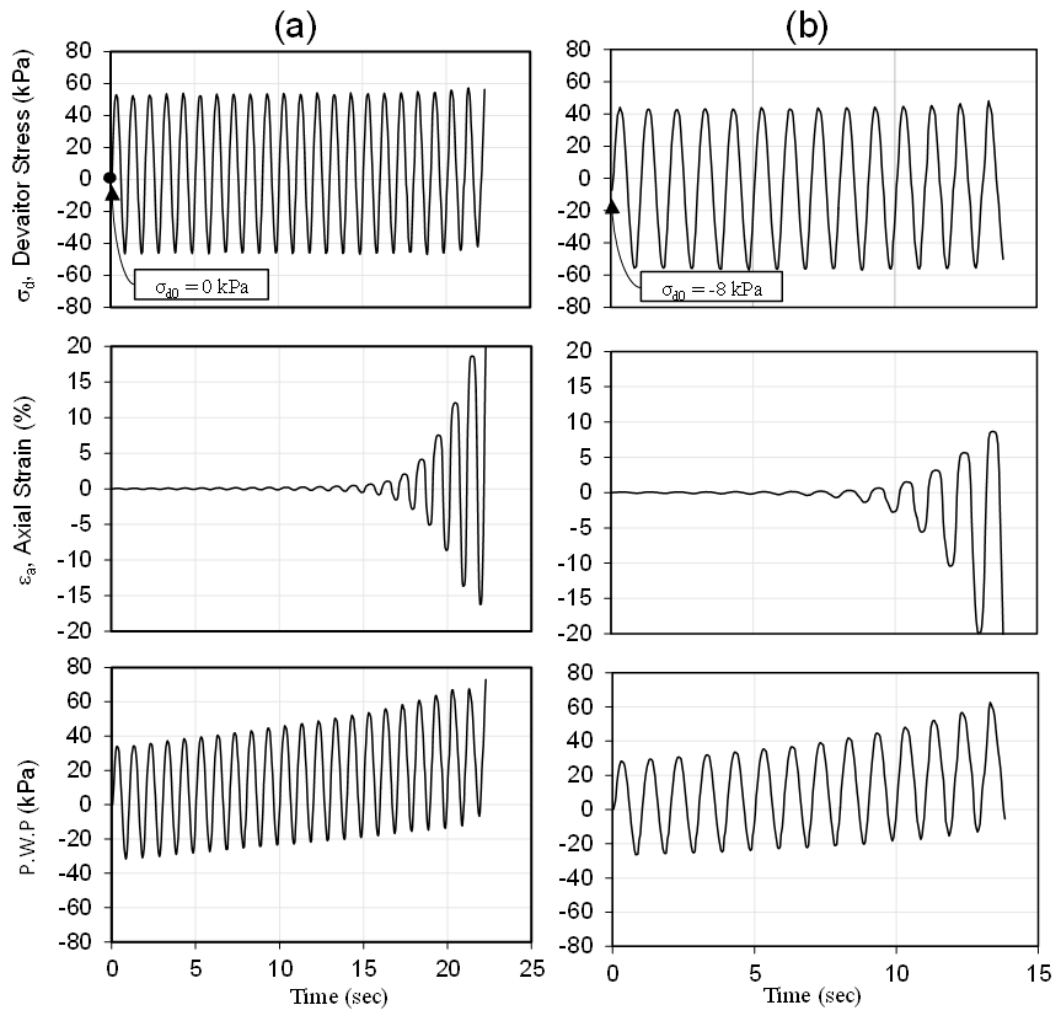


Figure 53. Cyclic triaxial test on (a) isotropically-consolidated and (b) anisotropically-consolidated clay samples

100

### 4.2.3 Testing

#### 4.2.3.1 Apparatus

The updated CKC Automated Triaxial Testing System was used to conduct stress-controlled cyclic tests on anisotropically-consolidated specimens. A full description of the apparatus is presented in chapter 5.

#### 4.2.3.2 Material

A local soil (Ashrafieh Clay) was used as the "native"/natural matrix material in all the tests. This soil was sourced from a construction site in Beirut, Lebanon. This clay has a c/p ratio of about 0.30; thus the undrained strength at 100kPa confinement is ~30kPa. Ottawa sand (C 109) was used as the reinforcing granular soil. The relevant geotechnical characteristics of the matrix clay and reinforcing sand are given in Table 5 Table 6, respectively.

#### 4.2.3.3 Testing Procedure and Program

Similar procedure as described in previous section is adopted here. Saturated sand columns were prepared via freezing at densities of 17.0, 16.5, and $16.2kN/m^3$ for dense (D), medium dense (MD), and loose (L) granular columns respectively. Table 7 summarizes the set of tests performed.

Table 7. Testing program

| Test | CSR | Column Density |
|------|-----|----------------|
| 1 | 0.2 | - |
| 2 | 0.25 | - |
| 3 | 0.35 | - |
| 4 | 0.25 | D |
| 5 | 0.35 | D |
| 6 | 0.45 | D |
| 7 | 0.2 | MD |
| 8 | 0.25 | MD |
| 9 | 0.3 | MD |
| 10 | 0.25 | L |

After placing the specimens in the triaxial chamber, the samples were back-pressure saturated and reconsolidated anisotropically under 100kPa±2kPa lateral pressure and 90kPa±2kPa vertical pressure (i.e. $\sigma_{d0} \approx$ -8kPa) for 24 hrs. Once the consolidation phase was completed, sinusoidal stress-controlled loading under undrained conditions was performed with different cyclic stress ratios (CSR = $\sigma_d/2\sigma_c$) to replicate possible field excitations. Totally, eleven tests were performed, three of which were on control samples and eight on reinforced samples, all reaching 20% axial strain. The loading frequency adopted was 1Hz.

### 4.2.4    Test Results and Analyses

4.2.4.1    Effect of Reinforcement

Excess pore water pressure and axial strain versus time plots were generated for each of the triaxial tests. Results of control and reinforced clay samples with medium dense and dense sand columns are presented in Figure 55Figure 56Figure 57, respectively. It is clear from the results presented that, for all test conditions and as expected, as the CSR increased, the number of cycles to failure decreased. It was also

observed that all samples failed in necking, at a distance of roughly one diameter from the top as shown in Figure 54.

The inclusion of a sand column had three main effects on the recorded response of the composite specimen tested. First, it was noticed that a larger number of cycles was needed to reach failure when samples were reinforced, when compared to unreinforced samples tested at the same CSR. Second, although pore water pressure measurements are not representative of the actual pore pressures in the sample due to high loading rates, they are suggestive of a major difference between control and reinforced samples. Generated pore water pressures in control clay samples did not exceed 60% of the confining pressure whereas in reinforced samples pore water pressure ratios reached 100%. Finally, focusing on early cycles, it was noticed that reinforced samples exhibited higher stiffnesses, as compared with unreinforced specimens.

The number of cycles to reach 5% and 20% axial strains for all the samples tested at every CSR is presented in Figure 58. The positive effect of the presence of the sand column is clearly seen as an increase in the cyclic resistance. This increase becomes more significant as the axial strain increases. For example, under a number of cycles of 20, the cyclic stress ratio needed to reach 5% and 20% axial strains increases from 0.23 for unreinforced soil to 0.27 and 0.31 for samples reinforced with dense columns, respectively.

103

Figure 54. Necking failure for a clay sample reinforced with sand column
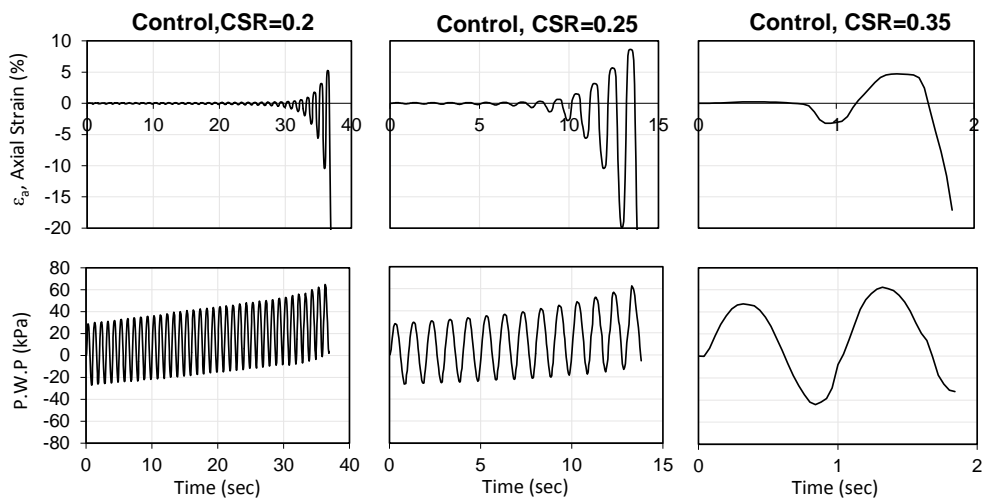


Figure 55. Cyclic tests results from control clay samples
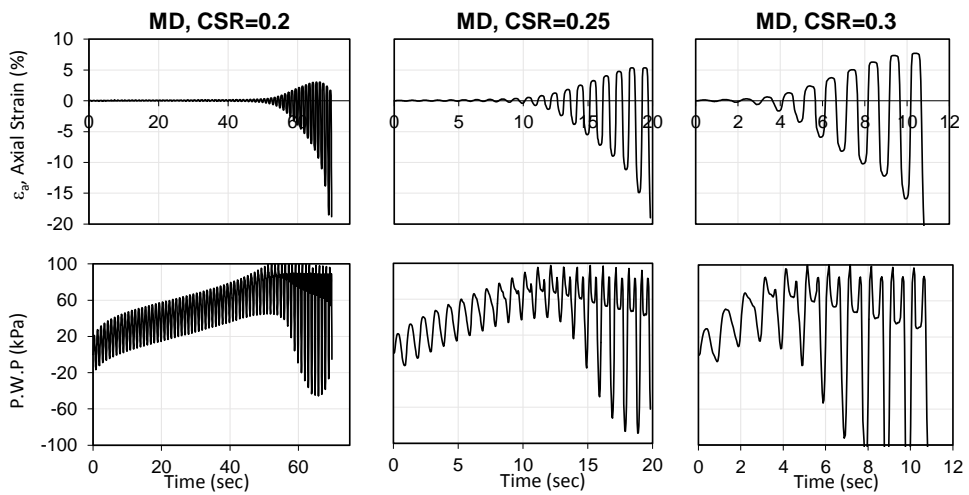


Figure 56. Cyclic test results for samples reinforced with medium dense columns
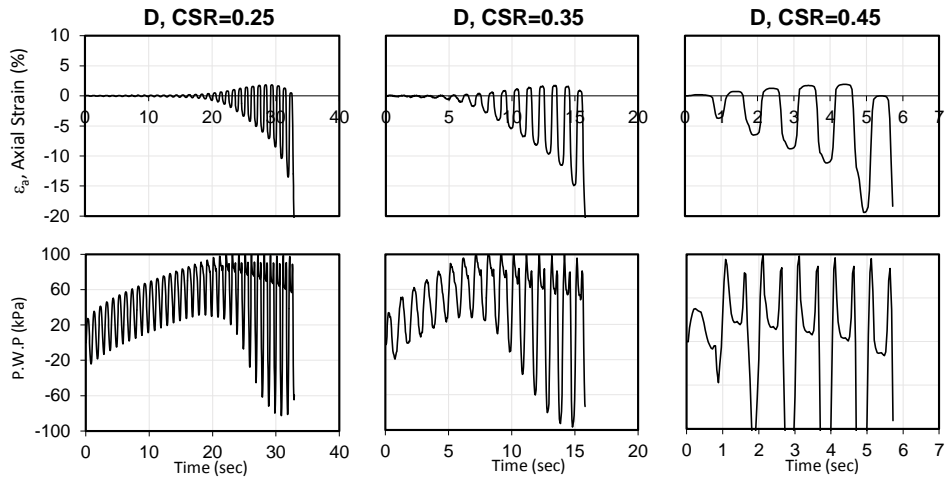
Figure 57. Cyclic test results for samples reinforced with dense columns
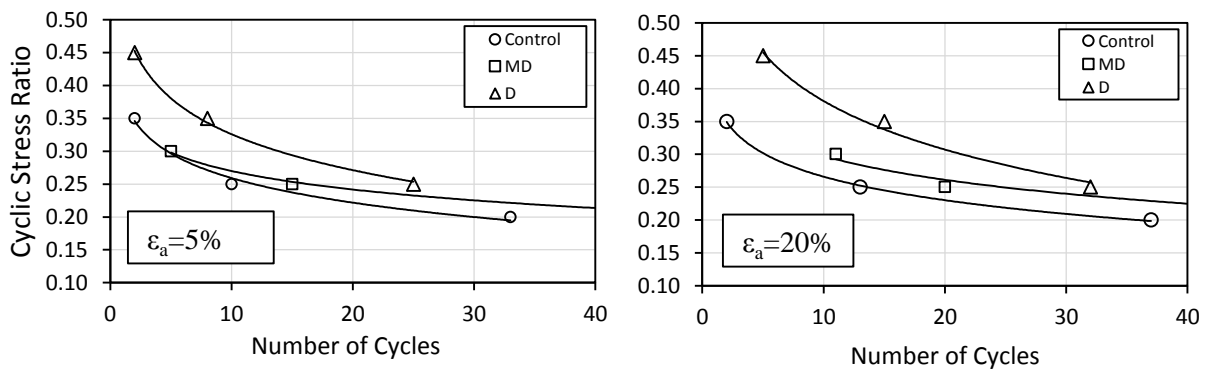


Figure 58. Required number of cycles to reach 5% and 20% axial strains

For the reinforced samples, it was noticed that at low strains, pore water pressures oscillated in phase with the applied deviatoric stress along an increasing trend line. The slope of this line was found to increase with increasing cyclic stress ratio and decreasing column density. However, at large strains, double-peak cycles appeared which may be attributed to the dilative tendency of the sand column.

## 4.2.4.2  Effect of Column Density

In an effort to further investigate the effect of column density, one additional test was performed at a cyclic stress ratio of 0.25 on a clay sample reinforced with a loose sand column. Figure 59 shows the axial strain and generated pore water pressure

varying with time. The results of the tests at a CSR of 0.25 for the three sand column

densities are summarized in Figure 60a. The effect of the column density on the

observed responses and consequently on the efficacy of the improvement, is clear.

Installing a relatively loose column will lead to no improvement when compared to the

unreinforced soil.
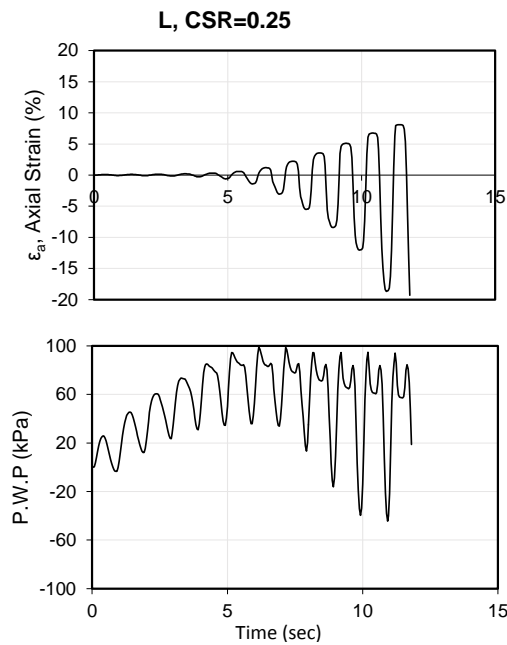


Figure 59. Cyclic test on clay reinforced with loose sand column.
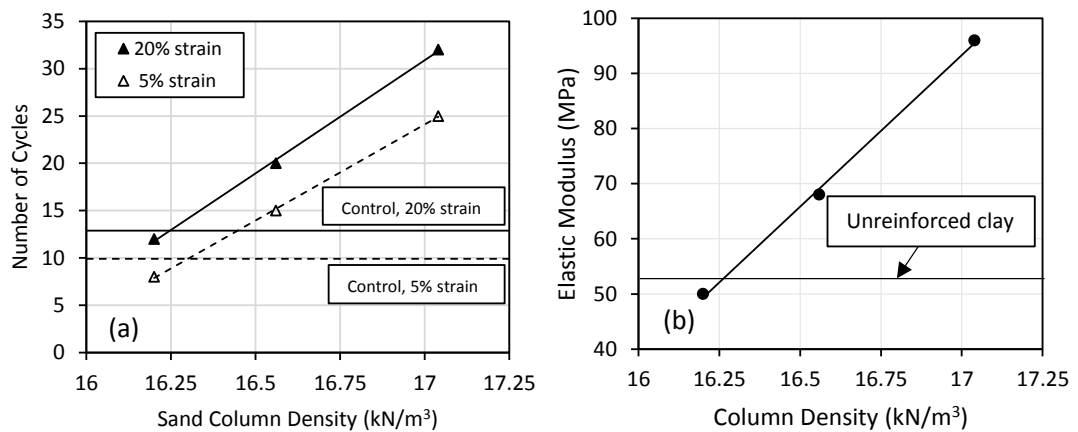


Figure 60. (a) Variation of number of cycles to reach specific strains with column
density; (b) Low strain elastic modulus vs. column density

106

Figure 60b shows the variation of the initial elastic modulus of the composite samples as a function of the column density. The elastic modulus of the samples reinforced with dense sand columns almost doubled when compared with that for the control clay. Conversely, using a loose sand column resulted in no improvement of the stiffness of the composite system.

4.2.4.3    Comparison with design methods

Due to the difference in stiffness between the sand column and the surrounding clay, it is expected to have non-uniform stress distributions across the composite sample. To estimate the CSR "felt" by the sand column and that sensed by the clay at small strains, relationships could be developed based on the assumption of compatibility of strains between the sand and clay and are presented in the following equations:

$$\frac{CSR}{CSR_s} = \frac{1}{E_r} + a_r(1 - \frac{1}{E_r}) \tag{25}$$

$$\frac{CSR}{CSR_c} = 1 + a_r(E_r - 1) \tag{26}$$

where $E_r$ is the ratio of the elastic modulus of the sand, $E_s$, to that of the clay, $E_c$. The area replacement ratio $(A_s/A_t)$ is expressed as $a_r$, and $A_s$ and $A_t$ are the sand column and total area of the sample respectively. For the conditions adopted in our testing program, the CSRs felt by the sand column and the clay matrix are expected to be respectively larger and smaller than the applied CSR.

Available design tools/approaches proposed by (J. Baez & Martin, 1993) and (Rayamajhi et al., 2013) for the estimation of the field response of clays with granular columns were compared with the results obtained from the testing program. The

107

comparison was based on the reduction factor ($K_G$) which should be calculated in the

elastic range of the materials and is defined as:

$$K_G = \frac{\tau_s}{\tau} = \frac{CSR_c}{CSR} \tag{26}$$

where $\tau_s$ is the shear stress felt by the soil in the reinforced ground, $\tau$ is the shear stress

felt by the soil in the unreinforced ground, $CSR_c$ is the cyclic stress ratio felt by the clay

in the reinforced samples and calculated using Equation 2, and $CSR$ is the average

cyclic stress ratio applied on the soil sample. Figure 10 shows the CSR required to reach

0.2% double amplitude in a given number of cycles for the control and reinforced

samples with dense sand columns. In the range of this specific strain, it is stipulated that

the clay and sand may still be roughly considered to exhibit an elastic behavior.
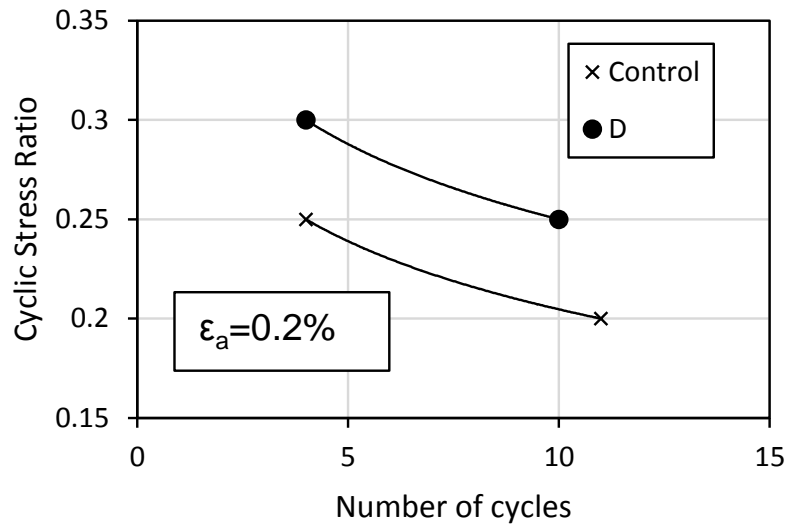


Figure 61. Cyclic stress ratio to reach 0.2% double amplitude strain with number of
cycles

For a number of cycles of 4, the CSR needed to reach 0.2% strain is 0.3 for the

sample. Using equation 2, the CSR felt by the clay is estimated to be $CSR_c$=0.2. $E_s$=200

MPa, $E_c = 53MPa$, $\vartheta_c = 0.5$, $\vartheta_s = 0.5$, and $a_r = 17\%$ were assumed in the

calculation, where $\vartheta_c$ and $\vartheta_s$ are Poisson's ratio for the clay and sand respectively. The

selection of Poisson's ratios was based on the fact that the cyclic tests were undrained constant-volume tests. This results in a reduction factor of $K_G$ ~0.66 using Equation 3. Field stress reduction factors of 0.67 and 0.91 were obtained from (J. Baez & Martin, 1993) and (Rayamajhi et al., 2013) respectively. It is notable that the reduction factor obtained from the testing program and that from (J. Baez & Martin, 1993) are comparable, since they are both based on the same assumptions, whereas the other approach resulted, as anticipated, in higher reduction factor due to the non-compatible deformation effects. Also it is worthy to note that the resultant reduction factors from these two methodologies were not significantly sensitive to the assigned Poisson's ratio values for both sand and clay.

### 4.2.5   *Summary and Conclusions*

The stress state-induced anisotropy in slopes has a significant effect on the strength of soil elements along the slip surface. This paper investigated the reinforcing effect of columnar inclusions on the cyclic response of anisotropically-consolidated clays in a laboratory framework. The results showed that the reinforcement of clay in this weakened initial stress state with sand columns increases their cyclic resistance and low-strain elastic moduli. This effect can be attributed to higher stiffness and dilative tendency of the reinforcing column material. The results of the testing program indicated that columns should be installed in a relatively dense state in order to guarantee any significant improvement. Due to similar mechanistic behavior, the reduction factors obtained from the testing program were closer to reduction factors obtained from design approaches that assume compatible deformations.

However, the following limitations still hinder the application of these

results/observations at field-scale, and should be taken into consideration in future research:

1. Non-compatible deformations between the column and surrounding soil are present in the field and cannot be reproduced in conventional small-scale laboratory setups.

2. The use of sand columns to represent granular columns leads in some cases to the generation of pore pressure ratios ~100% in the laboratory experiments. Such may not be the case in the field, where pore pressure dissipation from the granular columns is more efficient.

3. Typical triaxial loading mechanism results in a stress path that differs from what a soil element is ideally subjected to during a seismic event (assumed to be simple shear).

Based on that, additional research is required to investigate more realistically the response of columnar inclusions-soil systems. This might include large scale or centrifuge tests aided by image processing and tomographic techniques to track boundary deformation of the inclusions and have a decisive output about the degree of shear strain compatibility between the column and the soil.

# CHAPTER 5

# UTILIZATION OF IMAGE PROCESSING TO MONOTIR RADIAL DEFORMATION

## 5.1    Introduction

Image processing technique was increasingly utilized in the past five decades in many engineering research applications. It proved to be a reliable tool in tracking the motion of marked targets (soil particles), monitoring deformation of continuums, locating plane of shear failure, and measuring volume change of soil samples during consolidation and/or shearing.

(Gachet, Geiser, Laloui, & Vulliet, 2006) presented an image processing technique for volume change measurement during triaxial testing. Images collected by Kodak DVC 300 Camera were first enhanced (improved contrast) binned (black and white), and black-hole filled. A special filter was used to capture the edge of the specimen. Vertical calibration was assumed to be linear. In the horizontal direction the authors approximated the relation between pixels and radial distances using simple linear and second order function. They validated their approach with test on dummy sample. In their approach, a fitted model was used to account for the refraction effects. The resulting absolute measurement error over the specimen volume was 1.26%.

(Macari, Parker, & Costes, 1997) presented a pioneering procedure for measuring volume change during triaxial testing while correcting for distortion due to refraction. Both 2-dimensional and 3-dimensional models were described and validated through experimental results.

(Lenoir, Bornert, Desrues, Bésuelle, & Viggiani, 2007) used 3-D digital image correlation technique for X-ray images for an argillaceous rock specimens subjected to displacement-controlled triaxial shearing to detect the onset of shear strain localization.

The major advantage of using image processing to track sample deformation is that it can replace LVDT's and provide data with comparable accuracy. All this can be done without going into worrying about sensors installation, data acquisition, and calibration processes.

From an optical point of view, infinite light rays emerge from each point of the samples surface (membrane surface) as shown in the figure below. These rays are diffused in all directions in the water surrounding the samples. When a ray reaches the water-plexi interface, it follows refraction rules and deviates from its initial direction. This processes is repeated on the plexi-air interface. Theoretically speaking, by placing a camera in front of the sample, only one light ray passes through its pinhole and it is projected on the image plane Figure 62.
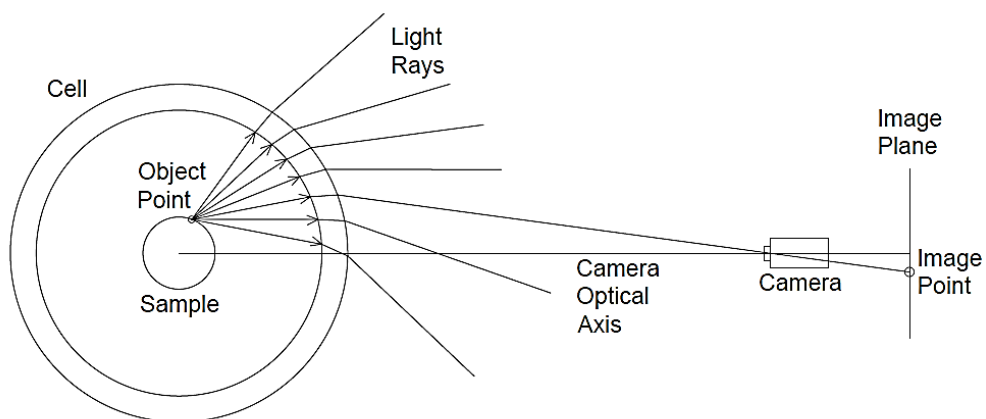


Figure 62. Layout of triaxial cell and camera

The principle of reversibility of light states that light will follow exactly the same path if its direction of travel is reversed. Based on that, we can start from a ray defined by the line connecting the image point and the pinhole of the camera. This light

112

ray will eventually reach the corresponding object point on the sample. However, since imaging projects a 3-dimensional object (sample) into a 2-dimensional plane (image), a problem emerges when we try to determine the location of the object point. In other words, when back-tracing the light ray from the image point, this gives only the line at which the object point will fall on. An additional camera (Figure 63) or a mirror (Figure 64) is needed to get an additional light ray passing through the image point. Thus the image point location can be determined as the intersection of these two lines.
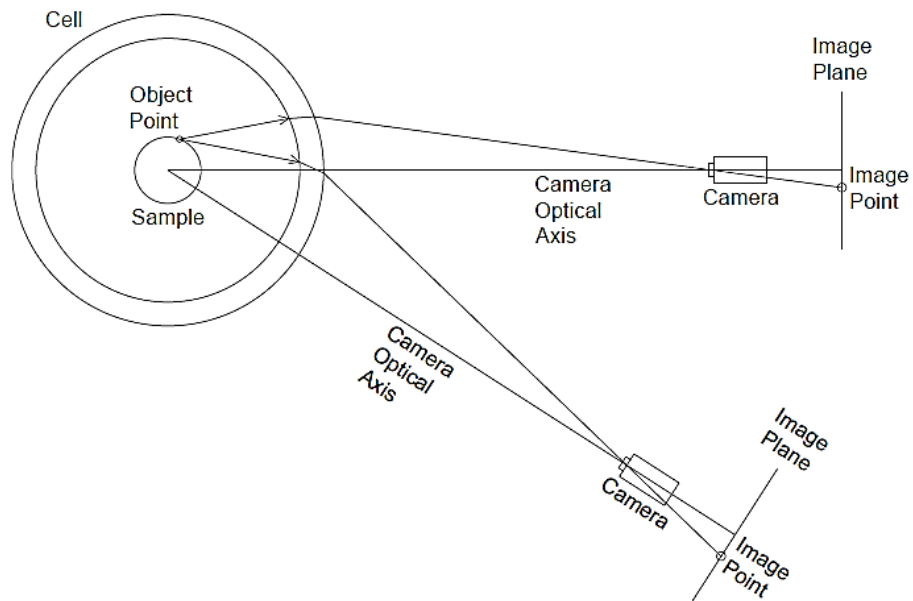


Figure 63. Incorporating two cameras to aid in object detection
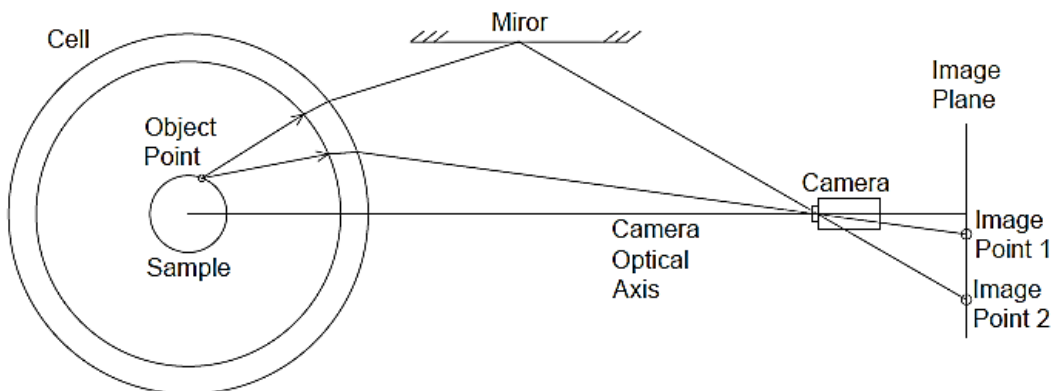


Figure 64. Incorporating a mirror to aid in object detection

However, the samples in this testing program were failing in either bulging or

necking symmetrically around the sample axis. This assumption simplifies the problem into just capturing the edge of the sample and full deformed shape is obtained by revolving the edge profile around the sample axis.

The edges on two sides of the samples are obtained and compared to check the validity of the assumption of symmetrical deformation of the sample. Since nothing is ideal as theory, it is expected to have some differences between the two profiles. To minimize this error, the two profiles are averaged and the resulting profile is adopted in further analysis.

## 5.2   Procedure

In this section, the procedure of mapping the image points to the real-world object is demonstrate. Images are composed of 2D grid that contain value (or multiple values). It can be viewed mathematically as a matrix. Each pixel in the 2D grid corresponds to a projection of point in the 3D space covered by the camera. As a first step, the edge points of the specimen at each frame are detected. This is done using the edge detection function available in Matlab. Luminous sources are concentrated at the specimen to have a greater contrast between the specimen and the background. This results in sharper edge and facilitates the edge detection process. Figure 65 shows a frame of a tested specimen during the cyclic phase. It is clear from the figure the bulging of the specimen. Edge detection tool in Matlab captures the edges within this frame (Figure 66). A code is then used to capture the pixel coordinates of the edge points as can be seen in Figure 67. The "Camera Calibration Toolbox" in Matlab provides the capability to get the transformation matrices (translation and rotation) by which the conversion between pixel coordinates and real world coordinates of the image points onto a given plane  in space (plane XY(Z=0) in Figure 68) is performed. So for any given pixel in the captured image, its corresponding projection can be obtained

(point A in Figure 68).



Figure 65. Frame shows a deofrmed specimen during a cyclic test
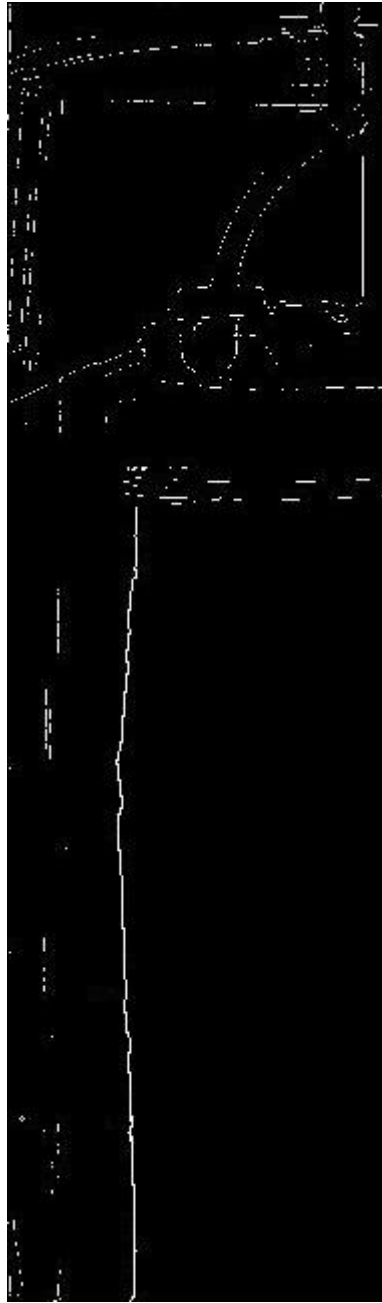
Figure 66. Edge of specimen deteted using the Matlab (left half of speciemn)
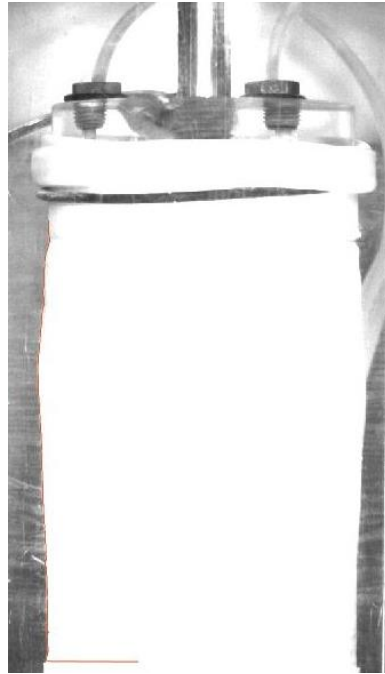
Figure 67. Digitized left edge plotted along with the image (in orange)

The law of rectilinear propagation of light, the principle of reversibility of light propagation, and Snell's law are the major three physical rules utilized in the digitizing the edge of the specimen during the cyclic phase of the triaxial tests.
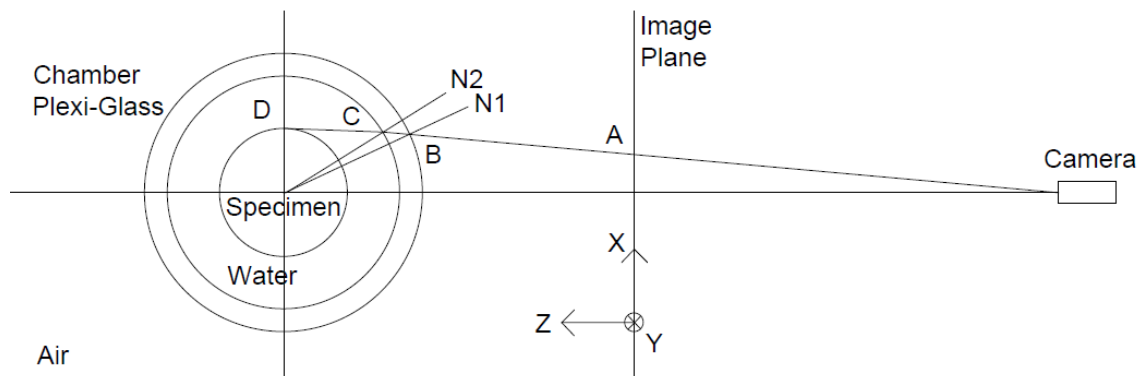


Figure 68. Illustrative plan view of of the camera and triaxial chamber.

Once the real world image coordinates are obtained for all edge points (similar to point A), 3D space geometry and optical rules are used to go from image points (point A) to their corresponding object point (point D). This process starts by connecting the image point to the pinhole of the camera to define the light ray which is extended

until it reaches the air-plexi interface (point B). The angle of incidence is defined as the angle between this light ray and a normal (N1) to the interface at the point of intersection of the light ray and the interface in the plane defined by the light ray and normal. The refraction angle is determined using Snell's law:

$$\frac{n_1}{n_2} = \frac{sin\theta_2}{sin\theta_1} \tag{27}$$

where $n_1$ and $n_2$ are the refraction indices of the medium of incidence and medium of refraction respectively. The refractive indices are 1, 1.15, and 1.33 for the air, plexi-glass, and water respectively. And $\theta_1$ and $\theta_2$ are the incident and refracted angles respectively. The difference between the refracted and incident angles defines the deviation in the light ray. This deviation can be applied to the incident ray to get the refracted ray using the following rotation matrix:

$$R = \begin{bmatrix} \cos\theta + u_x^2 (1 - \cos\theta) & u_x u_y (1 - \cos\theta) - u_z \sin\theta & u_x u_z (1 - \cos\theta) + u_y \sin\theta \\ u_y u_x (1 - \cos\theta) + u_z \sin\theta & \cos\theta + u_y^2 (1 - \cos\theta) & u_y u_z (1 - \cos\theta) - u_x \sin\theta \\ u_z u_x (1 - \cos\theta) - u_y \sin\theta & u_z u_y (1 - \cos\theta) + u_x \sin\theta & \cos\theta + u_z^2 (1 - \cos\theta) \end{bmatrix}.$$

where θ is the angle of rotation (difference between incident and refracted rays) and $u_x$, $u_y$ and $u_z$ are the components of the normal vector to the plane containing the incident and N1 around which rotation is taking place.

The obtained vector represents the direction vector if the refracted ray which is then extended to reach the plexi-water interface where the previously described steps performed at the air-plexi interface are repeated to get the light ray directed toward the edge of the specimen. Specimen edge points have a unique criteria that provides an additional equation which in turn helps in solving the problem of mapping image points (2-D image plane) to their corresponding object points (3-D sample). This additional equation comes from the fact that the object edge point on the sample will have the minimum distance to the back-traced light ray originating from the edge in the image

plane and the sample vertical axis as shown in Figure 69. Mathematically, the dot

product of light ray vector and the radius should be zero.
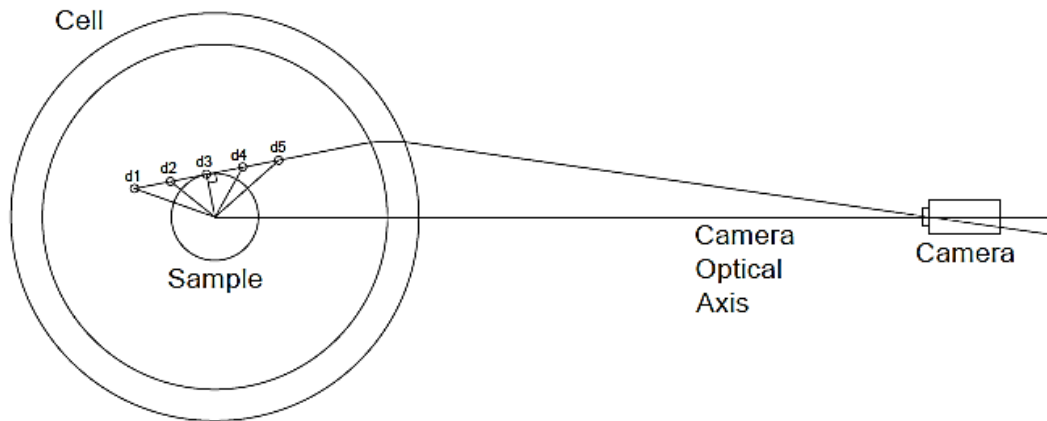


Figure 69. The light ray and distances to speciemn. Notice that the sought point has the minimum distance to the center of the specimen.

This procedure is looped over all edge points in each frame of the video and

then on all the frames. A Matlab code was developed to automate this process.

## 5.3 Demonstrative Example

Shows series of frames that were captured during a cyclic test. The bulging and

necking of the specimen is clearly demonstrated in the frames presented. Applying the

previously described approach to digitize the specimen edge of the presented frames

results in Figure 71.
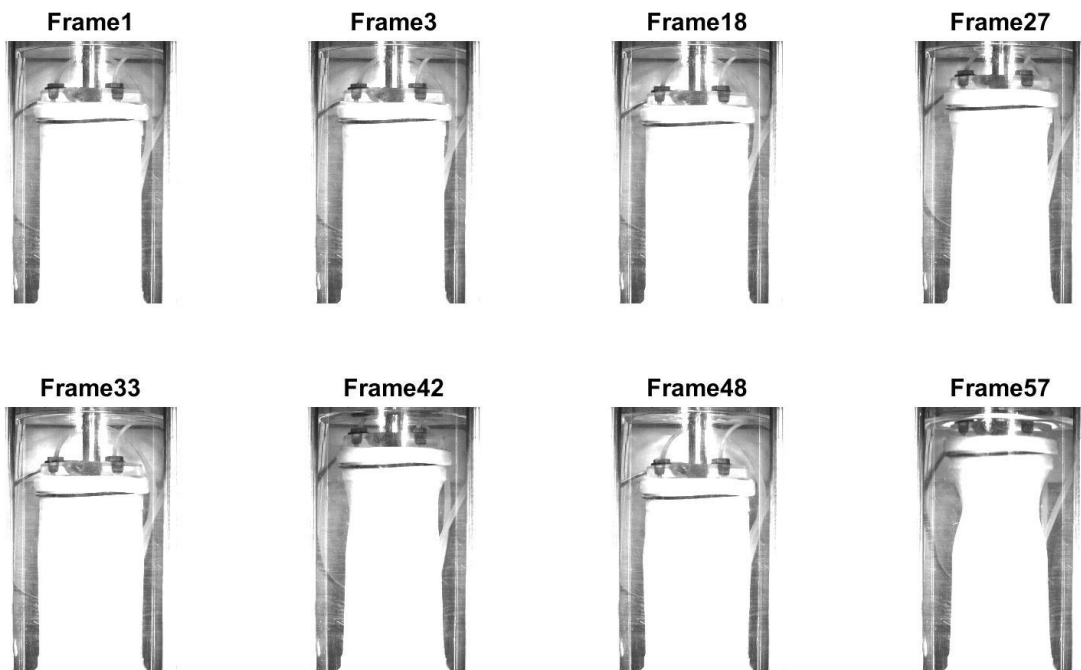
Figure 70. Group of frames showiung the deformed specimen during the cyclic phase of the triaxial test.
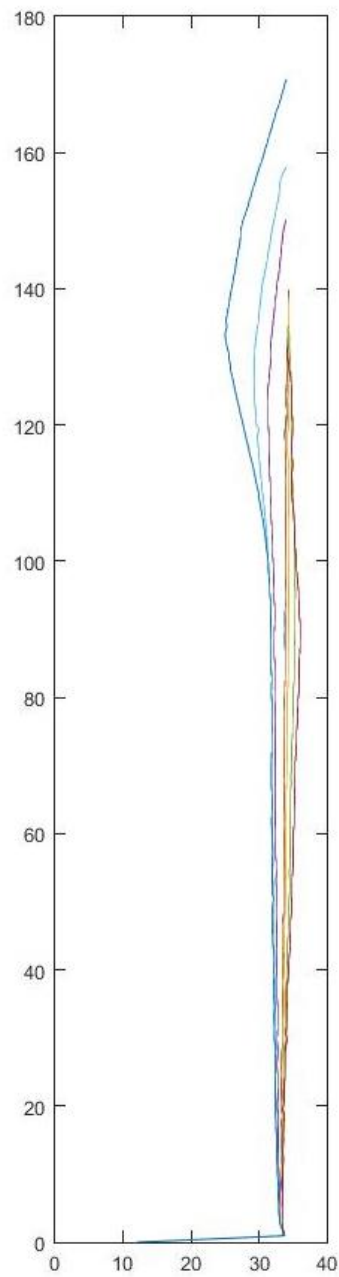
Figure 71. Digitized edges of the frames

## 5.4 Results and Analysis

As the imaging part was developed while the testing program was running, some tests weren't video recorded. The results are displayed for only three tests: one control clay test (Figure 72), one 3cm-reinforced clay specimen test (Figure 73), and one 4cm-reinforced clay specimen test (Figure 74). The selected edges are at the peak and troughs of a given cycle. Normalized time by the loading period adopted in the test

121

(t/T) is displayed for each edge.
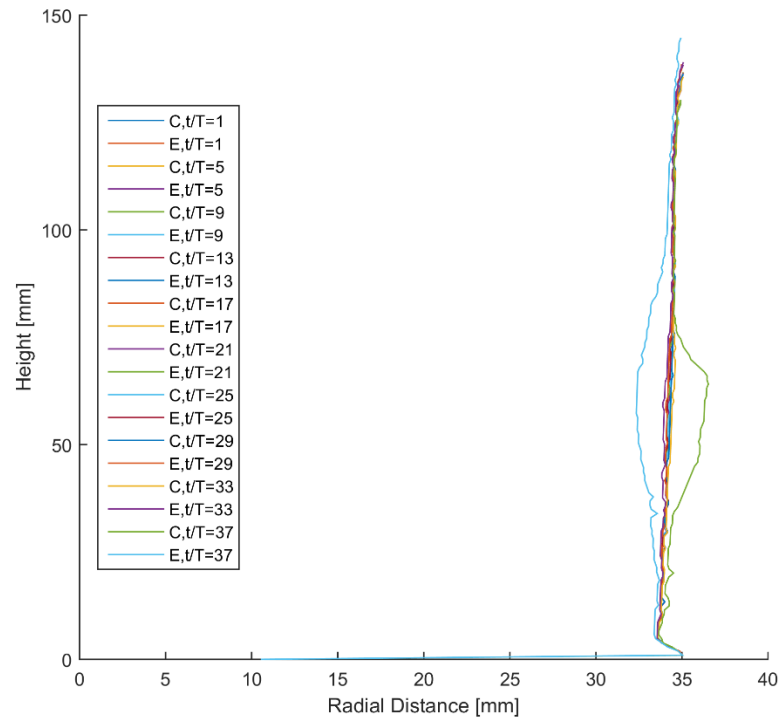


Figure 72. Edges of scpeimen at peak and trough axial strains for different cycles for the clay test, CSR=0.25, T=1sec
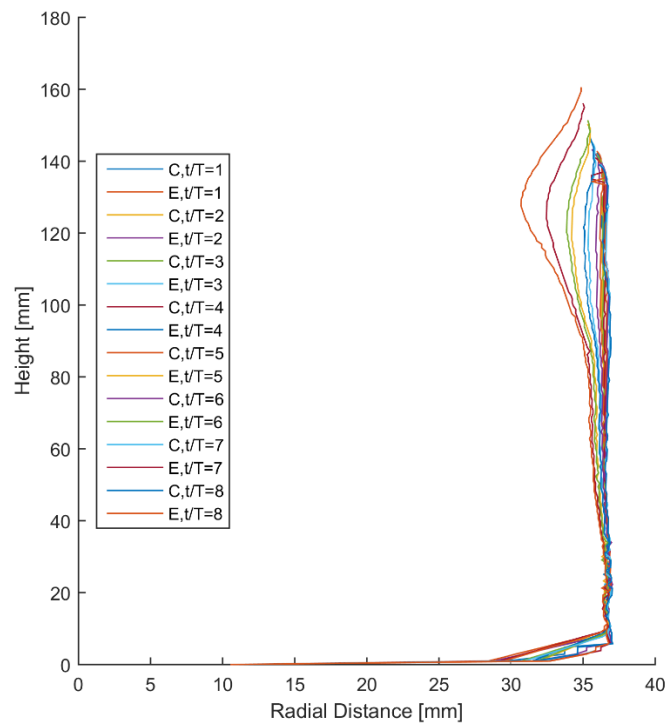


Figure 73. Edges of scpeimen at peak and trough axial strains for different cycles for the 3cm reinforced clay test, CSR=0.35, T=1sec
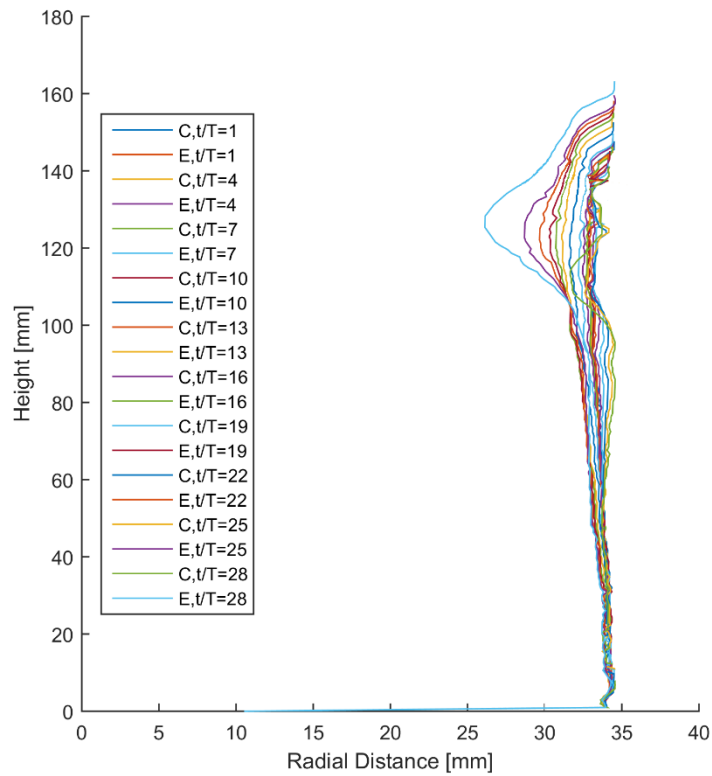
Figure 74. Edges of scpeimen at peak and trough axial strains for different cycles for the 4cm reinforced clay test, CSR=0.35, T=1sec

For the clay test (Figure 72), it can be noticed that the lateral deformation remained small for the first 33 cycles then strains developed rapidly after that. Strains were concentrated at middle of the specimen approximately as can be noticed from the last edges taken at t/T=37 in both extension and compression half cycles.

On the other hand, lateral strains appear to develop gradually with number of cycles in the reinforced specimens. Deformations are concentrated in upper quarter of the specimen. Direct correlation can be generally noticed between axial deformation and lateral deformation. This is a clear demonstration of the Poisson's effect.

## 5.5    Conclusion

Image processing is a robust tool for detecting the lateral deformation of specimens in triaxial test. It can be noticed from the results that as the global axial strain increases, the deformations will concentrate at a certain location across the height of the

specimen. The benefits of this technique may be expanded to calculate the localized

vertical strain and recalculation of deviatoric stresses based on the cross-sectional area

obtained from digitized images. In addition, the output of the imaging could be coupled

with finite element softwares for calibration of soil models.

# CHAPTER 6

# INCORPORATING MODEL UNCERTAINTY AND SPATIAL VARIABILITY IN THE DESIGN OF FOOTINGS ON CLAYS REINFORCED WITH STONE COLUMNS

## 6.1  Abstract

Monte-Carlo simulations are conducted in the context of a reliability-based framework that incorporates model uncertainty and spatial variability with the objective of calibrating resistance factors for the ultimate limit state design of footings resting on clays improved with granular columns. Resistance factors are calibrated for different design scenarios to ensure target reliability levels. Results indicate that the required resistance factors are mainly dependent on the ratio of the dead to live load, clay sensitivity, area replacement ratio, and the target probability of failure. From a practical design standpoint, it is recommended that resistance factors in the range of 0.5 to 0.55 be used for cases involving sites with relatively low variability in the undrained shear strength. These resistance factors ensure designs with a probability of failure of 1%. For more stringent target probabilities of failure ($p_f = 0.1\%$), the resistance factors have to be decreased to about 0.4. For sites that are more variable, the resistance factors are smaller and range from 0.38 to 0.55 (for $p_f = 1\%$) and from 0.25 to 0.40 (for $p_f = 0.1\%$).

## 6.2  Introduction

Granular columns are widely used to improve several aspects of soil behavior.

The installation process involves replacing part of the soft soil with an array of densified granular columnar elements covering the influence zone of a footing. These columns exhibit better characteristics with regards to strength, stiffness, and drainage, and less variability relative to the native soil. Reinforcement by granular columns has been proven to be effective in solving various geotechnical engineering problems. For applications of granular columns in soft clays, the main performance indicators that govern the response are the ultimate bearing capacity and the stiffness of the composite clay-column system. For the ultimate limit state which is the main focus of this paper, the literature includes several models ((Vesic, 1972), (Hughes, Withers, & Greenwood, 1975), (M. Madhav & Vitkar, 1978), (Brauns, 1978), and(Mitchell, 1981)) that aim at quantifying the ultimate bearing capacity of a single granular column that is installed in a clay matrix. Since foundations are generally supported on clay that has been reinforced with single or multiple stone columns, simplified composite models that aim at incorporating the contribution of the matrix clay to the bearing capacity of the system have been developed by several researchers (ex. (Barksdale, 1987)and (Stuedlein, Huffman, & Reddy, 2014)).

A common attribute of the above methods is that they are empirical or at most semi-empirical in nature. As such, there is a degree of model uncertainty that is expected to be inherent in the ultimate bearing capacity predictions of these models on top of the conventional sources of uncertainty that originate from spatial variability in soil properties of both the soft soil and the compacted column. This additional uncertainty will translate into a source of risk that has to be accounted for in the design. As a result, the required resistance factor that would ensure an acceptable level of reliability or risk for improved ground in the context of LRFD could differ from the

conventional resistance factors that are typically used in foundations on unreinforced soil.

Reliability-based design (RBD) techniques which combine all sources of uncertainty have been effectively utilized in the last two decades in almost all fields of geotechnical engineering design. More recently, RBD principles have started to infiltrate into the soil improvement field through many applications. Examples include the work of (Nishimura & Shimizu, 2008), (Zheng, Liu, & Xu, 2009), (Najjar, Sadek, & Alcovero, 2012), (Stuedlein et al., 2014), and (Bergman, Ignat, & Larsson, 2013). (Huffman & Stuedlein, 2014) and (Stuedlein et al., 2014) developed RBD procedures that are based on Monte Carlo simulations to assess the allowable bearing capacity of aggregate pier-reinforced clay and to calibrate ultimate limit state resistance factors, respectively. Recently, (Kahiel, Najjar, & Sadek, 2017) presented charts of factors of safety corresponding to different design scenarios for the ultimate bearing capacity of footings supported on clays reinforced with stone columns for targeted probabilities of failure.

The objective of this paper is to calibrate resistance factors that are compatible with the conventional bearing capacity models for stone columns in clay while considering the different sources of uncertainty that affect the design problem. The methodology uses the traditional models for stone column capacity prediction as a basis for the analysis, given the past experience that geotechnical designers and contractors have in these methods. The parameters that are included in the reliability analysis in addition to the model uncertainty are the area replacement ratio under the foundation, the undrained shear strength of the clay, the friction angle of the granular column and the sensitivity of the clay as reflected in the ratio of the undisturbed undrained shear

127

strength to the remolded undrained shear strength. To achieve the above objective, a probabilistic approach that is based on Monte Carlo simulations is proposed to quantify the probability distribution of the ultimate bearing capacity of foundations that are supported on reinforced clay for practical design scenarios. To add robustness to the reliability analysis, a lower-bound estimate of the shear strength as reflected in the remolded undrained shear strength of the clay is incorporated in the probabilistic model of the bearing capacity to yield a more realistic model of the left-hand tail of the distribution. The outcome of the reliability analysis is a set of recommended resistance factors that could be used in the context of LRFD codes for foundations to achieve a target level of risk for a comprehensive set of realistic design scenarios.

## 6.3    Model and Spatial Uncertainty

Despite the availability of several models for the estimation of the ultimate bearing capacity of clays reinforced with granular columns (Stuedlein et al., 2014) and (Najjar, 2013b)), the reliability analysis was limited in this paper to the method presented in Hughes and Withers (1974) and Hughes et al. (1975) in its modified version as presented in (Stuedlein et al., 2014). In this method, the ultimate bearing capacity is expressed as:

$$q_{ult} = [\sigma'_{r0} + 4 \cdot s_u] \cdot tan^2\left(45 + \frac{\varphi_p}{2}\right) \cdot a_r + d_c d_d N_c \cdot s_u \cdot (1 - a_r) \tag{28}$$

where $q_{ult}$ is the column ultimate bearing capacity, $s_u$ is the undrained shear strength of the surrounding clay, $\sigma'_{r0} = \gamma'_s \cdot d/2 \cdot (1 - sin\varphi'_s)$ is the average effective lateral stress of the clay along a distance equal to $d = d_p \cdot tan(45 + \frac{\varphi_p}{2})$, $d_p$ is the diameter of the column, $\varphi_p$ is the friction angle of the column material, $k_p = -1.45 \cdot ln(s_u) + 8.52$ is the aggregate pier cavity expansion factor, $\varphi'_s$ and $\gamma'_s$ are the drained angle of

friction and effective unit weight for the surrounding clay, $d_c$ and $d_d$ are shape and depth correction factors respectively, $N_c$ is the bearing capacity factor of cohesion, and $a_r$ is defined as the ratio of the total area of the stone columns under the footing to the area of the footing. This model includes the contributions of granular columns and the surrounding soil matrix scaled by the area replacement ratio which makes it useful in a wide range of practical design scenarios. (Kahiel et al., 2017) report that Equation 1 exhibits a lognormally distributed bias with a mean of around 1.19 and a COV of 0.31 for predictions involving footings on clay reinforced with single or multiple stone columns.

To quantify the total uncertainty in the bearing capacity of footings supported on stone columns in clay, the uncertainty in soil properties has to be combined with the uncertainty of the models used to predict capacity. An investigation of Equation 1 indicates that the undrained shear strength $(s_u)$ of the clay is expected to be a main contributor to the uncertainty in the bearing capacity predictions. According to (Phoon & Kulhawy, 1999a; Phoon & Kulhawy, 1999b), the coefficient of variation of $s_u$ ranges from 18% to 80%. In this paper, $s_u$ was modelled as a lognormally distributed random variable with three coefficients of variations (0.3, 0.4, and 0.5) covering the realistic common range of the uncertainty in $s_u$ in practical design scenarios. It is worth noting that due to the inversely proportional relation between $\ln(s_u)$ and $k_p$, a lower limit of unity was set to the value of $k_p$ in the Monte Carlo simulations to eliminate unrealistic realizations of $k_p$ that are not practically or physically possible.

In this paper, a lower-bound shear strength that is defined by the remolded undrained strength was incorporated in modeling the left hand tail of the truncated lognormal distribution of the undrained shear strength of the clay. Since the remolded

undrained shear strength is a physical soil property, it should be also considered as an

uncertain parameter that exhibits spatial variability. (Najjar & Gilbert, 2009) proved

through an analysis of two offshore case histories that the uncertainty in the remolded

undrained shear strength is generally much smaller than that of the undisturbed

undrained shear strength since the remolded strength is expected to be less sensitive to

the depositional environment and to disturbance during sampling and testing. In this

paper, the remolded undrained shear strength $S_{u,LB}$ is assumed to follow a lognormal

distribution with a mean ($\mu_{Su,LB}$) that is equal to the mean of the undisturbed undrained

shear strength ($\mu_{Su}$) divided by the sensitivity of the clay ($\mu_{Su,LB} = \mu_{Su}$ / Sensitivity), with

an associated coefficient of variation of 0.15.

The uncertain remolded undrained shear strength $S_{u,LB}$ was used to truncate the

distribution of the undrained strength. More details about how the lower bound is

mathematically incorporated to define the CDF of ($s_u$) are presented in (Kahiel et al.,

2017).

Other contributors to the uncertainty in the bearing capacity are the drained

angle of internal friction and unit weight of the clay surrounding the column. Based on

the recommendations of (Phoon & Kulhawy, 1999a; Phoon & Kulhawy, 1999b), the

friction angle and unit weight of the clay were modelled as normally distributed random

variables with coefficients of variation of 0.2 and 0.1, respectively. The internal friction

angle of the column material was also assumed to be a random variable. To account for

the curvature in the Mohr-Coulomb failure envelope of the aggregates, the angle of

internal friction ($\varphi_p$) was assumed to vary linearly with the logarithm of the confining

pressure such that:

$$\varphi_p = \varphi_0 + \Delta\varphi \cdot ln \left[ \frac{\sigma'_{r0} + k_p.s_u}{\sigma_{atmospheric}} \right] \qquad (29)$$

where $\varphi_p$ and $\varphi_o$ are the angles of internal friction of the aggregate at confining

pressures of $(\sigma'_{r0} + k_p.s_u)$ and $\sigma_{atmospheric}$, respectively, and $\Delta\varphi$ is the change in $\varphi_p$

in one logarithmic interval of normalized confining pressure (slope of the relationship

between friction angle and logarithm of confining pressure). Mean values of 40° and 50°

for $\varphi_0$ were adopted in the analysis to represent granular columns of different densities

and compositions. Since the results of the reliability analysis showed that the mean of

$\Delta\varphi$ does not have a significant impact on the results, a mean value of -8° was adopted in

the reliability analyses conducted in this paper. Both $\varphi_0$ and $\Delta\varphi$ were taken as normally

distributed with a relatively low coefficient of variation of 0.05. This is due to the fact

that the nature of the granular material used in the column (generally gravel) and the

method of installation of the column are generally well-controlled by the contractor,

resulting in column properties that are less uncertain than the properties of natural soils.

Finally, the area replacement ratio was also assumed to be a random variable

that is normally distributed with a coefficient of variation of 0.05. The uncertainty in the

area replacement ratio was incorporated in the reliability analysis to reflect variations in

the diameter of the column due to the process of installation.

From the load side, both dead and live loads were taken into considerations as

lognormally distributed variables with mean biases of 1.05 and 1.15 and COVs of 0.1

and 0.2, respectively. In the LRFD equation, load factors of 1.25 and 1.75, respectively

were considered for the dead and live load and different combinations of nominal dead

and live load ratios "η" were adopted. To limit the scope of this paper, only results for η

of 1 and 3 are presented.

## 6.4    Monte-Carlo Simulations

The LRFD equation used as a basis to calibrate resistance factors in the analysis is:

$$\gamma_{DL}DL_n + \gamma_{LL}LL_n < \varphi R_n \tag{30}$$

where $R_n$ is the nominal resistance obtained from the selected bearing capacity equation, $DL_n$ and $LL_n$ are the nominal dead and live loads respectively, $\gamma_{DL}$ and $\gamma_{LL}$ are the dead load and live load factors, and $\varphi$ is the resistance factor to be calibrated. A total of approximately 2300 practical design scenarios were analyzed within a probabilistic framework to (1) quantify the mean, COV, and distribution of the ultimate bearing capacity of footings supported on stone-column reinforced clays for different combinations of input parameters, (2) evaluate the probability of failure (reliability index) associated with designs that are conducted using different resistance factors, and (3) recommend resistance factors needed to achieve a target level of reliability based on the important design parameters (ex. area replacement ratio, COV of $s_u$, and η).

The design cases that were analyzed involved a wide representative range of combinations of design parameters as listed in Table 8.

Table 8.Mean values of major parameters used in the simulations.

| Random Variable | $S_u$ $(kPa)$ | $\varphi_0$ | $a_r(\%)$ | Sensitivity |
|---|---|---|---|---|
| Mean values | 20, 40, 80 | 45, 50 | 10 to 40 by 10 | 1.15, 1.25, 1.5, 1.75, 2, 3, 5 |

Mean values of undrained shear strength ranged from 20 kPa to 80 kPa. To account for practical cases with different lower-bound remolded shear strengths, cases with different clay sensitivities (range from 1.15 to 5) were analyzed. In addition, the area replacement ratio was varied from 10% to 40% to cover different percentages of

clay replacement/reinforcement under the footing. It should be noted that the COV of $s_u$

was also varied between 0.3 and 0.5 for all cases analyzed. For each design scenario

considered (combination of input parameters), Monte Carlo simulations were conducted

using 500,000 realizations of the input parameters to quantify the variations of the

mean, COV, and the probability distribution of the resulting ultimate bearing capacity of

the footing with different input parameters. The number of simulations was chosen to

ensure less than 10% error in the probability of failure with 95% confidence.

Since the main objective of the paper is to recommend resistance factors that

would ensure a target reliability level for footings on reinforced clay, the results of the

Monte Carlo analyses were also used to determine the dependency of the required

resistance factor on the main input design parameters. Mathematically, this was

achieved by plugging different resistance factors in equation 2 while recording the

resulting reliability index. The resistance factor that would result in the required target

reliability index was then selected. More details and results are presented in the

following section.

## 6.5   Results

### 6.5.1   *Resistance: mean, COV, and distribution*

Based on the simulations described above, the mean and COV of the ultimate

bearing capacity were determined. For illustration, the variations of the mean and COV

of the $q_{ult}$ as a function of clay sensitivity are presented in Figure 75 for the case having

area replacement ratio of 20% and $\varphi_0$ of 40°. Results on Figure 75 indicate that the

effect of the sensitivity of the clay on the mean ultimate bearing capacity appears to be

negligible for sensitivities above 2.5. For smaller clay sensitivities, the truncation of the

left-hand tail of the probability distribution of $s_u$ increases the mean value of the

resulting bearing capacity of the foundation. This minor effect of the clay sensitivity on the mean of $q_{ult}$ is more evident for cases with a high COVs$_u$.

Unlike the mean of $q_{ult}$, the COV of $q_{ult}$ was found to be sensitive to the COV of $s_u$ and to the assumed clay sensitivity. Results on Figure 75b indicate that as the clay sensitivity decreases, the uncertainty in the bearing capacity decreases. This result is important since it indicates that when the effect of the clay sensitivity in the form of a lower-bound undrained shear strength is included in the reliability analysis, it is expected to affect the resulting probability of failure. The effect of the clay sensitivity on the COV of $q_{ult}$ becomes more clearly evident for sensitivities below 2.0 and for the higher COV of su. It could be noted that the maximum uncertainty in $q_{ult}$ is reached at sensitivities of 5 and 3 for COV of undrained shear strength of 0.5 and 0.3, respectively.



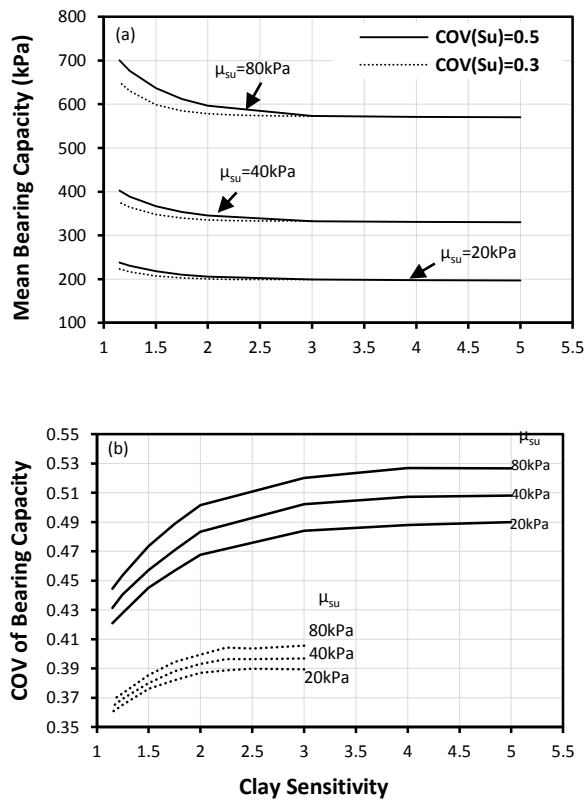Figure 75. Variation of mean and COV of qult with clay sensitivity.

The resulting resistance factors for the simulated design scenarios are presented in Figs. 2 and 3 for $COV_{su}$ of 0.3 and 0.5, respectively. The resistance factors were plotted for two probabilities of failure (1% and 0.1%), two dead to live load ratios (1 and 3), four area replacement ratios (10, 20, 30 and 40%), three mean undrained shear strengths (20, 40, and 80kPa), and two mean aggregate friction angles ($\varphi_0$ of 40° and 50°). Results on Figure 76Figure 77 indicate that the required resistance factors were found to be highly dependent on (1) the target reliability level, (2) the area replacement ratio, (3), the clay sensitivity, (4) the COV of $s_u$, and (5) the ratio of dead to live load, and slightly dependent on the mean friction angle of the granular column and the mean of the undrained shear strength of the clay. Comparing Figure 76Figure 77, the following observations can be made:

For cases where the uncertainty in $s_u$ is relatively small (COV = 0.3), results on Figure 76 indicate that resistance factors in the order of 0.35 to 0.40 and 0.5 to 0.55 are required to achieve target $p_f$ of 0.1% and 1%, respectively for the case with a relatively large sensitivity (~ 3). For cases involving less sensitive clays (ex, sensitivity of 1.5), the required resistance factors decrease to about 0.38 to 0.47 (compared to 0.35 to 0.40) and 0.55 to 0.6 (compared to 0.5 to 0.55), respectively. For any given clay sensitivity, the higher resistance factors are typically associated with the higher mean undrained shear strength and the lower dead to live load ratio. For a $COV_{su}$ of 0.3, the sensitivity of the resistance factors to the assumed area replacement ratio was observed to be relatively low.

For the cases where the uncertainty in the undrained shear strength is expected to be relatively large (COV = 0.5), results on Figure 77 indicate that resistance factors in the ranges of 0.25 to 0.40 and 0.35 to 0.50 are required to achieve a target $p_f$ of 0.1%

and 1%, respectively for cases with large clay sensitivity (~ 5). The relatively wide ranges indicate that the required resistance factors for cases with a $COV_{su}$ of 0.5 are more sensitive to the area replacement ratio and the mean $S_u$ compared to the cases where the $COV_{su}$ was 0.3. More importantly, results on Figure 77 indicate that the clay sensitivity plays a significant role in increasing the required resistance factors for any target probability of failure. For illustration, the range of the required resistance factors for a target $p_f$ of 0.1% increases to 0.35 to 0.45 for cases involving a clay sensitivity of 2.0. These results portray the importance of incorporating the clay sensitivity as a parameter that affects the design of footings on clays that are reinforced with stone columns.

For all the cases analyzed, the required resistance factors were found to be larger (by about 0.025 to 0.075) for the cases involving dead loads to live load ratios of 1.0 compared to the cases involving a ratio of 3.

### 6.5.2 *Practical recommendations for resistance factors*

Based on the results presented in Figure 76Figure 77 and to simplify the results presented in this study, the following recommendations are suggested to determine the recommended resistance factor to be used in the LRDF design of shallow footings on clays reinforced with stone columns. The recommendations are presented in Table 2 and are based on two categories for the area replacement ratio ("L" for $a_r$ below 25% and "H" for $a_r$ above 25%), three categories for the clay sensitivity ("L" for clay sensitivity below 2, "I" for sensitivity between 2 and 3, and "H" for sensitivity above 3). The recommended resistance factors were conservatively chosen to produce designs with probabilities of failure that are less than 1% and 0.1%, respectively as indicated in Table 9.

A comparison between the resistance factors presented Table 9 and those presented in (Stuedlein et al., 2014) indicates that the ranges are generally comparable, despite the fact that the resistance factors presented by (Stuedlein et al., 2014) are based on a newly developed empirical model that includes 6 regression coefficients and 4 regression variables to predict the bearing capacity of footings on improved ground. The fact that the resistance factors from the two studies are similar indicates that although the uncertainty in the model used to predict the bearing capacity plays a role in the reliability analysis, other sources of uncertainty (ex. uncertainty in the undrained shear strength, friction angle of the column, etc.) could mask the effect of the model uncertainty and govern the risk of failure of the foundations. It is worth noting that the most important differences in the resistance factors calculated in this study and in (Stuedlein et al., 2014) study pertained to cases with clays of low sensitivity where the lower-bound undrained shear strength played a role in increasing the required resistance factor. In these cases, the recommended resistance factors in this study were higher by about 0.1 compared to those recommended in (Stuedlein et al., 2014).
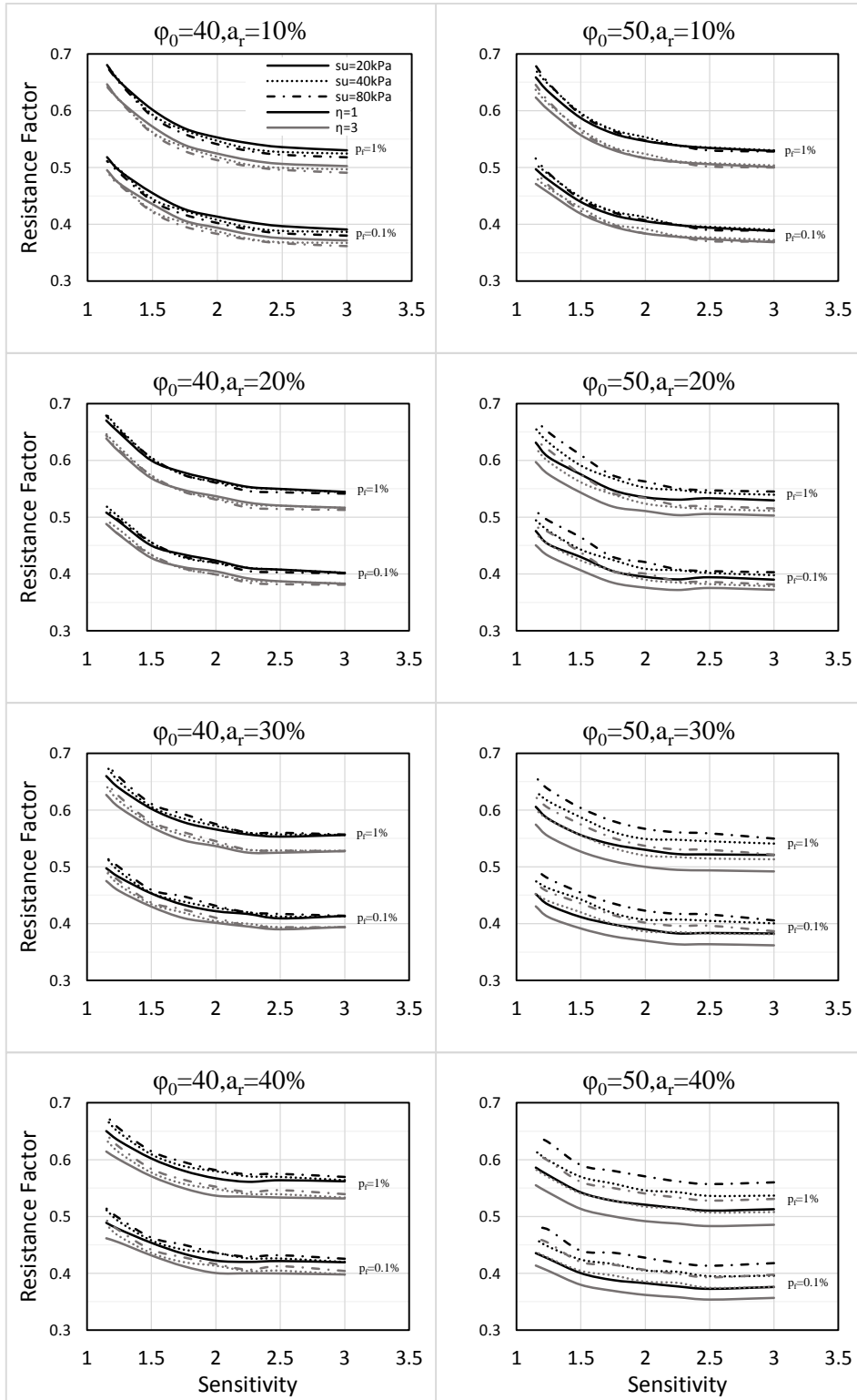
Figure 76. Variation of resistance factors with sensitivity for COVSu = 0.3
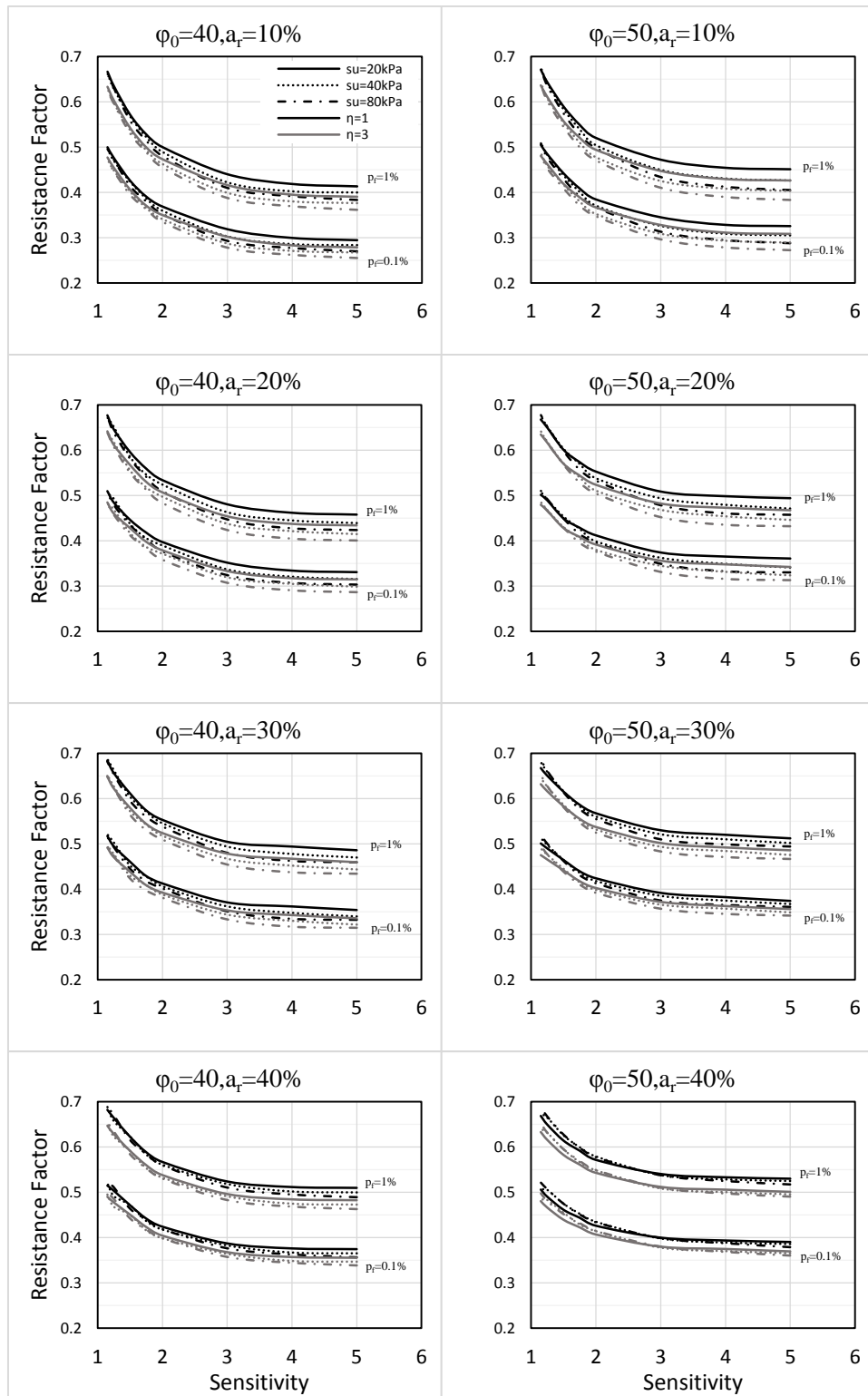
Figure 77. Variation of resistance factors with sensitivity for COVSu = 0.5

Table 9. Recommended resistance factors for practical design scenarios.

| COV$_{su}$ | η | A$_r$ | Sensitivity | Φ (p$_f$=1%) | Φ (p$_f$=0.1%) |
|---|---|---|---|---|---|
| 00.3 | 1 | - | - | 0.55 | 0.40 |
| | 3 | - | - | 0.50 | 0.38 |
| 00.5 | 1 | L | H | 0.40 | 0.28 |
| | | | I | 0.43 | 0.30 |
| | | | L | 0.48 | 0.35 |
| | | H | H | 0.45 | 0.33 |
| | | | I | 0.48 | 0.35 |
| | | | L | 0.55 | 0.40 |
| | 3 | L | H | 0.38 | 0.25 |
| | | | I | 0.40 | 0.28 |
| | | | L | 0.45 | 0.33 |
| | | H | H | 0.43 | 0.30 |
| | | | I | 0.45 | 0.33 |
| | | | L | 0.53 | 0.38 |

### 6.5.3 *Comparison between static and cyclic resistance*

In practice, water tanks and silos are designed for static loading patterns. The cyclicity of the load that occurs due to the continuous filling and discharging is commonly neglected. Given the static ultimate resistance of the reinforced clay specimens (Rayess, 2015), the developed resistance factors allows the calculation of an allowable shear stress that will guarantee the targeted probabilities of failure (1% and 0.1%). As the resistance factors are a function of the clay sensitivity, the allowable stress are plotted for different sensitivities. Figure 78 shows the allowable shear stress that the reinforced specimens can resist. The calculations are based on the undrained ultimate resistance of the 3cm and 4cm given by (Rayess, 2015) (80kPa and 150kPa respectively). The allowable stress is normalized by the initial effective confining pressure the specimens experienced.
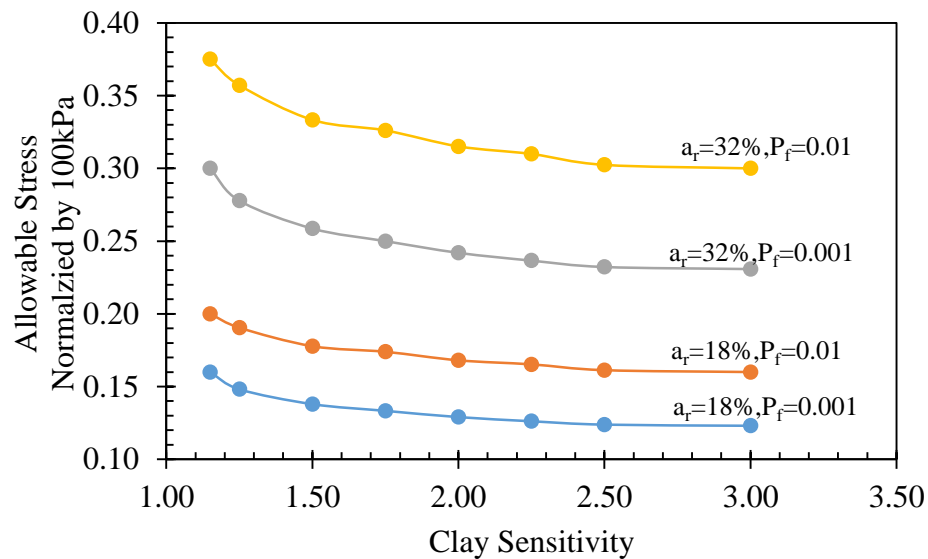
Figure 78. Allowable shear stress based on the developed resistance factorsversus clay sensitivity.

Assuming that the total load is being cycled, though in realty the dead weight remains constant and part of the stored material or water load undergoes cyclic patterns, a direct comparison between the allowable stress normalized by the confining pressures and the cyclic stress ratio can be performed. From this plot, for a clay sensitivity of 1.15, the allowable shear stress normalized by 100kPa is 0.35 for an area replacement ratio of 32% ($p_f$=0.01). Under this cyclic stress ratio (0.35), clay specimen with 32% area replacement ratio will fail after about 30 cycles applied at a loading period of 1sec while it not reach failure if the loading frequency exceeds 10sec as can be seen from Figure 49.

## 6.6 Conclusion

In this paper, a robust reliability-based design methodology is presented for footings that are supported on granular columns in cohesive soils. The main outcome of this methodology is a set of resistance factors that are associated with the use of the modified model of Hughes and Withers to design practical foundations on reinforced

141

clay. The novelty in the proposed methodology is the incorporation of a lower-bound shear strength that is based on the remolded undrained shear strength in the reliability analysis.

Results indicated that the resistance factors that need to be used in conjunction with the modified Hughes and Withers model are considerably affected by the COV of $s_u$, dead to live load ratio, the sensitivity of the clay, and area replacement ratio. The resistance factors are less sensitive to the mean of $s_u$ and the mean of the friction angle of the column.

From a practical design standpoint, it is recommended that resistance factors in the range of 0.5 to 0.55 be used in the LRFD of footings on clays reinforced with stone columns for cases involving sites with relatively low variability in the undrained shear strength. These resistance factors ensure designs with a probability of failure of 1%. If more stringent target probabilities of failure are required ($p_f$ = 0.1%), the resistance factors have to be decreased to about 0.4. For sites that are more variable, the resistance factors are smaller and range from 0.38 to 0.55 (for $p_f$ = 1%) and from 0.25 to 0.40 (for $p_f$ = 0.1%) depending on the clay sensitivity, area replacement ratio, and dead to live load ratio.

# CONCLUSIONS

This thesis dealt with different aspects of stone columns. The invasion clay into the pores of coarser granular packing is investigated. Models that predict the magnitude of invasion are developed and the field applications are demonstrated. For stone column application, the invasion of clay into the pores stone column depends on the available stress at the clay/gravel interface at the service of the supported structure as compared to the locked in stresses at that interface resulting from the installation process. Additional research can be performed to refine the prediction models to account for the effect of the tortuosity of the invasion path. The effect of granular packing gradation could be another parameter to investigate.

For the case of isotropically consolidated stress state, two major factors controlled the response of the sand column reinforced specimens for the range of loading periods adopted in the testing program: The viscous behavior of the clay and the drainage within the sand column. The clay strength decreases as the loading period increases, while the strength of the sand increases at the loading period increases. However, the tests results shows that the drainage in the sand increase the strength more than the drop in the clay strength causing an overall improvement in the response of the composite specimens. Future work can focus on relating experimental results to field scales.

The initial stress state (before being loaded by an earthquake) is critical in determining the response of clays. Anisotropically consolidated specimens showed a decreased cyclic resistance as compare to isotropically consolidated ones. The dilative tendency of sand column results in significant improvement.

The advantage of utilizing image processing techniques in triaxial tests are:

1. Measure lateral strains across the height of the specimen without the any modification to the triaxial device (installing sensors, leak-free connections…).

2. Check the assumption of perfect cylinder adopted in the determination of the cross-sectional area.

3. Calculate local axial strains across the height of the specimen.

Finally, safety factors for the static design of stone columns are found to be greatly dependent on the clay sensitivity. Relatively lower safety factors can be adopted for non-sensitive clays. However, these factors of safety may not guarantee targeted safety requirements under cyclic loading conditions.

# REFERENCES

Aboshi, H., Mizuno, Y., & Kuwabara, M. (1991). Present state of sand compaction pile in japan. *Deep foundation improvements: Design, construction, and testing* () ASTM International.

Adalier, K., Elgamal, A., Meneses, J., & Baez, J. (2003). Stone columns as liquefaction countermeasure in non-plastic silty soils. *Soil Dynamics and Earthquake Engineering, 23*(7), 571-584.

Adalier, K., & Elgamal, A. (2004). Mitigation of liquefaction and associated ground deformations by stone columns. *Engineering Geology, 72*(3), 275-291.

Alamgir, M., Miura, N., Poorooshasb, H., & Madhav, M. (1996). Deformation analysis of soft ground reinforced by columnar inclusions. *Computers and Geotechnics, 18*(4), 267-290.

Andersen, K. (1980). Cyclic and static laboratory tests on drammen clay. Paper presented at the *Asce, , 106*(5) 499-529.

Ansal, A., Iyisan, R., & Yıldırım, H. (2001). The cyclic behaviour of soils and effects of geotechnical factors in microzonation. *Soil Dynamics and Earthquake Engineering, 21*(5), 445-452.

Ansal, A. M., & Erken, A. (1989). Undrained behavior of clay under cyclic shear stresses. *Journal of Geotechnical Engineering, 115*(7), 968-983.

Ashour, S. (2016). *The Response of Stone Columns Under the Cyclic Loading,*

ASTM Committee D-18 on Soil and Rock. (2004). *Standard test methods for one-dimensional consolidation properties of soils using incremental loading* ASTM International.

Baez, J., & Martin, G. (1993). Advances in the design of vibro systems for the improvement of liquefaction resistance. Paper presented at the *Proc. Symposium on Ground Improvement, 62-70.*

Baez, S. J. (1997). A design model for the reduction of soil liquefaction by vibro-stone columns.

Baghdikian, S. Y., Sharma, M. M., & Handy, L. L. (1987). Flow of clay suspensions through porous media. Paper presented at the *SPE International Symposium on Oilfield Chemistry,*

Balaam, N., & Booker, J. (1985). Effect of stone column yield on settlement of rigid foundations in stabilized clay. *International Journal for Numerical and Analytical Methods in Geomechanics, 9*(4), 331-351.

Barksdale, R. D. (1987). *State of the Art for Design and Construction of Sand Compaction Piles,*

Barron, R. A. (1900). Consolidation of fine-grained soils by drain wells.

Basack, S., Indraratna, B., & Rujikiatkamjorn, C. (2015). Modeling the performance of stone column–reinforced soft ground under static and cyclic loads. *Journal of Geotechnical and Geoenvironmental Engineering, 142*(2), 04015067.

Bergman, N., Ignat, R., & Larsson, S. (2013). Serviceability limit state design of lime-cement Columns–A reliability based design approach. *Geotechnical Safety and Risk IV,* , 417-422.

Beroya, M., Aydin, A., & Katzenbach, R. (2009). Insight into the effects of clay mineralogy on the cyclic behavior of silt–clay mixtures. *Engineering Geology, 106*(3), 154-162.

Brauns, J. (1978). Initial bearing capacity of stone columns and sand piles. Paper presented at the *Int. Symp. on Soil Reinforcing and Stabilizing Techniques in Engineering Practice, , 1* 497-512.

Bray, J. D., Sancio, R. B., Riemer, M., & Durgunoglu, T. (2004). Liquefaction susceptibility of fine-grained soils. Paper presented at the *Proc., 11th Int. Conf. on Soil Dynamics and Earthquake Engineering and 3rd Int. Conf. on Earthquake Geotechnical Engineering, , 1* 655-662.

Buckingham, E. (1915). The principle of similitude. *Nature, 96*(2406), 396.

Castro, J., & Sagaseta, C. (2009). Consolidation around stone columns. influence of column deformation. *International Journal for Numerical and Analytical Methods in Geomechanics, 33*(7), 851-877.

Deb, K., & Behera, A. (2016). Rate of consolidation of stone column–improved ground considering variable permeability and compressibility in smear zone. *International Journal of Geomechanics, 17*(6), 04016128.

Deb, K., & Shiyamalaa, S. (2015). Effect of clogging on rate of consolidation of stone column–improved ground by considering particle migration. *International Journal of Geomechanics, 16*(1), 04015017.

Duncan, J. M., Wright, S. G., & Brandon, T. L. (2014). *Soil strength and slope stability* John Wiley & Sons.

Engelhardt, K., & Golding, H. (1975). Field testing to evaluate stone column performance in a seismic area. *Geotechnique, 25*(1), 61-69.

Gachet, P., Geiser, F., Laloui, L., & Vulliet, L. (2006). Automated digital image processing for volume change measurement in triaxial cells.

Goughnour, R. R., & Pestana, J. M. (1998). *Mechanical behavior of stone columns under seismic loading*

Han, J., & Ye, S. (2001). Simplified method for consolidation rate of stone column reinforced foundations. *Journal of Geotechnical and Geoenvironmental Engineering, 127*(7), 597-603.

Han, J., & Ye, S. (2002). A theoretical solution for consolidation rates of stone column-reinforced foundations accounting for smear and well resistance effects. *The International Journal Geomechanics, 2*(2), 135-151.

Hanna, A. M., & Javed, K. (2008). Design of foundations on sensitive champlain clay subjected to cyclic loading. *Journal of Geotechnical and Geoenvironmental Engineering, 134*(7), 929-937.

Hird, C., & Moseley, V. (2000). Model study of seepage in smear zones around vertical drains in layered soil. *Geotechnique, 50*(1), 89-97.

Huffman, J. C., & Stuedlein, A. W. (2014). Reliability-based serviceability limit state design of spread footings on aggregate pier reinforced clay. *Journal of Geotechnical and Geoenvironmental Engineering, 140*(10), 04014055.

Hughes, J., Withers, N., & Greenwood, D. (1975). A field trial of the reinforcing effect of a stone column in soil. *Geotechnique, 25*(1), 31-44.

Hyodo, M., Sugiyama, M., & Yamamoto, Y. (1996). Cyclic shear behaviour of clay subjected to initial shear stress. Paper presented at the *7th Australia New Zealand Conference on Geomechanics: Geomechanics in a Changing World: Conference Proceedings, 312.*

Indraratna, B., & Redana, I. (1998). Laboratory determination of smear zone due to vertical drain installation. *Journal of Geotechnical and Geoenvironmental Engineering, 124*(2), 180-184.

Kahiel, A., Najjar, S., & Sadek, S. (2017). Reliability-based design of spread footings on clays reinforced with aggregate piers. *Georisk: Assessment and Management of Risk for Engineered Systems and Geohazards, 11*(1), 75-89.

Kim, Y. S., & Whittle, A. J. (2009). Particle network model for simulating the filtration of a microfine cement grout in sand. *Journal of Geotechnical and Geoenvironmental Engineering, 135*(2), 224-236.

Kramer, S. (2005). L.(1996). geotechnical earthquake engineering. *Pren-Tice Hall, New Jersey,*

Kumar, S. (2001). Reducing liquefaction potential using dynamic compaction and construction of stone columns. *Geotechnical and Geological Engineering, 19*(2), 169-182.

Lenoir, N., Bornert, M., Desrues, J., Bésuelle, P., & Viggiani, G. (2007). Volumetric digital image correlation applied to x-ray microtomography images from triaxial compression tests on argillaceous rock. *Strain, 43*(3), 193-205.

Liu, Q., & Santamarina, J. (2018). Mudcake growth: Model and implications. *Journal of Petroleum Science and Engineering, 162*, 251-259.

Macari, E. J., Parker, J. K., & Costes, N. C. (1997). Measurement of volume changes in triaxial tests using digital imaging techniques.

Madhav, M. R., Park, Y., & MIURA, N. (1993). Modelling and study of smear zones around band shaped drains. *Soils and Foundations, 33*(4), 135-147.

Madhav, M., & Krishna, A. M. (2008). Liquefaction mitigation of sand deposits by granular piles-an overview. *Geotechnical engineering for disaster mitigation and rehabilitation* (pp. 66-79) Springer.

Madhav, M., & Vitkar, P. (1978). Strip footing on weak clay stabilized with a granular trench or pile. *Canadian Geotechnical Journal, 15*(4), 605-609.

Mitchell, J. K. (1970). In-place treatment of foundation soils. *Journal of the Soil Mechanics and Foundations Division, 96*(1), 73-110.

Mitchell, J. K. (1981). Soil improvement-state of the art report. Paper presented at the *Proc., 11th Int. Conf. on SMFE, , 4* 509-565.

Najjar, S. S. (2013a). A state-of-the-art review of stone/sand-column reinforced clay systems. *Geotechnical and Geological Engineering, 31*(2), 355-386.

Najjar, S. S. (2013b). A state-of-the-art review of stone/sand-column reinforced clay systems. *Geotechnical and Geological Engineering, 31*(2), 355-386.

Najjar, S. S., & Gilbert, R. B. (2009). Importance of lower-bound capacities in the design of deep foundations. *Journal of Geotechnical and Geoenvironmental Engineering, 135*(7), 890-900.

Najjar, S. S., Sadek, S., & Alcovero, A. (2012). Quantification of model uncertainty in shear strength predictions for fiber-reinforced sand. *Journal of Geotechnical and Geoenvironmental Engineering, 139*(1), 116-133.

Nieto-Leal, A., & Kaliakin, V. (2013). *Behavior of Cohesive Soils Subjected to Cyclic Loading "an Extensive Review of Pertinent Literature",*

Nishimura, S., & Shimizu, H. (2008). Reliability-based design of ground improvement for liquefaction mitigation. *Structural Safety, 30*(3), 200-216.

Okamura, M., Ishihara, M., & Oshita, T. (2003). Liquefaction resistance of sand deposit improved with sand compaction piles. *Soils and Foundations, 43*(5), 175-187.

Olgun, C. G., & Martin, I., James R. (2008). Numerical modeling of the seismic response of columnar reinforced ground. *Geotechnical earthquake engineering and soil dynamics IV* (pp. 1-11)

Parsa Pajouh, A., Fatahi, B., & Khabbaz, H. (2010). Uncertainties of smear zone characteristics in the design of preloading with prefabricated vertical drains. Paper presented at the *International Conference on Geotechnical Engineering and Soil Mechanics,*

Peck, R. B., & Terzaghi, K. (1948). *Soil mechanics in engineering practice*

Phoon, K., & Kulhawy, F. H. (1999a). Characterization of geotechnical variability. *Canadian Geotechnical Journal, 36*(4), 612-624.

Phoon, K., & Kulhawy, F. H. (1999b). Evaluation of geotechnical property variability. *Canadian Geotechnical Journal, 36*(4), 625-639.

Procter, D. C., & Khaffaf, J. H. (1984). Cyclic triaxial tests on remoulded clays. *Journal of Geotechnical Engineering, 110*(10), 1431-1445.

Rayamajhi, D., Nguyen, T., Ashford, S., Boulanger, R., Lu, J., Elgamal, A., & Shao, L. (2012). Effect of discrete columns on shear stress distribution in liquefiable soil. *GeoCongress 2012: State of the art and practice in geotechnical engineering* (pp. 1908-1917)

Rayamajhi, D. (2016a). Dense granular columns in liquefiable ground. I: Shear reinforcement and cyclic stress ratio reduction. *Journal of Geotechnical and Geoenvironmental Engineering, 142*(7), 04016023.

Rayamajhi, D. (2016b). Dense granular columns in liquefiable ground. II: Effects on deformations. *Journal of Geotechnical and Geoenvironmental Engineering, 142*(7), 04016024.

Rayamajhi, D., Nguyen, T. V., Ashford, S. A., Boulanger, R. W., Lu, J., Elgamal, A., & Shao, L. (2013). Numerical study of shear stress distribution for discrete columns in liquefiable soils. *Journal of Geotechnical and Geoenvironmental Engineering, 140*(3), 04013034.

Rayess, A. Z. (2015). *Triaxial Response of Natural Clay Reinforced with Sand Columns Under Partially Drained Conditions,*

Rollins, K. M., Quimby, M., Johnson, S. R., & Price, B. (2009). Effectiveness of stone columns for liquefaction mitigation of silty sands with and without wick drains. *Advances in ground improvement: Research to practice in the united states and china* (pp. 160-169)

Rudolph, R., Serna, B., & Farrell, T. (2011). Mitigation of liquefaction potential using rammed aggregate piers. *Geo-frontiers 2011: Advances in geotechnical engineering* (pp. 557-566)

Rujikiatkamjorn, C., & Indraratna, B. (2014). Analytical solution for radial

consolidation considering soil structure characteristics. *Canadian Geotechnical*

*Journal, 52*(7), 947-960.

Sharma, J., & Xiao, D. (2000). Characterization of a smear zone around vertical drains

by large-scale laboratory tests. *Canadian Geotechnical Journal, 37*(6), 1265-1271.

Sochi, T. (2010). Non-newtonian flow in porous media. *Polymer, 51*(22), 5007-5023.

Stuedlein, A. W., Huffman, J. C., & Reddy, S. (2014). Reliability-based ultimate limit

state design of spread footings on aggregate-pier-reinforced clay. *Proceedings of*

*the Institution of Civil Engineers-Ground Improvement, 167*(4), 291-300.

Valdes, J. R., & Santamarina, J. C. (2008). Clogging: Bridge formation and vibration-

based destabilization. *Canadian Geotechnical Journal, 45*(2), 177-184.

Vardanega, P., & Haigh, S. K. (2014). The undrained strength–liquidity index

relationship. *Canadian Geotechnical Journal, 51*(9), 1073-1086.

Vesic, A. S. (1972). Expansion of cavities in infinite soil mass. *Journal of Soil*

*Mechanics & Foundations Div, 98*(sm3)

Wang, G. (2009). Consolidation of soft clay foundations reinforced by stone columns

under time-dependent loadings. *Journal of Geotechnical and Geoenvironmental*

*Engineering, 135*(12), 1922-1931.

Wang, J., Cai, Y., & Yang, F. (2013). Effects of initial shear stress on cyclic behavior of

saturated soft clay. *Marine Georesources & Geotechnology, 31*(1), 86-106.

Wang, Q., Wang, S., Sloan, S. W., Sheng, D., & Pakzad, R. (2016). Experimental investigation of pressure grouting in sand. *Soils and Foundations, 56*(2), 161-173.

Weber, T. M., Plötze, M., Laue, J., Peschke, G., & Springman, S. M. (2010). Smear zone identification and soil properties around stone columns constructed in-flight in centrifuge model tests. *Géotechnique, 60*(3), 197.

Xie, K., Lu, M., & Liu, G. (2009). Equal strain consolidation for stone columns reinforced foundation. *International Journal for Numerical and Analytical Methods in Geomechanics, 33*(15), 1721-1735.

Xie, K., Lu, M., Hu, A., & Chen, G. (2009). A general theoretical solution for the consolidation of a composite foundation. *Computers and Geotechnics, 36*(1), 24-30.

Zheng, J., Liu, Y., & Xu, Z. (2009). Reliability-based design applied to multi-column composite foundations. *Advances in ground improvement: Research to practice in the united states and china* (pp. 83-91)